

# Assessment Of Efficiency Potential Hybrid Electric Turbocharging SI ICE

Future proofing the large spark ignited internal  
combustion engine for future fuels

G.J.H. Baan



# Assessment Of Efficiency Potential Hybrid Electric Turbocharging SI ICE

Future proofing the large spark ignited internal  
combustion engine for future fuels

by

G.J.H. Baan

to obtain the degree of Master of Science in  
Marine Technology at the Delft University of Technology,  
to be defended publicly on Thursday April 10th, 2025 at 13:30.

This thesis (MT.24/25.032.M) is classified as confidential in accordance  
with the general conditions for projects performed by the TUDelft.

Student Name	Student Number
G.J.H. Baan	5191165

Thesis committee:	Dr. ir. P. de Vos	TU Delft, Chairman
	Ir. J. Vollbrandt	TU Delft, Supervisor
	Dr. ir. R. D. Geertsma	NLDA, Supervisor
Project Duration:	April, 2024 - April, 2025	
Faculty:	Faculty of Mechanical Engineering, Delft	

Version: 1.0

Cover: Close-up of ABB turbocharger compressor



# Preface

*"How many times have you seen this already?"*, a question I've been asked many times by my parents and brothers while growing up. They would ask that when they peeked into my room or when they heard 'Jessica', the song that cues the intro of *Top Gear*. And I never could answer, but it genuinely was a lot. It was during my early years in secondary school that I always spent my spare time either watching *Top Gear*, playing *Need for Speed MW*, or taking apart devices like receivers just to see how their internals worked. It was during those years —and thanks to those blokes on the BBC and a certain 'silver BMW'— that my passion for cars, engines, machines, and engineering in general was largely sparked. As a consequence, I made the decision to start studying Mechanical Engineering at Avans in Den Bosch. At the same time, I started working in a local car workshop, getting hands-on experience working on cars. Meanwhile, studying Mechanical Engineering wasn't easy, but after finishing, I wasn't satisfied, I didn't feel like I had used my full potential.

So I went searching for an interesting study at TU Delft that covered internal combustion engine topics and came across the Diesel A and B courses. Instantly, I knew the next step in my journey was pursuing a master's in Marine Technology with a specialization in Marine Engineering. It was on the 1st of September 2020 that I started my bridging programme, at home, in the middle of COVID.

And now we are here, at the end, about to graduate. Looking back, I'm glad to say that I feel satisfied, especially with my graduation project, which feels like it was made tailor made just for me. It has been a joy to be able to use my passion to full extend and apply everything that I've learned about engines; the challenges during late hours tinkering with the M50B25t $\ddot{u}$  in the e34, my job in the workshop, watching countless engineering and engine rebuild videos, attending Diesel A & B lectures, and so on.

My special thanks go to the FMW NLDA, where I spent the last one and a half years working on both my individual research assignment and my graduation project. I am very grateful to my daily supervisor, Ir. Jasper Vollbrandt, for his valuable insights and technical support. I also thank the committee members Dr.ir. P. de Vos and Dr.ir. R. D. Geerstma for taking the time to be part of my thesis committee. Secondly, I want to thank the team at NLDA-Medemblik for always being willing to help or brainstorm. I also want to express my gratitude to the Marine Engineering team at TU Delft, particularly to Wieger and Konstantinos, for their support in the struggles with the GT-ISE engine model.

Finally, I cannot thank my family enough for being a constant source of motivation and moral support.

I would like to end with thanks to my biggest source inspiration;

*"I can do all things through Christ Who strenghtens me."*

— *Philippians 4:13*

G.J.H. Baan  
Zoetermeer, March 2025



# Summary

The transition to sustainable energy in the maritime sector necessitates innovative solutions to enhance efficiency and reduce emissions of internal combustion engines (ICEs). This thesis examines the efficiency potential of large hybrid electric turbocharging (HET) in spark-ignited (SI) ICEs, focusing on the CAT G3508a gas engine. The research is motivated by ever increasing environmental regulations, such as the Paris Greenddeal, IMO's MARPOL Annex VI, and the EU's FuelEU Maritime initiative, which impose strict greenhouse gas emissions limits. In response, the Dutch Ministry of Defence aims to integrate climate-neutral propulsion systems into its fleet, necessitating advanced engine technologies to improve energy efficiency and reduce operational dependency on fossil fuels.

HET integrates an electric machine into the turbocharger's rotating assembly, enabling turbo compounding, where excess exhaust energy is recuperated and converted into electrical power rather than being used to power the compressor. This process offers the potential to enhance overall system efficiency thus reduce specific fuel consumption. While HET has been studied extensively in automotive sized SI engines or large compression-ignited (CI) engines, its application in large SI engines remains to be researched, engines that have great potential for future implementation in maritime use cases. This study addresses this knowledge gap by evaluating the efficiency potential of HET in a large SI engine thus assessing its feasibility within naval propulsion systems.

A GT-ISE (simulation software part of the GT-POWER suite) simulation model of the CAT G3508a was developed to analyse HET's impact on engine performance. The model was validated using empirical data from a CAT G3508a in a controlled test environment, ensuring accuracy in predicting real-world engine behaviour. The research primarily focuses on efficiency improvements through turbo-compounding, optimizing the resistive torque of the electric machine, maintaining a consistent system power target, and reducing Brake Specific Fuel Consumption (BSFC). It also examines HET's influence on charge air pressure, temperature distributions, throttle behaviour, compressor-turbine interaction, and combustion characteristics under steady-state conditions.

This study assesses HET's efficiency potential in a large SI ICE using the GT-ISE model, focusing on steady-state performance. Despite the models capability of transient analysis, this research does not explore dynamic behaviour, load step responses, or advanced control strategies. System integration for maritime applications is not covered, nor is the direct impact of alternative fuels like methanol.

Findings indicate that HET significantly improves efficiency, reducing specific fuel consumption by up to 5.5 [%] in mid-range power settings. Efficiency gains primarily result from reductions in Pumping Mean Effective Pressure (PMEP) and Friction Mean Effective Pressure (FMEP). Compressor power is controlled via resistive compounding torque, altering the compressor's operational point. The lower-powered compressor produces a reduced charge air pressure, the engine control unit compensates by opening the throttle further, reducing PMEP or pumping losses.

Results suggest HET offers strong potential for applications prioritizing fuel economy and emissions reduction, such as maritime operations. By decreasing fuel demand and increasing efficiency, HET lowers operational costs and OPEC dependence while enhancing sustainability. This research provides a GT-ISE model of the CAT G3508a and a foundation for HET implementation in large SI engines. Future research should explore transient boost assist, where the electric machine aids the turbine in powering the compressor. Further investigation into HET's compatibility with alternative fuels like methanol and ammonia could enhance its role in climate-neutral propulsion. These insights contribute to more efficient, sustainable power solutions, supporting the goals of the Paris Greenddeal, IMO Annex VI, and the EU FuelEU Maritime Initiative.

# Contents

<b>Preface</b>	<b>i</b>
<b>Summary</b>	<b>ii</b>
<b>Nomenclature</b>	<b>vi</b>
<b>1 Introduction</b>	<b>1</b>
<b>2 Basics Of Internal Combustion Engine Theory</b>	<b>3</b>
2.1 Four stroke operation . . . . .	3
2.2 Ignition methods . . . . .	3
2.3 Valve actuation . . . . .	4
2.4 Injection types . . . . .	4
2.5 Air-fuel ratio . . . . .	4
2.6 Modern charge air systems . . . . .	5
2.6.1 Turbocharging . . . . .	5
2.6.2 Turbocharger maps . . . . .	6
2.6.3 Turbo-compounding . . . . .	7
<b>3 Background of Hybrid Electric Turbocharging</b>	<b>8</b>
<b>4 Research Foundation</b>	<b>11</b>
4.1 Knowledge gap and problem definition . . . . .	11
4.2 Research objective and questions . . . . .	13
4.3 Scope of research . . . . .	14
<b>5 Method</b>	<b>15</b>
5.1 Method introduction . . . . .	15
5.2 Engine introduction . . . . .	17
5.3 Model . . . . .	19
5.3.1 Model introduction . . . . .	19
5.4 Model description . . . . .	20
5.4.1 Pipe sections . . . . .	22
5.4.2 Fuel injection . . . . .	23
5.4.3 Compressors . . . . .	24
5.4.4 Aftercooler . . . . .	25
5.4.5 Throttle . . . . .	25
5.4.6 Valves . . . . .	26
5.4.7 Cylinder . . . . .	27
5.4.8 Turbine . . . . .	28
5.4.9 Turboshaft . . . . .	29
<b>6 Throttle Correlation Study</b>	<b>31</b>
<b>7 Initial Validation Complete Model</b>	<b>34</b>
7.1 Introduction . . . . .	34
7.2 Steady state power . . . . .	35
7.3 Average turbocharger speed . . . . .	35
7.4 Mass air flow and mass CNG flow . . . . .	36
7.5 Pressure compressor in . . . . .	36
7.6 Pressure compressor out . . . . .	37
7.7 Pressure ratio compressors . . . . .	37
7.8 Temperature compressor in . . . . .	38
7.9 Temperature compressor out . . . . .	38

7.10	Pressure ratio aftercooler	39
7.11	Pressure pre-throttle	39
7.12	Pressure ratio throttle	40
7.13	Manifold Absolute Pressure (MAP)	40
7.14	Manifold Air Temperature MAT	41
7.15	Pressure ratio cylinders	41
7.16	Pressure turbines in	42
7.17	Pressure turbines out	42
7.18	Pressure ratio turbines	43
7.19	Temperature turbines in	43
7.20	Temperature turbines out	44
7.21	Compressor maps	45
7.22	Turbine maps	46
7.23	Turbocharger speed	47
7.24	Validation and connection of throttle theory.	48
<b>8</b>	<b>Last Iteration And Re-validation</b>	<b>50</b>
8.1	Re-validation	52
8.1.1	Updated steady state power	52
8.1.2	Updated average turbocharger speed	52
8.1.3	Updated Mass air flow and mass CNG flow	53
8.1.4	Updated Manifold Air Temperature MAT	53
8.1.5	Updated average pressure ratio turbines	54
8.1.6	Updated average temperature turbine in	54
8.1.7	Updated average temperature turbine out	55
8.2	Validation conclusion and model assessment	55
<b>9</b>	<b>Hybrid Electric Turbocharging Compounding</b>	<b>57</b>
9.1	Method	57
9.2	Modification	57
9.3	Cases	60
9.4	Results of optimization	60
9.5	Constant power production	63
9.5.1	Implications on dynamics	64
9.6	Impact on fuel consumption	65
9.7	Efficiency gain cause	65
9.8	Efficiency exchange	68
9.9	Turbine exit temperature	70
9.10	Summary table	72
<b>10</b>	<b>Conclusion</b>	<b>73</b>
10.1	Model Development, Placement and Validation	73
10.2	Key findings:	75
10.2.1	Efficiency Gains Through Energy Recuperation and its optimalization.	75
10.2.2	Engine output control by hybrid electric turbocharging.	75
10.2.3	NOx reduction in e-compounding	75
10.2.4	Thermal signature and more efficiency potential.	75
10.2.5	Hybrid electric turbocharging versatility	76
10.2.6	Study scope and model limitations.	76
10.3	Final takeaway	76
<b>11</b>	<b>Recomendations for further research</b>	<b>77</b>
	<b>References</b>	<b>79</b>
<b>A</b>	<b>Remaining Re-validation graphs</b>	<b>82</b>
A.1	Re-validation graphs	82
A.2	Pressure compressor in	82
A.3	Pressure compressor out	82
A.4	Pressure ratio compressors	83

---

A.5	Temperature compressor in	83
A.6	Temperature compressor out	83
A.7	Pressure ratio aftercooler	84
A.8	Pressure pre-throttle	84
A.9	Pressure ratio throttle	84
A.10	Manifold Absolute Pressure (MAP)	85
A.11	Pressure turbines in	85
A.12	Pressure turbines out	85

# Nomenclature

## Abbreviations

Abbreviation	Definition
AFR	Air-Fuel Ratio
ATDC	After Top Dead Centre
BBDC	Before Bottom Dead Centre
BDC	Bottom Dead Centre
BMEP	Break Mean Effective Pressure
BSFC	Break Specific Fuel Consumption
BTDC	Before Top Dead Centre
CI	Compression Ignited
CIS	Continuous Injection System
DUT	Delft University of Technology
EGR	Exhaust Gas Recirculation
EGT	Exhaust Gas Temperature
EVO	Exhaust Valve Opening
FAT	Factory Acceptance Test
FMEP	Friction Mean Effective Pressure
GHG	Green House Gas
HET	Hybrid Electric Turbocharging
IMEP	Indicated Mean Effective Pressure
IMO	International Marine Organisation
IVC	Intake Valve Closing
MEPC	Marine Environment Protection Committee
MMEP	Mechanical Mean Effective Pressure
MVFP	Mean Value First Principle
NA	Naturally Aspirated
NLDA	Netherlands Defence Academy
NOx	Nitrogen Oxides
OPEC	Organization of the Petroleum Exporting Countries
PM	Particulate Matter
PMEP	Pumping Mean Effective Pressure
RPM	Rotations Per Minute
SCR	Selective Catalytic Reduction
SI	Spark Ignited
SOx	Sulphur Oxides
TDC	Top Dead Centre
TPS	Throttle Position Sensor
VVT	Variable Valve Timing
WOT	Wide Open Throttle

# 1

## Introduction

Environmental legislation has been active for the past decades across various sectors to mitigate exhaust emissions from fossil fuel combustion. The International Maritime Organization (IMO) introduced MARPOL Annex VI to regulate these emissions [1]. The IMO's Marine Environment Protection Committee (MEPC) has adopted an initial strategy aimed at reducing CO<sub>2</sub> emissions from shipping by at least 50% by 2050, aligning the IMO with the Paris Agreement's objective to lower or eliminate greenhouse gas emissions as soon as possible.

Additionally, to accelerate the energy transition within the shipping industry, regulatory authorities have intensified their regulations. In March 2023, the European Council and the European Parliament reached a provisional agreement on the FuelEU Maritime initiative, which establishes stringent limits on the average annual greenhouse gas (GHG) intensity as a result of energy used onboard by ships, measured on a well-to-wake basis. Compared to the 2020 GHG intensity levels, these limits are designed to become progressively more stringent over time, beginning with a 2% reduction in 2025, increasing to 6% in 2030, and ultimately reaching an 80% reduction by 2050 [2].

The Dutch Ministry of Defence is continuously seeking for innovations to improve the effectiveness, reliability and efficiency of their systems. Additionally, the ministry is expected to adhere to the Paris Agreement and pursue the emissions goals. One approach to addressing emissions in the fleet of the Royal Dutch Navy involves employing costly secondary methods, such as scrubbers to reduce sulphur oxides (SO<sub>x</sub>) and Selective Catalytic Reduction (SCR) to reduce nitrogen oxides (NO<sub>x</sub>). Alternatively, the adoption of advanced engine technologies and alternative fuels, such as methanol, ammonia and natural gas, offers significant environmental benefits. For example, an average reduction in SO<sub>x</sub>, NO<sub>x</sub>, CO<sub>2</sub>, and particulate matter (PM) by approximately 98%, 86%, 11%, and 96%, respectively in the case of LNG [3].

The current 10 support vessels of the Royal Dutch Navy are set to be replaced by 8 new vessels. These current vessels are engaged in various supportive tasks and are approaching the end of their operational life in the coming years. Last year, Secretary of State Christophe van der Maat informed the Parliament about the conclusion of the research phase (referred to as the B-phase) [4]. The decision has been made to introduce 4 ocean-going vessels and 4 diving vessels, all equipped with climate-neutral propulsion systems [5], partly by operating on bio-methanol fuel. Through the implementation of climate-neutral propulsion systems in these vessels, the Ministry of Defence aims to reduce dependency on fossil fuels, which can possibly be delivered by untrustworthy OPEC, and to contribute to the societal imperative of combating climate change [4][6].

A large role of this climate-neutral objective is assigned to the energy systems and internal combustion engines of these vessels. These engines self-evidently need to meet a very large set of innovative and demanding requirements. Traditionally, the engines needed to be effective and reliable while maintaining their efficiency to ensure the necessary endurance required in the numerous naval situations. Recently, the environmental legislation of modern times needs to be incorporated and given some priority in developing the new engine strategy. The implementation of alternative fuels is seen as an attractive solution by the Ministry of Defence to comply with the latest environmental legislation developments.

A significant disadvantageous aspect of the implementation of alternative fuels is the reduced energy density of the total storage system [7]. The implementation of alternative fuels onboard new vessels poses a significant design challenge, as concessions need to be made regarding the size, weight, cost, employability and endurance. This evermore underscores the importance of the development and optimization of total system efficiency on board these vessels. Reducing the energy consumption and fuel quantity needed today is vital, as this will be multiplied by the factor of fuel-system-storage-density-ratio in the future, as these new alternative fuel systems are much less energy dense.

The Ministry of Defence has a specific department for research dedicated to its own engine technology implementation, referred to as NLDA (NetherLands Defence Academy). At the NLDA, interest has been piqued by the apparent benefits that hybrid electric turbocharging can offer in their ongoing research into the behaviour of operating compression ignited and spark ignited internal combustion engines [8][9], specifically a Wärtsilä 6L20DF compression ignited (CI) dual fuel engine and a CAT G3508a spark ignited (SI) gas engine. A hybrid electric turbocharger is composed by integrating an electric machine into the turbochargers rotating structure, creating a hybrid electric turbocharger. This innovation serves two purposes: firstly, it can extract power from the turbocharger to enhance overall system efficiency, a phenomena called turbo-compounding. And secondly, the possibility to aid the turbochargers' ability in controlling and optimizing engine transient response. Apparent benefits of hybrid electric turbocharging include but are not limited to; improved dynamic response, control over unstable turbocharger phenomena and improved mean system efficiency among others [10] [11][12][13]. The objective for the research in this study is to assess the efficiency part of those benefits for the CAT G3508a gas engine. The apparent benefits of hybrid electric turbocharging have great potential for realization and application of alternative fuels in SI engines, for both performance and efficiency aspects. This is the basis for the initiative to research the effects of hybrid electric turbocharging of a SI engine that is at the core of the research at the NLDA.



**Figure 1.1:** The CAT G3508A engine installed at the NLDA in Den Helder

# 2

## Basics Of Internal Combustion Engine Theory

### 2.1. Four stroke operation

Four stroke internal combustion engines, function through a four-phase cycle: intake, compression, power, and exhaust. Starting the intake stroke at top dead centre (TDC), the piston moves downward and draws air (and possibly also fuel in the case of certain types of fuel systems) into the combustion chamber through the opened intake valve. Next the compression stroke starts at bottom dead centre (BDC), during which the intake and the exhaust valves are closed, the piston moves upwards and compresses the air-fuel mixture to significantly increased pressures and temperatures. After the compression stroke, the highly compressed air-fuel mixtures ignites around TDC due to spark or compression ignition and initiates the power or combustion stroke. During the power stroke the piston is driven downward by the rapid expansion of the combustion products and produces mechanical work. Finally at BDC the exhaust valve opens and the piston is driven upward, forcing the burned mixture out of the cylinder, after which the cycle is repeated.[14]

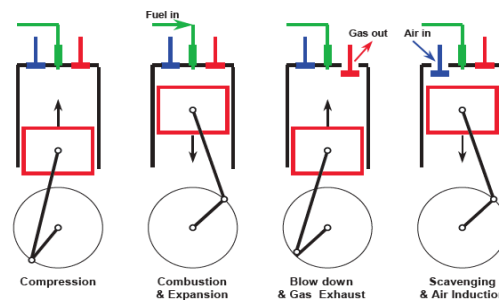


Figure 2.1: Operation principle of a 4-stroke diesel engine [14]

### 2.2. Ignition methods

Today, various types of ignition systems exist. These can mainly be categorized into two types; spark ignition and compression ignition. Spark ignition (SI) engines, like Otto-cycle engines, use an electrically generated spark between two electrodes inside the combustion chamber to ignite the present compressed air-fuel mixture. The firing of the spark plug doesn't ignite the entire air-fuel mixture in an instant, rather it sets of a flame front that propagates from the electric spark radially through the combustion chamber. Compression ignition (CI) engines, like Diesel-cycle engines, don't depend on a spark plug for ignition but use a higher compression ratio resulting in higher temperature and pressure that auto ignites the present air-fuel mixture. This ignition occurs relatively simultaneously throughout the homogeneous mixture in the combustion chamber. [14]

## 2.3. Valve actuation

The correct and timely actuation of the intake and exhaust valves is crucial for the smooth and efficient operation of a four stroke internal combustion engine. The intake and exhaust valves don't necessarily open and close exactly at TDC or BDC. Rather they open before or after those moments, valves are typically opened before top dead centre (BTDC) or before bottom dead centre (BBDC) because of the inertia of the air-fuel media. In charged engines in between the exhaust and intake stroke both the intake and exhaust valves can be designed to remain open at the same time to create a valve overlap (if  $P_{ir} > P_{or}$ ). This valve overlap allows the high pressure from the intake to scavenge the cylinder from the remaining burned mixture, completely flushing the remaining in-cylinder volume with fresh air, while also providing additional cooling for some engine components, mainly the exhaust valves [15]. Valve overlap is however undesired in the case of non-direct injection types, see section 2.4. The scavenging air-fuel mixture then directly enters the exhaust without being combusted, expulsion of unburned fuel is undesired for efficiency, health- and environmental reasons.

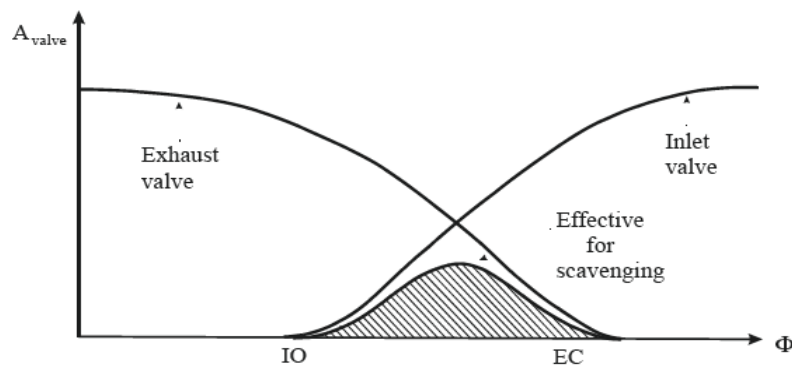


**Figure 2.2:** Inlet and outlet valve area as function of crank angle and resulting effective valve area for 4-stroke engine with small valve overlap [15]

## 2.4. Injection types

Fuel admission into the combustion chamber is possible in various methods. In 2016 Georgescu et al. recognized nine differing types of fuel injection and ignition methods of internal combustion engines operating on a gaseous fuel [16]. All types share the same objective; mixing the fuel with air to convert the internal chemical energy into mechanical energy. Fuel admission can be done using several injection systems, there are basically three types of injection. 1: A unipoint system, where at a single point in the intake air path fuel is injected into the air flow for all the cylinders combined. 2: Port injection, where the fuel is injected into the intake air very close to the intake valve and each cylinder has its own injector, this system is widely used in a lot of SI engines. 3: Direct injection where the fuel is injected directly into the cylinders, where evidently also each cylinder has its own injector, this is becoming more common in SI engines and is common practice for Diesel engines. A problem that arises when combining valve overlap with unipoint or port injection is that a premixed charge of air and fuel is used to scavenge the cylinder and isn't used for combustion. This premixed charge of air and fuel is then expelled out of the exhaust without being ignited, thus not used for power generation. The expulsion of unburned fuel is undesired for efficiency, health- and environmental reasons.[14][15]

## 2.5. Air-fuel ratio

Spark ignited internal combustion engines convert the chemical energy in the fuel to mechanical work through the exothermic reaction of deflagration with air. Deflagration is the combustion of a pre-mixture of fuel and oxidizer where the flame propagates through the explosive mixture at sub-sonic speeds [17]. To initiate and sustain a correct deflagration combustion a correct air-fuel ratio (AFR) is required as a mixture inside the combustion chamber. SI engines can operate on a relative small window of adequate AFR's because of the phenomena called 'knocking' and 'misfire' [18]. The AFR is referring to the average air-fuel mixture in the cylinder. A perfect homogeneous AFR through the entire cylinder is desired but due to design and other aspects this is rarely the case. A cylinder filled with a combustible average AFR will contain pockets of rich mixture, and pockets of lean mixture. During the design

process of internal combustion engines a lot of care is taken to disperse the fuel as homogeneous as possible by means of measures like; turbulence inducing, elongating evaporation times or decreasing the droplets of the injected fuel.

$$afr = \frac{m_{ca}}{m_f}$$

with

$afr$	air fuel ratio [-]
$m_{ca}$	mass of combustion air in cylinder, mainly fresh air also partly residual gasses [kg]
$m_f$	mass of fuel in cylinder [kg]

A low AFR, I.E. a rich mixture, is known to cause knocking. 'Knocking' is the self-ignition of the unburned fuel/air mixture somewhere in the combustion chamber, after the spark has fired, that also isn't the initiated flame front from the spark plug. Knocking is known to cause overheating and failure of components due to the pressure oscillations and increased heat flux as a result of the rapid combustion [19]. A 'misfire' can be caused by a AFR mixture that is high, I.E. a lean mixture. A lean mixture has too little fuel mixed in the charge that a deflagrating flame front cannot be initiated or sustained. The (partly) unburned mixture is then expelled from the cylinder without being fired, hence the name 'misfire'. Misfiring engines have deteriorated performance and often show increased vibrations, leading to premature wear and failure. SI engines control this AFR by controlling the mass air flow into the engine by means of a throttle. A throttle smothers the air flow by a adjustable restriction. This is often done by implementation of a butterfly valve. The resulting air flow is calculated by the engines control unit which then injects the correct fuel quantity to obtain a specified AFR. CI engines operate in a differing technique. CI engines can run on a relatively wide range of AFR's, such that they don't require measures like a throttle to modulate the incoming mass air flow as precisely to suit a specified AFR. After the fresh air mass has been compressed in the compression stroke the required fuel quantity is directly injected into the cylinder BTDC, which directly initiates ignition. The AFR of CI engines is limited by the smoke limit or thermal management at approximately a lambda of 1.5 - 1.8, depending on the fuel type [20]. Above those values a wide range of air-fuel ratios are possible up to a lambda of approximately 4.45 [21].

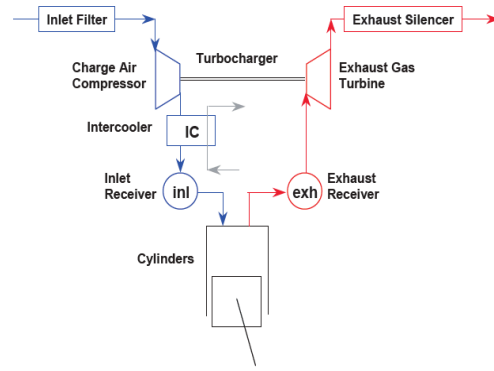
## 2.6. Modern charge air systems

### 2.6.1. Turbocharging

The main objective for an internal combustion engine is to produce mechanical power in the form of a rotating shaft at the correct time, speed and torque. Mechanical power that is converted from chemical energy by means of combustion. In the vast majority of engines, during this conversion most of the energy available is not effectively converted to mechanical power but is lost to heat. A large part of the energy flow is lost by not capturing the remaining exergy in the exhaust flow [22]. This is where turbocharging is a known and effective solution. A turbocharger is composed of a turbine in the exhaust, that is mounted close to the engines exhaust ports. In this turbine the exhaust flow is expanded and mechanical energy is recuperated. This mechanical energy is then used in a compressor in the intake to increase the air density, and thus the mass air flow. Due to the increased mass air flow more fuel can be injected in a cycle. This increases the specific power output of the engine, as the higher mass air flow allows for a greater quantity of fuel to be combusted per cycle, resulting in increased energy release. Furthermore, the efficiency of the engine improves because the relative increase in specific power output is greater than the proportional increase in heat and mechanical losses. This is due to the fact that many losses, such as friction and heat transfer to the surroundings, do not scale linearly with power output, meaning that a well-optimized turbocharged engine can achieve a higher overall thermal efficiency compared to a naturally aspirated counterpart. The compression of the charge air however leads as well to a rise of temperature, which lowers the air density. Therefore, turbocharging systems are practically always combined with a 'charge-air-cooler', or 'aftercooler'. The compressed charge air passes through the aftercooler which reduces the charge air temperature, raising the density further. As the charge air temperature is lower, also the peak temperature during combustion is slightly cooler, allowing for more ignition advance and higher break mean effective pressure (BMEP).



(a) Sankey diagram illustrating how the ingoing exergy is transferred due to work, via heat transfer, via the exhaust gases, and destroyed due to irreversibilities in the high-pressure phase of the engine operating cycle[22]



(b) Principle of single stage turbocharging [15]

### 2.6.2. Turbocharger maps

A turbochargers behaviour is captured and characterized in graphs that are called the compressor-and turbine map. The former being especially interesting as it has the most data and captures most critical limitations. A compressor map is shown in Figure 2.4.

On the vertical axis is the pressure ratio as a function of corrected mass flow on the horizontal axis. The black lines running relatively horizontal are constant speed lines for the rotating assembly of the turbocharger. The contour lines depict a region of constant efficiency. The line on the far left depicts the so called 'surge line'. This line distinguishes stable and normal operation on its right from unstable and unsafe operation on its left. Compressor surge is the unstable phenomena where the pressure ratio over the compressor is too high to sustain the mass air flow, causing turbulent fluctuations or even reversal of the air flow through the compressor stage. During normal operation the operational point of the compressor may not exceed the surge line, as compressor surge under load is known to cause major mechanical damage and deterioration of engine performance. On the far right is the barrier that is known as the choke line. Choke is the operational barrier at which point the compressor cannot increase its airflow regardless of the pressure ratio as it reaches supersonic air speeds [23].

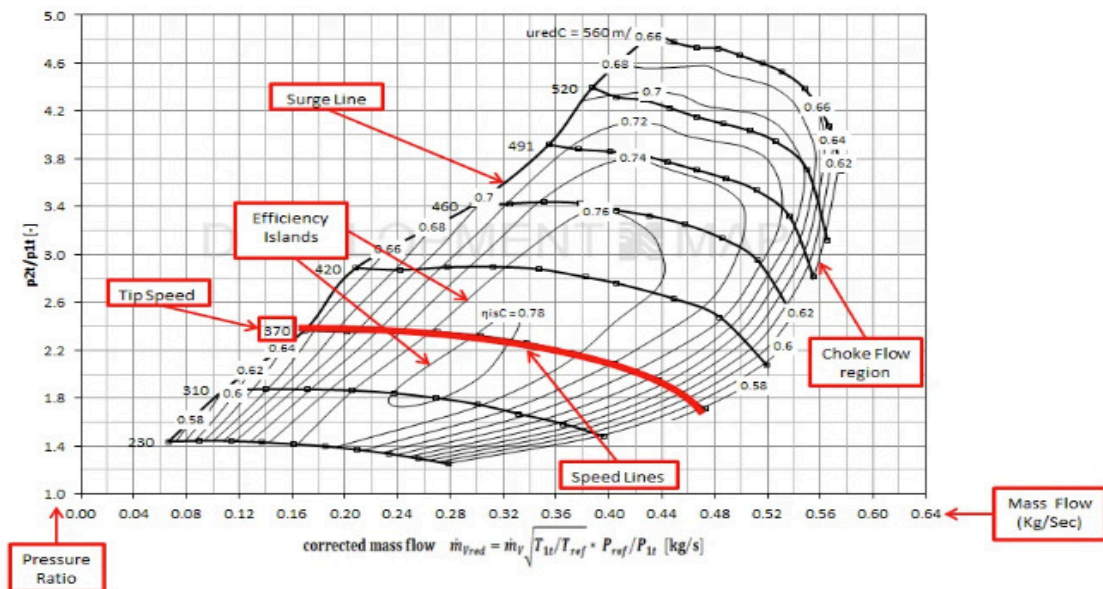
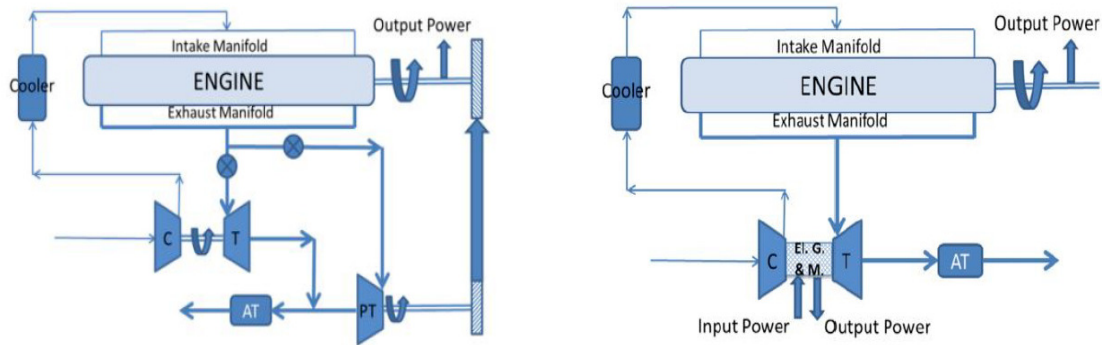


Figure 2.4: Example of a compressor map[23].

### 2.6.3. Turbo-compounding

The goal of the turbochargers turbine is to recuperate as much of the available exergy in the exhaust flow as possible and convert it to mechanical energy. The turbochargers construction directs the recuperated mechanical energy to the compressor. However, there are alternatives for use of the available mechanical energy. When the mechanical energy is captured and not used for the compressor it is named 'Turbo-compounding'. Turbo-compounding can be done mechanically or electrically, using the turbochargers turbine or with a separate additional power turbine [24]. The goal of turbo compounding is to enhance the total system efficiency, with the additional benefit to have the possibility of better control over rotational speed and pressure, and thus possibly eliminate the need for a waste gate [25].



(a) Example of mechanical turbo-compounding using a separate power turbine [24]. (b) Example of electrical turbo-compounding using the integrated turbine [24].

A disadvantageous effect of turbo-compounding is the effect it has on engine operation. In a traditional turbocharger all recuperated energy of the turbine is used by the compressor for an improved gas exchange, assuming no losses. However, when some of the recuperated mechanical energy is used for other purposes, less energy is available for the compressor. On CI engines, that operate with a large air excess ratio, this implies a deteriorated gas exchange, resulting in a reduced scavenging air flow and lower air excess ratio [10]. On spark ignited engines that operate with a throttle and need a specific air mass in the cylinders this has presumably divergent implications that need to be studied. For example, the valve overlap in non-direct-injected natural gas engines is non-existent to prevent the expulsion of unburned fuel, indicating little to no scavenging to begin with. Additionally, the exhaust gas mass flow on spark ignited engines on low load will also be reduced when compared to the compression ignited counterparts, as the throttle will severely smother the flow to control the air-fuel ratio.

# 3

## Background of Hybrid Electric Turbocharging

The system that is comprised of a hybrid electric turbocharger isn't completely new. It is used in Formula-1 since the 2014 racing season [26] and Mercedes-AMG has per 2023 some streetcars available that use a similar commercial version of the technology. In addition, as per September 2024 Porsche starts delivery of their facelifted 992.2 911 Carrera GTS T-hybrid. A new model that similarly uses a new hybrid electric single-turbocharged engine, called 9A3B6, that replaces the previous parallel-sequential twin-turbocharged 9A2B6 engine. The new hybrid electrically turbocharged system allows the engine to run a stoichiometric air-fuel ratio throughout the entire load and speed range, without the need for a waste gate. Reducing the emissions on high load, where the previous system would run a rich mixture up to [8%], which resulted in reduced three-way catalysts effectiveness. Additionally, the new system reduces the transient boost response from closed throttle by over 60[%,] and is capable to recuperate up to 11 [kW] of electrical energy from the exhaust gas flow [25].

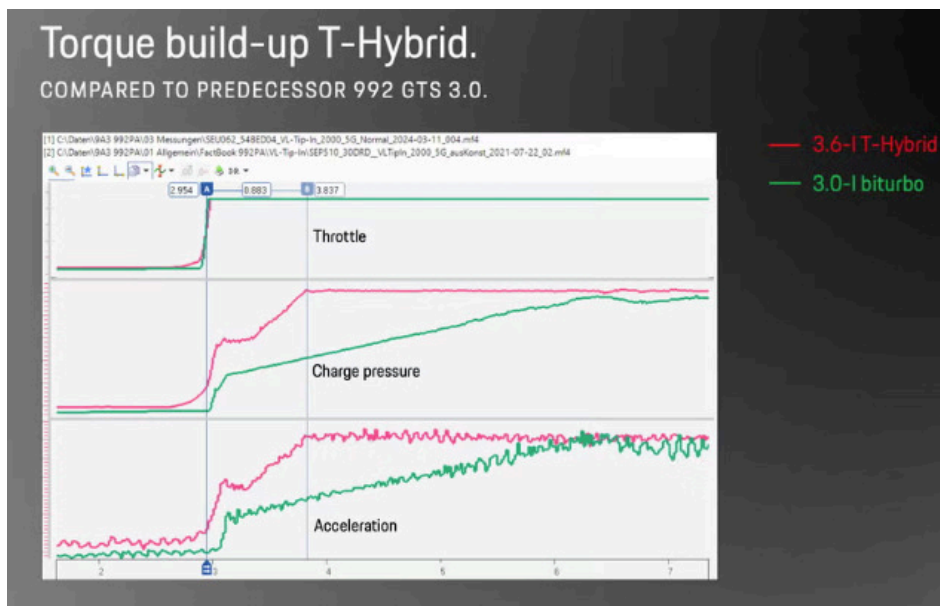


**Figure 3.1:** The difference in transient response of the new hybrid electric turbocharged system between the 992.1 and 992.2 911 Carrera GTS [25]

The Delft University of Technology (DUT) has facilitated master students with relevant research topics in the past. Westhoeve (2018) [10] has evaluated the effectiveness and implementation of hybrid electric turbocharging on a CI dual fuel engine for dredging purposes in 2018. He used a model comprised of a combination of two mean value models, the then latest Diesel B model and a dual fuel engine model by Georgescu et al. (2016) [16] which is based on the Seiliger cycle. This model was matched to a Wärtsilä 6L43DF and then reasonably verified with available, but limited, engine data. This model notably considered limitations like the surge limit of the turbocharger. The research reports; when a waste-gated turbo is replaced with a hybrid electric turbocharger a potential nominal system efficiency increase of 2.3[%] in turbo-compounding mode is possible, albeit with a decreased engine efficiency as a result of a deteriorated gas exchange. Other notable findings are the almost constant engine torque output that can be obtained when a hybrid electric turbocharger assists the turbine in combination with a bypass valve. Westhoeve (2018)[10] concluded that further research should be done with regard to a hybrid electric turbocharger for the natural gas combustion of the dual fuel engine.

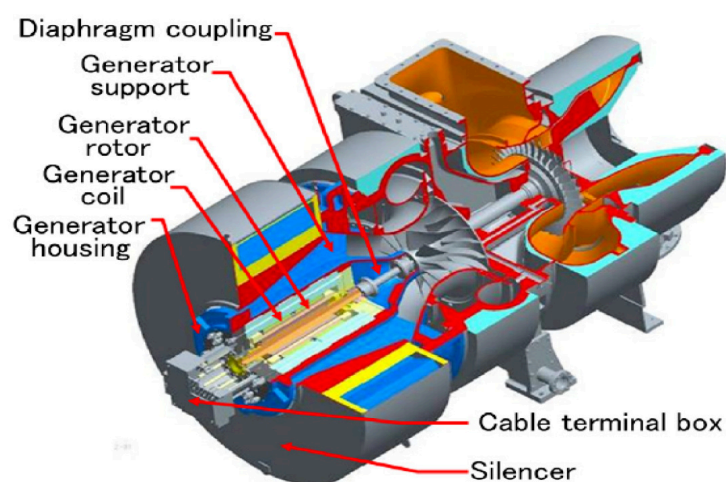


**Figure 3.2:** Example of a large hybrid electric turbocharger [27]

Another recent study facilitated by Delft University of Technology and Dutch Ministry of Defence has been done by Rusman (2018)[11] into various charge air configurations for propulsion diesel engines aboard fast naval frigates. Research based on a Mean Value First Principle model by Geerstma et al. (2017) [28] and Loonstijn (2017) [29], using motion based relations by Colonna et al. (2007) [30], was done to evaluate a parallel sequential and hybrid electric turbocharger setup on a Wärtsilä W26-STC diesel engine. This model was reasonably satisfactory validated, partly with FAT and project guide data, and partly with experimental data that was generated onboard Zr. Ms. De Ruyter, a 'LCF'-frigate powered by a CODOG configuration partly consisting of 2 Wärtsilä W26-STC. Rusman (2018) [11] concluded similar remarks from the study into hybrid electric turbocharging. In combination with shifting the operating point of the diesel engine, efficiency in part load can increase with approximately 15[%] in comparison with a single charged diesel engine as reported, which seems questionable. Further findings include: considerable improvements in the efficiency, acceleration performance, and emissions of diesel engine. However, Rusman (2018) [11] also concludes that the effect of hybrid electric turbocharging on NO<sub>x</sub> emissions are positive. Stating that: 'Hybrid turbocharging increases the pressure ratio over the cylinder resulting in a better scavenge process. Therefore, the cylinder will be cooler which is beneficial for NO<sub>x</sub> reduction. Further, it was shown that the thermal loading during acceleration could be reduced significantly. The exhaust valve temperatures were decreased with almost 430 [K].' This seems counterintuitive at this introductory stage. In compounding mode, the energy is recuperated from the turboshaft, leaving less power available for the compressor. A lower powered compressor intuitively generates a lower pressure ratio, conflicting with the stated findings. Presumably, the stated decrease in thermal loading was not a result of the efficient compounding mode, but rather in a mode where the electric machine assists the turbine in powering the compressor. Additionally, Rusman (2018)[11] indicates that a lot of uncertainties were encountered during the measurement campaign, making it hard to draw reliable conclusions. Recommending a measurement campaign in a

controlled environment, like a test bench, for validation. Finally, Rusman (2018) [11] concludes that the hybrid electric turbocharger can play a major role in the application of alternative fuels. Therefore, it has been recommended to investigate the application of hybrid electric turbochargers on gas SI engines.

Both studies cited above have researched similar research topics using similar models and methods of validation. As the methods are comparable and the research is thorough the findings are also notably analogous. The authors in both studies extensively report the challenges in adapting the existing Diesel B and MVFP models to their respective relevant engines and altering the model to include a hybrid electric turbocharger. This is a result of the incomplete available engine data, being limited to the existing product guide of the manufacturer and the available FAT data. Moreover, the authors of both studies have also reported uncertainties regarding the validation of the models. Both having limited real world data from measurements of their respective engines, as the engines in the real world are bound to the operational profile and conditions.

Another especially noteworthy paper has been done by Figari et al. (2022) [31] on the optimal selection of the hybrid electric turbocharger for large marine four-stroke dual-fuel engines. Figari et al. (2022) [31] evaluated a hybrid electric turbocharger by taking an existing model of a large 9-cylinder 8775 [kW] engine and extend it to include the hybrid electric turbocharger. This model was previously built in the commercial simulation software GT-POWER. This simulation software package is widely recognized and utilized by the automotive sector to simulate engine, drivetrain and subsystems. The software however is also capable of simulating gas turbines, FEM and CFD analysis among other systems. The model comprises of a zero-dimensional in-cylinder Wiebe process for the estimation of the working media temperature, mass, pressure, and mixture composition. In combination with a one-dimensional modelling of the air path. The air path model that is used for modelling the gas exchange is of much higher resolution compared to the emptying and filling approach of the afore mentioned Diesel B and MVFP models. The study investigated a wide range of hybrid turbocharger electric motor power and its impact on marine dual fuel four-stroke engines. Results show that the optimal nominal motor size is 300 kW for their respective engine, resulting in an averaged energy surplus of 2[%] to 3[%]. Also reporting that the NO<sub>x</sub> emissions increased 15[%] on average in the Diesel mode, contrary to the findings by Rusman (2018) [11].

Along with the cited relevant research at Delft University of Technology multiple relevant studies are available in published literature regarding the scope of this study. The potential of hybrid electric turbocharging has been studied by Mitsubishi heavy industries [32][13][12][33], early on recognizing the operational and efficiency benefits it could bring. Shiraishi et al. (2015) [13] concluded that the hybrid turbocharger was able to reduce fuel oil consumption and black smoke emission at start-up, studied from in-house developed code and test banks.

Both the automotive and motorsport sector have, as previously mentioned, already set precedent in reality in exploiting and applying the hybrid electric turbocharger. Hence why in literature a relative majority is available that regards the hybrid-electric-turbocharging of specifically automotive engines. Research in the automotive sector into hybrid electric turbocharging almost exclusively involve spark ignited Otto cycle engines in the 1.6 [L] to 2 [L] displacement range. In the paper by Dong et al. (2020) [34], a comprehensive simulation and experiment on the optimization of a gasoline vehicle applying a hybrid electric turbocharger was done. A simulation platform was built that linked GT-SUITE, SIMULINK and GT-POWER, extensively covering the energy use and management of an entire vehicle. The one-dimensional numerical engine model from GT-POWER was integrated into an algorithm that optimized the energy use of the electric machine integrated in the turbocharger assembly. The developed model's prediction of cumulative fuel consumption was found to deviate by only 0.7[%] during the real experiment. Dong et al. (2020) [34] reported tank-to-Wheel energy savings of different driving cycle norms were reported to be between 1[%] to 5[%]. The deviations of the model's prediction used in this paper compared to reality have shown significant improvements over the MVFP models used in earlier research, this can be partially accredited to the fact that the authors used a model of higher resolution with respect to the gas exchange, but also to the fact that the simulation and experiment could be better matched and reproduced in controlled scenario and conditions. Additionally, both studies by Figari et al. (2022)[31] and Dong et al. (2020)[34] have been done by validating a traditionally turbocharged engine, after which its converted to a hybrid electric system. The authors of these studies have reported less challenges in validating these models when compared to Westhoeve (2018)[10] and Rusman (2018)[11].

# 4

## Research Foundation

### 4.1. Knowledge gap and problem definition

The existing literature has covered a considerable range of topics that characterize the behaviour of operating internal combustion engines with hybrid electric turbochargers. Precedent has been set, theoretically and in reality, for the beneficial potential that hybrid electric turbocharging can bring to the energy savings onboard the vessels of the Royal Dutch Navy.

Another important potential that hybrid electric turbocharging can offer is aiding in the realisation of the adaption of future alternative fuels in the maritime sector. Traditionally, the vast majority of marine engines are operated on HFO and MGO, which are CI fuels. The engines that operate on these fuels are primarily regulated by controlling the injected fuel mass, implying that the air-fuel ratio can fluctuate within a set range. This range is relatively large for compression ignition engines. For compression ignition engines is the lowest air-fuel ratio limited by either the smoke limit or thermal management at approximately a lambda of 1.5 - 1.8 [-], depending on the fuel type [20]. Above those values a wide range of air-fuel ratios are possible up to a lambda of approximately 4.45 [-] [21].

Marine engines are typically highly charged and often use a constant pressure exhaust system, implying that they are characterized by a relatively long transient response with respect to the mass air flow and a relatively large boost threshold. However, due to the large range of air-fuel ratios they are known to have adequate load step capabilities. In some cases, a load step causes the engine to run richer than the smoke limit, causing black soot to be expelled from the exhaust pipe. This can happen on start-up or on large load steps for example. In these cases the engines management system injects the required quantity of fuel without having necessarily the adequate quantity of air to remain below the smoke limit. The air is supplied by the turbocharger's compressor, which has a delayed response.

This practice is not possible when running purely on future alternative fuels. The combustion of pure methanol or ammonia for example cannot be done using CI engines. It is possible to combust these fuels in a dual fuel engine. However, this engine type still requires diesel as a pilot fuel for ignition. When moving away from diesel, an alternative ignition method is required, namely spark ignition. SI engines running on natural gas, methanol or ammonia need a specific air-fuel ratio for combustion [18]. As can be seen in Figure 4.1, a small range of air-fuel ratio is available at a high load or break mean effective pressure.

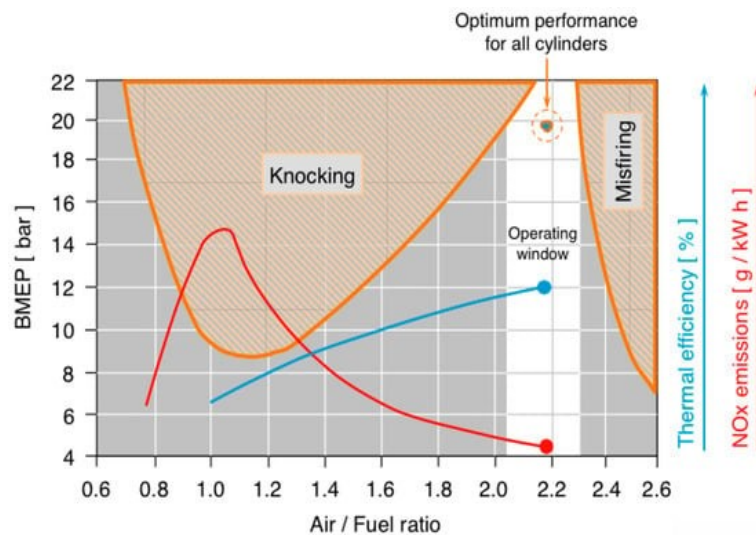


Figure 4.1: Air-fuel ratio range against BMEP for a Wärtsilä 9L50DF on LNG fuel [18]

Hybrid electric turbochargers can aid in this twofold. Firstly, hybrid electric turbocharging has the potential for increasing the efficiency of the engine. When an engine can only operate by opening a wastegate, valuable high energy is redirected through that waste gate. High energy exhaust gas that would otherwise be expanded in the turbine to be recuperated to mechanical energy. A hybrid electric turbocharging system would make this possible. The excess energy that would be redirected through the waste gate can now be fully directed through the turbine. The extra energy, that would be too much for a conventional turbocharger, is now used to generate electricity, reducing the specific fuel consumption. This is the case in diesel and dual fuel engines as reported by [10] and [11]. What implications hybrid electric turbochargers has on a large SI engine such as the CAT G3508a remains to be studied. The diesel-cycle engines from [10] and [11] operate on a large air excess ratio and do not require a throttle. A SI engine requires a throttle to reduce the mass flow through the engine and consequently has higher pumping losses and/or throttle losses for moving the working media past the restrictive throttle. Efficiency gains are a benefit for any engine, but especially for engines that run on fuels with a low energy density like methanol or ammonia. An increase in efficiency results in a reduced necessitated fuel quantity for a given autonomy, decreasing both CAPEX and OPEX.

Secondly, hybrid electric turbocharging has the potential to increase the performance of an engine by assisting the turbine in powering the compressor. The assist can aid in the control of the air mass entering the cylinders. This is vital as a mixture that is too rich can cause knocking while a mixture that is too lean can be cause for misfire. This implies that spark ignited engines on fuels like natural gas, methanol or ammonia cannot only increase the fuel mass flow on a load step with a latency in the air mass flow. These engines need the correct amount of air for the injected fuel quantity. The massflow of airflow is regulated by means of controlling a throttle valve and/or a by-pass valves or a blow off valves if fitted. Critically, the long transient response nature of the turbocharge system of these large marine SI engines remains. This all means that large, highly charged SI engines can only take reduced load steps, limited by the maximum amount of mass air flow available at that static operational starting point. This is where hybrid electric turbocharging can be a fitting solution. It has been shown in literature that hybrid electric turbochargers decrease the transient response of the turbocharger [10][11][31][13]. A hybrid electric turbocharger can therefore (pro)actively increase mass flow of air to the engine while or even before the loads step is taken, whereas a traditional turbocharger would build air mass flow reactively. This means that bigger load steps, faster recovery of load steps and more control over those load steps is possible [10]. These are highly supportive aspects in making future alternative fuels viable and high performing.

The NLDA is currently researching the behaviour of operating their internal combustion engines on bio-methanol. Both the engines, the Wärtsilä 6L20DF CI dual fuel engine and a CAT G3508a SI gas engine, are being modified to operate on methanol. The CAT G3508a spark ignited gas engine is of specific interest in this research for reasons listed above. This engine is a 500 [kW] 34.5 [L] 4-stroke SI twin turbocharged V8 engine. This engine operates on a specified air-fuel ratio by control of a throttle valve and electronic fuel injection, similar to a lot of automotive engines and unlike common marine diesel engines. Research into the behaviour of the combination of hybrid-electrical-turbocharged SI gas engines of similar scale of displacement with regards to both performance and efficiency potential has not been found during the literature review, this defines the key knowledge gap.

As previously mentioned, the development and optimization of total system efficiency is of high importance. The reduction of energy consumption directly translates into a reduction of OPEX, as the fuel quantity needed for a set scenario will be reduced. Additionally, the reduction of energy consumption and fuel quantity needed today gets multiplied by the factor of fuel-system-storage-density-ratio in the future, as those fuel systems will be less dense. As the research into the implementation of methanol advances, so does the need for high efficiency internal combustion engines. This sets the foundation for this research into the implementation of hybrid electric turbocharging the CAT G3508a SI gas engine. The results in a later stage can be used to more comprehensively estimate the total energy demand of operating a methanol powered hybrid electrically turbocharged SI gas engine onboard a specific vessel of the fleet of the Royal Dutch Navy.

## 4.2. Research objective and questions

The hybrid electric turbocharging system carries a lot of potential as mentioned, consequently a lot of aspects of hybrid electric turbocharging of large SI engines can be researched. Aspects like; static and dynamic behaviour, wherein the electric motor of the hybrid electric turbocharger assists in transient response or spooling and reducing the boost threshold for a more direct response. Electrically assisting the turbocharger changes the power balance between the turbocharger's turbine and compressor, potentially changing its operating point. Assisting the compressor with electric assist combined with a bypass valve potentially solves unstable phenomena in low speed high load scenarios. However, the operational point of the compressor may not breach the surge line, as compressor surge under load is known to cause major mechanical damage. Conversely, the case where a default in the electric part of the system has resulted in a situation where it is not operational. A defective electric machine in the turbocharger may result in significant compromises on the engines delivery and response, especially from a dynamic high demand naval point of view.

Additionally, static high-load scenarios can be studied wherein the electric motor of the hybrid electric turbocharger extracts energy from the high-energy exhaust flow by directing the full exhaust flow through the turbocharger's turbine and not partially through a wastegate, I.E. turbo-compounding. This also alters the power balance between the turbine and the compressor. When the electric machine withdraws energy from the turbine, it automatically implies that there will be less energy available for the compressor. On CI engines, that operate with a large air excess ratio, this implies a deteriorated gas exchange, resulting in a reduced scavenging air flow and lower air excess ratio, as Westhoeve (2018) [10] pointed out. On spark ignited engines like the CAT G3508a that operate with a throttle body and need a controlled air mass in the cylinders this has presumably divergent implications that need to be studied.

This topic carries more aspects than can be covered in this single study. The objective for this study is mainly focussed on the potential efficiency gains as a result of turbo-compounding by a hybrid electric turbocharger, which is described in the first paragraph of this section 4.2. This objective can be broken down into the following questions;

**Main question:**

Investigate the potential of a hybrid electric turbocharged CAT G3508a spark ignited engine to enhance the system efficiency in turbo-compounding mechanism.

**Sub questions:**

How is it possible to model a (hybrid electric) turbocharged CAT G3508a spark ignited engine in the GT Power simulation tool and validate this model with measurement data?

Evaluate the impact of recuperating energy (compounding) from exhaust gases with the turbocharger's turbine on the overall efficiency of the power plant in a static running condition.

Investigate what the engines and turbochargers behavioral changes are to this compounding mechanism.

### 4.3. Scope of research

This research will study, model, predict and evaluate a model of an experimental CAT G3508a spark ignited engine that will be converted to hybrid electric turbocharging. This simulation model will be constructed to virtual prototype the engine and relevant turbocharger systems. Virtual prototyping is a widely acknowledged method for analysis and development of systems without the necessity of building them in reality. Which is valuable in this case, as building a hybrid electrically turbocharged internal combustion engine requires significant investments and development dedication. For example; back when Formula 1 introduced the system in 2014, the Mercedes-AMG team had invested significantly more into the development of the MGU-H (Formula 1 terminology for a hybrid electric turbocharger) compared to the competition. The Mercedes-AMG PU (Power Unit) was superior in almost every measure of performance and reliability over the competing PU's from competing suppliers; Scuderia Ferrari, Honda Racing Powertrains and Renault Racing, who initially underestimated the complexity of the MGU-H. This to remark the value of research and development, partly by virtual prototyping.

The model before the conversion to hybrid electric turbocharging will be validated with the existing experimental testbench setup in a controlled environment. These zero-/one-dimensional models will be constructed in a simulation software package called GT-POWER suite, now an available tool at Delft University of Technology. As stated in the literature review, the GT-POWER suite is expected to be capable of simulating an engine and drivetrain system more accurately than the previously used Diesel B and MVFP models, which is supported in the cited research. GT-POWER models accurately predict engine performance by effectively representing component interactions. It uses both zero- and one-dimensional modeling to enhance precision in key areas, unlike Diesel B and MVFP models, which rely on a filling and emptying approach. GT POWER captures the full air path geometry in one dimension and uses a zero-dimensional model for in-cylinder processes, improving gas exchange resolution. While three-dimensional CFD models offer higher accuracy, they are impractical due to their heavy computational demands.

# 5

## Method

### 5.1. Method introduction

This study focuses on modelling and analysing the behaviour of the Caterpillar G3508a engine using GT-ISE, a one-dimensional engine simulation tool within the GT-POWER suite <sup>1</sup>. The primary objective is to assess the impact of turbocharger electrification on engine behaviour and efficiency, particularly its influence on the fresh air supply and exhaust gas disposal system. A structured modelling approach, based on the methods outlined by Sargent (2010) [35], has been employed to ensure systematic development, verification, calibration, and validation of the simulation. This approach is visually represented in Figure 5.1.

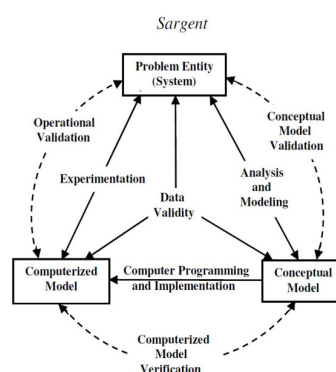


**Figure 5.1:** Simplified version of the modeling process as proposed by Sargent [35]

By following this methodology, a GT-ISE model has been systematically developed to capture the relevant physical and thermodynamic processes of the engine with high accuracy. The focus of the model development has been the airpath geometry, airpath restrictions and turbocharger behaviour. The reference for this is based on measurement data from the CAT G3508a that contains intake and exhaust flow specifics, including pressure and thermodynamic data. The measurements also include readouts of air and fuel mass flows, crank power readouts, turbocharger speed data, among others. Information sources for the models construction include manufacturer specifications, physical measurements, computational techniques, and experimental data. Through this engine geometry, airpath design, fuel injection characteristics, turbocharger behaviour and combustion modelling have been implemented based on the best available data sources. Calibration efforts prioritized matching steady-state power output, mass flow rates, pressure ratios, and thermodynamic conditions within acceptable error tolerance of max. +/- 10 [%].

<sup>1</sup><https://www.gtisoft.com/gt-power/>

An inspiring reference during development has been the GT-ISE Performance Tutorial [36], this provides instructions in sequence of engine modelling and setup. The process began with a simplified engine setup similar to naturally aspirated, followed by a stepwise integration of subsystems, including turbochargers and aftercooling. At each stage, validation was performed using sensor data from the G3508a to ensure the model accurately represents real-world operating conditions. The chronological development of the GT-ISE model for the CAT G3508a is schematically illustrated in Figure 5.2. This specific structure is relatively hectic and isn't further elaborated, rather chapter 8 describes a component-level walkthrough of the model, in the same sequence as the air passes through the engine.

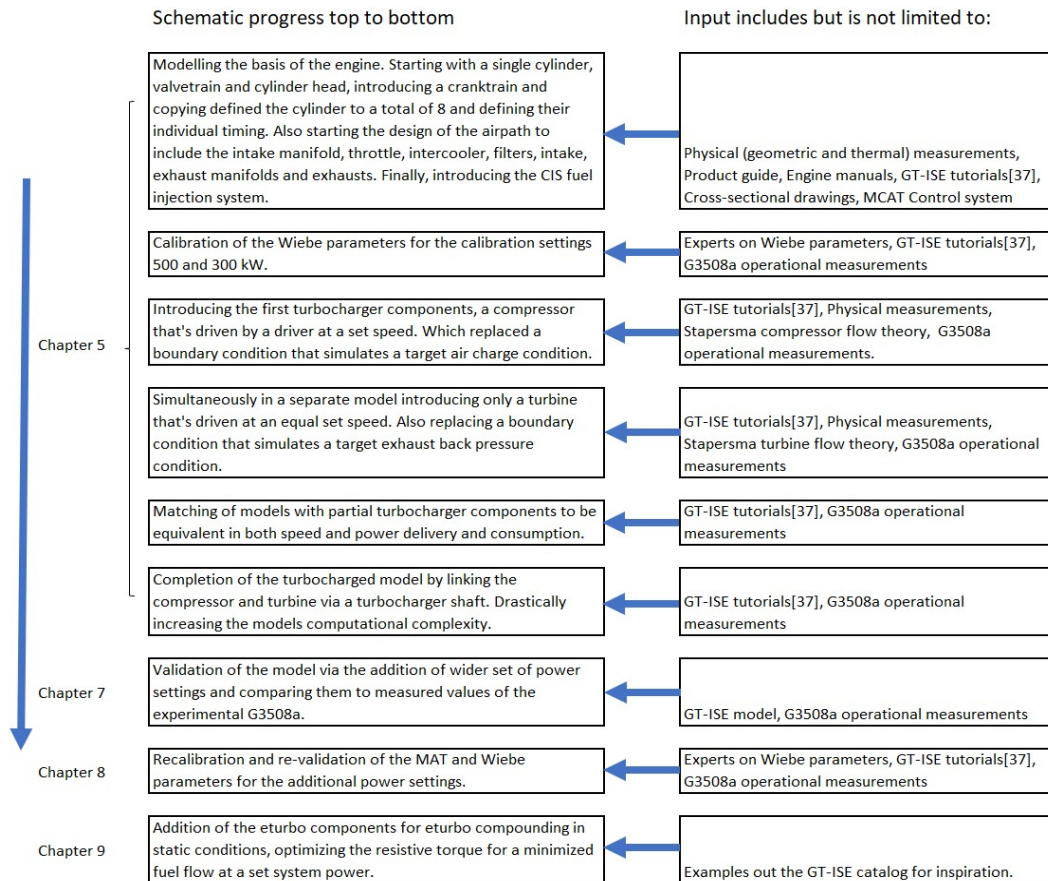


**Figure 5.2:** Chronological illustration of development of GT-ISE model.

Model choices and prerequisites are discussed in chapter 5, while chapter 6 presents a throttle correlation study that provided key insights into throttle system behaviour. The initial verification and calibration of the model are covered in chapter 7, comparing measured and predicted values. chapter 8 details further optimization, recalibration, and re-validation, ensuring the model accurately represents the G3508a and is fit for further research. Following this, the model was adapted to incorporate hybrid electric turbocharging components, with chapter 9 their effects on engine behaviour.

## 5.2. Engine introduction

The Caterpillar G3508a used in this study is part of the Caterpillar 3500 engine family. The engine concept originates from 1972, starting production of the V8 (3508) and V12 (3512) in 1981, later adding a V16 in 1983. The engine family is designed as a high speed 4-stroke twin turbocharged engine, ranging from 1400 to 1800 [RPM]. The family was designed to be used for multiple purposes like; heavy 'off highway' trucks, generator sets, industrial uses and prime movers for vessels. The original engine concept was originally designed to be fuelled by MGO with an cetane number of 40 using CI [37]. The engine in this study is currently fuelled by natural gas supplied by the grid, but has run on a variety of fuels like methanol and blend of hydrogen with natural gas.

The CAT 3500 family has a bore of 170 [mm] and stroke of 190 [mm], originally designed with a compression ratio of 14:1. The gas fuelled SI G3508a has a reduced compression ratio of 12:1 with a con-rod length of 861 [mm] (this has in a later stage turned out to be incorrect and has later been corrected to 380 [mm]). The CAT 3500 family has a stroke volume of 4.425 [L] per cylinder, making the CAT G3508a 35.4 [L] total stroke volume.

The engine in this study (G3508a) is an adaptation of the original CI design and now uses SI that is throttle controlled. This adaptation also includes a change in compression ratio, however the in-cylinder geometry is presumably largely unchanged as a bowl shaped piston is untypical for SI gas engines. SI engines typically feature a flat piston with a hemispherical head, such that the spark plug initiated flame front can propagate radially through the combustion chamber. However, the studied SI G3508a's heads are mostly flat and the pistons feature a significant bowl, which is typical for CI engines. The bowl predominantly serving to increase swirl inside the combustion chamber, improving diffused combustion of CI engines. This effect is not necessary beneficial for the SI G3508a in this study as the fuel is injected early on and has been thoroughly premixed through the entire intake system. Online reports of repair shops show images of a CAT 3508 with more flat head pistons <sup>2</sup>, so varying pistons are available, but are not used in this study.



(a) The CAT G3508a engine at the NLDA in Den Helder with the individual cylinder heads removed of bank 2, notice the bowl shaped pistons.

(b) A CAT 3508 up for repair in Greece notice the more flat head pistons. Work done contains at least; new pistons, piston rings, rod bearings, valve lash adjustment.

**Figure 5.3:** Comparison of CAT G3508a and CAT 3508

<sup>2</sup><https://www.euromarine.gr/episkeves-mihanon-caterpillar/episkevi-mihanis-caterpillar-cat-3508>

The engine family is based on the V12, as indicated by the bank angle of 60 [degree]. The V8 however needs a firing interval of 90 [degrees]. Therefore, the crankshaft has offset crankpins of 30 [degree] to make the engine run as smooth as possible. It must be noted that as a result of the 60 [degree] bank angle and V8 layout the primary and secondary balance are not optimal. However, it is not expected that this aspect will be of further relevance in this study.

The V8 engine has a cylinder count order that alternates between each bank, having the odd cylinders on one bank and the even on the other bank. The V8 uses a crossplane crank with a firing order of 1-2-7-3-4-5-6-8, firing at 24 [CA] BTDC. Consequently of the crossplane firing order receives each exhaust manifold of each bank thus an unequal exhaust pulsing of 180-90-180-270 [crank angle].

Each cylinder has its own individual cylinder head. Mounted between the engine block and the heads is an aluminum spacer. This spacer plate eliminates the need for a fitted edge for the liner in the cylinder block, which increases reliability and simplifies maintenance. The multivalve cylinder head features 4 valves of equal size fitted with valve rotators. The valves are actuated by pushrods that run on one of two camshafts which are mounted on each bank on the outside of the V. The heads on the engine used in this study are modified to fit water-cooled piezo electric Kistler 7061B sensors for in-cylinder pressure measurements.

The layout of the 3500 series is peculiar as both the intake and exhaust manifold of the engine are fitted on the inside of the V of the engine. This combined with the bank angle of 60 [degrees] makes for a relatively compact engine. As a result of the placement of the manifolds the flow design of the heads is untypical. Typically on multivalve heads are the ports of either intake or exhaust placed in parallel, with the intake and exhaust on either side of the cylinder head. On this engine the intake and exhaust flow parallel to each other, so the ports to both intake or exhaust are staggered, the valves on the 'back' flowing over the 'front' valve. This means that the intake and exhaust are fitted to the same side of the cylinderhead, see Figure 5.3. This staggered layout of valves is peculiar and will have suboptimal flow characteristics but these specifics should largely be captured by using the same staggered setup in GT-ISE.

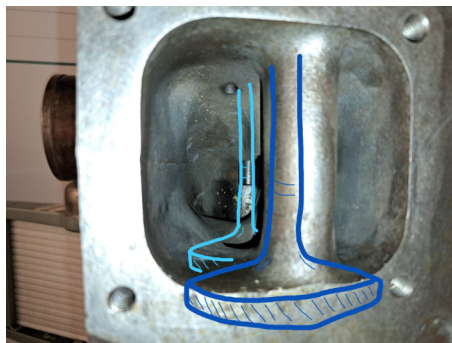


**Figure 5.4:** Downstream view of the inside of the exhaust ports, notice how the valves are staggered instead of next to each other. Side note; the dark blue valve in front does not run through that cast piece but sits behind it.

The log style intake manifold are placed in the valley between each bank, from there flowing into the heads on both banks via an intake runner. Each bank has its own water cooled log style exhaust manifold, fed by runners of the cylinder heads and flowing into one of the turbochargers.

The 3508 is turbocharged by two fixed and water cooled Garrett TW6146 (89 [mm] turbine inducer and 94 [mm] compressor exducer) turbochargers that are placed in parallel. The exhaust turbine has a area-radius-ratio ( $A/R$ ) of 1.37 [-] and the compressor a trim of 46. A small pipe joins the exhaust manifolds to equalize pressure between each bank.

The G3508a in this study can be fueled by various fuel supply systems for the varying fuel types. Only the relevant natural gas fuel supply system in this study will be modelled. The CIS (Continuous Injection System) is mounted just after the air filters. The air fuel mixture thus will pass through the compressor and charge air cooler for compression. The injection rate is calculated using a predefined fuel map based on pressure and temperature conditions in the inlet manifold.

## 5.3. Model

### 5.3.1. Model introduction

The software package used in this study is GT-ISE as part of GT-POWER (Gamma Technologies, 2016), a one-dimensional simulation tool that's widely adopted for modelling engine behaviour and analysis. By using advanced solvers and algorithms, GT-ISE effectively replicates the physical processes occurring within a running engine, allowing simulation of both steady-state and transient operations. The software's functionality and quality relies on the modellers ability to design a model that captures the engine behaviours accurately using the graphical user interface and a wide-ranging library of predefined engine components.

GT-ISE uses one-dimensional (1-D) gas dynamics to simulate fluid flow in pipes and a zero-dimensional (0-D) Wiebe approach for modelling the combustion model in the engines cylinders. This approach allows the software to predict key engine operating parameters of the air path, such as pressures, mass flow rates, and temperatures. GT-ISE is recognized as a highly effective tool for engine simulation due to its computational efficiency, high accuracy of results, and rapid execution times. Furthermore, its flexibility in customization and applicability across a wide range of use cases and scenarios made it a fitting choice for the present study.

The data required for constructing the engine model were sourced from the product guide, engine manuals, GT-ISE tutorials[36], cross-sectional drawings, control system, physical measurements and compressor flow theory. During the development process for the engine model the included Performance Tutorial was used for inspiration, this can be summarized in the following steps: Selecting objects from the library that accurately represent the engine components and establish their relation. Assigning relevant input data to each object. Making preliminary calibrations of model constants by referencing measurements of a set operating point, followed by simulation runs. Fine-tuning model constants to achieve the desired level of accuracy, refer for this to Figure 5.2.

For modelling in-cylinder heat transfer, the Woschni heat transfer model [38] was employed, a method widely utilized in engine studies as outlined by Merker et al. (2006)[39]. The heat release rate for SI operation was simulated using the single Wiebe model, also described by Merker et al. (2006)[39]. The theory developed by Stapersma [40] was used for the definition of the compressor and turbine mapping outside the known operational range, up to the still undefined limits.

Firstly, a model of a throttle controlled eight-cylinder engine block without turbochargers was developed and validated. This model was adjusted by altering the Wiebe parameters to values that fall in an acceptable range and produce satisfactory fuel efficiency, power and Exhaust Gas Temperatures (EGT) values. The model was later expanded and validated to include the charge air cooler and the compressors, these compressors then being driven by a simulated driver at a set speed that matches the measurements. The exact same was done by adapting the model to only include the turbines. After both models where validated they were combined to include the complete turbochargers, again see Figure 5.2 for reference.

The input data required for this model setup included geometric engine details, material properties, thermal engine management and other thermal details, throttle flow information, fuel composition, intake and exhaust valve lift and flow profiles, performance maps for both compressor and turbine and control parameters, and constants for engine sub-models such as combustion, heat transfer and friction. Additional inputs included the engine's operating point (load/speed), ambient conditions, and initial conditions for temperature, pressure, and the composition of the working medium in engine cylinders, pipes, and receivers.

On the CAT G3508 the throttle is actuated by a hydraulically powered and electronically controlled actuator, mounted on the front timing cover and connected to the throttle by a throttle linkage. The operator of the generator sets a loading setting for the load bank, the engines ECU responds by adjusting the throttle actuator signal to produce adequate torque at the target speed of 1500 rpm. The power output in the model is controlled by adjusting the throttle angle using the throttle controller which is integrated in GT-ISE. By setting the desired power output the controller adjusts the throttle based on GT-ISE set P.I.D. parameters. The speed of the engine is set in the model to be a constant 1500 rpm at all times. So the G3508a engine is throttle controlled to a target speed at a set load, the model is throttle controlled to a target output power or load at a set speed.

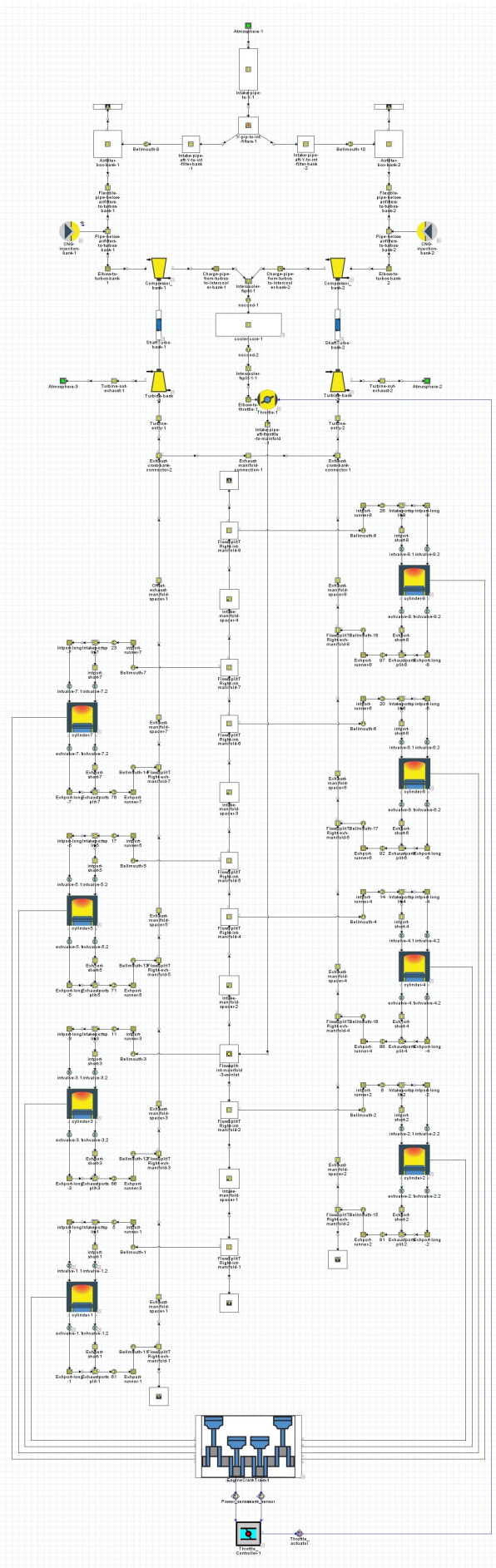
## 5.4. Model description

In this chapter, a brief description will be given of the main components that the model has been built with. The components, called objects, are provided by the 'Template library' that is built into GT-ISE. The objects used in the model have been introduced and learned through the 'Performance tutorial' included with the GT-ISE software package. Through this tutorial the user gets introduced into various modelled systems that gain in complexity. From these tutorial models relevant subsystems and objects have been put together and adapted to simulate the CAT G3508a.

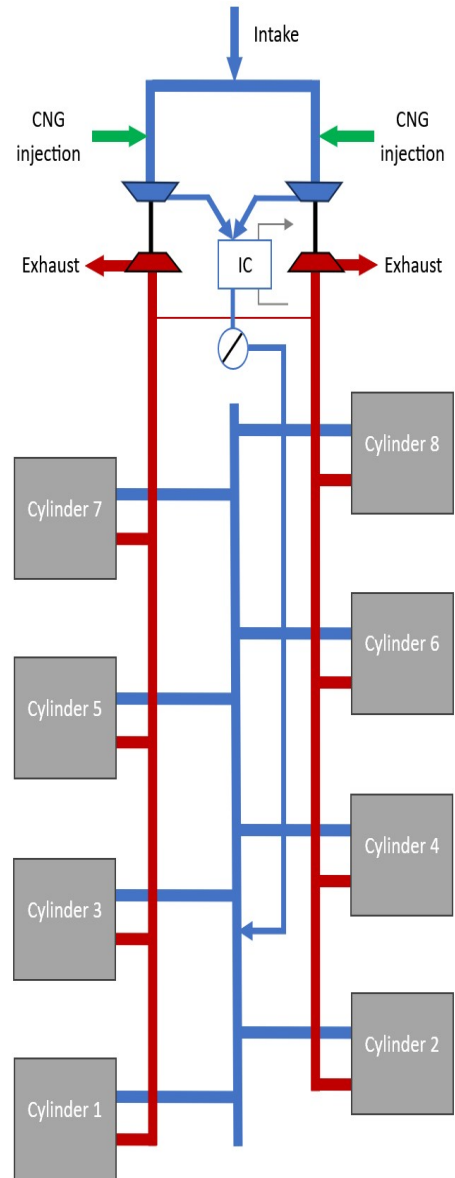
The GT-ISE's Performance Tutorial advises to follow a systematic method for integration of the turbocharger into the model. This method is necessary because identifying the root cause of performance issues in a complete engine model is challenging. For example, if turbocharger speed, boost pressure, and/or back pressure exceeded experimental data, it is difficult to determine whether the issue came from turbine or compressor maps. Adjusting an incorrect input could introduce additional errors, leading to further problems under different operating conditions, therefore the advised method has been followed.

The main objective for this model is to be able to assess the measure in which the engine behaviour responds to changes in the way the air is managed. The electrification of a turbocharger changes the way air is boosted or restricted at the compressor or turbine wheel. What the behaviour changes are for this specific engine depends on the design of the air path. For that reason has the focus during the design of the model mainly been on the geometry of the airpath.

The fresh air starts at the intake (at the top of Figure 9.3a), through the split into the air filter boxes. From the air filter boxes down along the CNG fuel injectors into the compressors. From the turbos into the charge air cooler and through the throttle into the intake manifold. Then from the intake manifold to the intake runners and through the cylinder head into the cylinder. Then after combustion back through the cylinder head and exhaust runners into the exhaust manifold. Then finally through the turbine wheel into the exhaust.



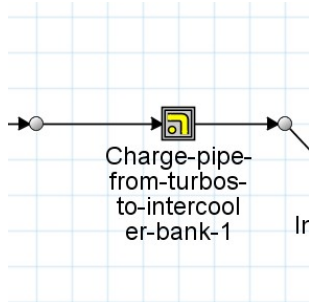
(a) Complete overview of the graphical user interface of the GT-ISE model of the CAT G3508a



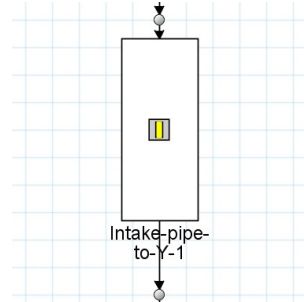
(b) Schematic overview of the airpath of the CAT G3508a.

### 5.4.1. Pipe sections

The main building block for this model is a pipe section, which objective is to replicate a straight air path section with a constant cross sectional shape without any intersections. However, it also can incorporate bends or a growing cross sectional area. GT-ISE has several options for this, starting with the type of cross section shape. Mainly round cross sections are used but rectangular are used where applicable. The PipeRound or PipeRectangle object in GT-ISE is designed to model a circular or rectangular cross-section, optionally including bends. This model calculates the pressure distribution and associated losses along the length of the pipe while accounting for fluid dynamics and heat transfer. One of the relevant key aspects of the model is its ability to discretize a single pipe into multiple sub-volumes, allowing calculations of pressure, temperature, and other variables at multiple points for each time step. The discretization length determines the size of the sub-volumes, which in turn impacts the resolution of the calculations.



(a) Example of a PipeRound object including a bend.



(b) Example of a PipeRound object section.

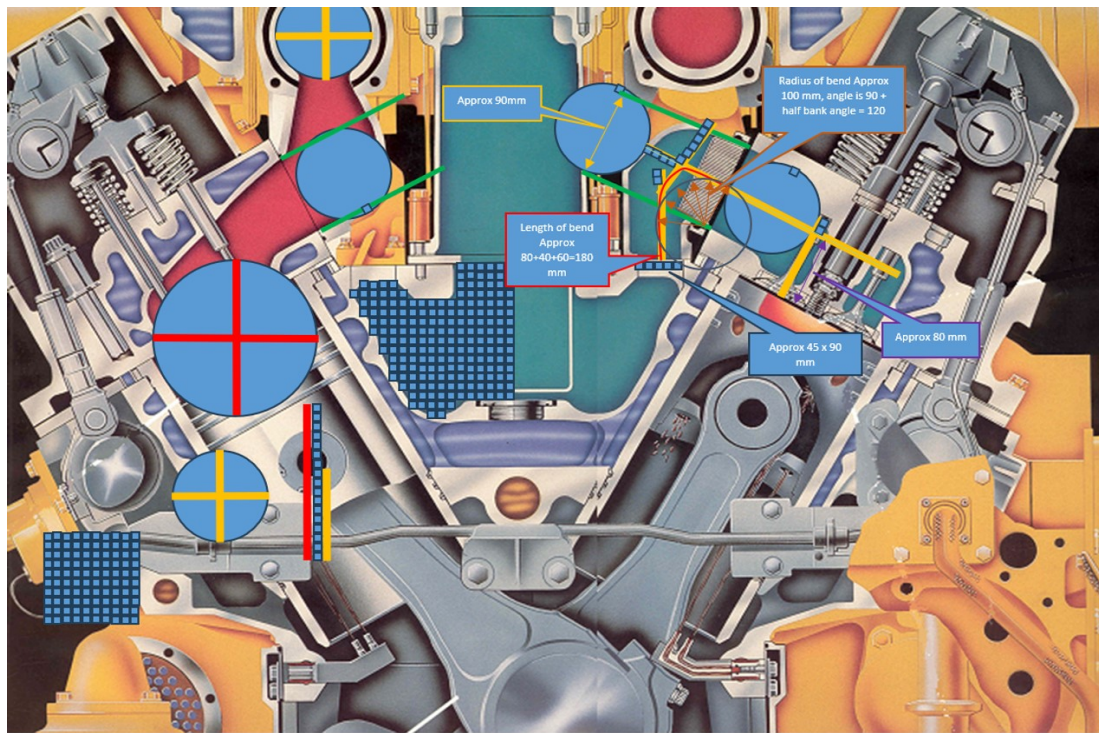
The geometry and initial conditions of the pipe are defined by parameters such as the inlet and outlet diameters, overall length, and radius and angle of bends. The time step for the explicit solver is proportional to the discretization length, fluid speed, and wave speed. Smaller discretization lengths allow for finer resolution of variables but can result in longer run times due to the need for more calculations and smaller time steps. The Performance Tutorial advises to set the discretization length on the intake side of the engine to be 40[%] of the engine cylinder bore, and 55[%] on the exhaust side. Coming down to 68 [mm] and 93.5 [mm] respectively, cutting even the ports in the heads and runners into multiple segments.

$$\Delta t_{\text{explicit}} \propto \frac{\Delta x}{c + |u|}$$

with

$\Delta t_{\text{explicit}}$	time step for the explicit flow solver only
$\Delta x$	pipe discretization length
$c$	fluid speed of sound
$u$	fluid velocity

An especially noteworthy section is the intake manifold that is being housed inside the V of the engine block. This manifold is being fed by a pipe section that comes down from the throttle body, and flows into the runners towards the cylinder head of each cylinder. The inside of the V features all kind of uneven surfaces due to it being a cast piece. Additionally, due to the fact that this portion of the intake is buried so far down in the V of the engine means that a lot of systems are mounted above it. This means that making a good approximation for the geometry and volume of this portion is difficult. The best indication for the cross sectional geometry came from a cutaway drawing of the CAT 3500 series, the specific drawing likely being the V12 version. The dimensions of the cylinder bore are known, which made it possible to get an indication of cross sectional area of the intake manifold. Assuming it as constant, which neglects the unevenness of the cast surface, and combining it with estimations of the internal length resulted in the best approximation of the internal volume. The cutaway drawing has been used extensively for volume and length estimations of the drawn air path sections, mainly the insides of the cylinder heads and runners, as indicated by Figure 5.7.



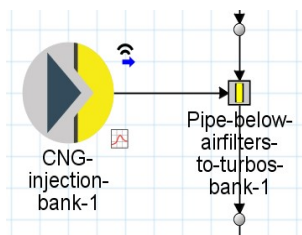
Large blue circle diameter = bore = 170 mm.  
 Red lines are diameter blue circle = 170 mm  
 Blue squares are square and have sides of  $1/17^{\text{th}}$  of red lines = 10 mm  
 Yellow lines are 10 blue squares = 100 mm  
 Small blue circle has diameter 100 mm

Figure 5.7: Cross section view of the CAT 3500 series

### 5.4.2. Fuel injection

The Continuous Injection System or CIS of the G3508a is replicated in the model by two InjAF-RatioConn objects in the intake system just after the air filter boxes. These objects replicate the fuel injectors that inject a determined amount of CNG into the airstream. The objects in the model are set to create a given lambda according to the same fuel mapping as the CAT G3508a. A fuel map has been composed in the model that alters the resulting lambda based on the injected fuel mass flow of the previous cycle. This is where the model differs from the real system. On the CAT G3508a the injected fuel mass is determined by the pressure and temperature conditions in the intake manifold, combined with the targeted power. It takes some delay for these conditions to change and stabilize as the sensors aren't placed close to the injectors, compressors or throttle. Additionally, the feed from these sensors needs to be processed, introducing more latency to the system. The model doesn't suffer from these aspects, the injectors in the model are able to produce the targeted lambda after just one cycle.

The chemical composition of the fuel that has been put in to the model is based on a chemical analysis done by Kiwa Technology B.V.. The reported chemical composition has been copied into the 'Fluid object' of the injector object, only taking chemical components that are present above a mass fraction that's higher than a per mille. The small sum of neglected parts are compensated for by slightly increasing the inert nitrogen content.



(a) Example of the injector object on the side of bank 1.

Attri...	Fluid Object	Mass or Volume Fraction
		%
1	methane-vap...	80.81...
2	ethane-vap...	3.18...
3	propane-vap...	0.706...
4	n2-vap...	13.3115...
5	n-butane-vap...	0.1627...
6	isobutane-vap-NASA...	0.1498...
7	co2-vap...	1.69...

(b) Chemical composition in GT-ISE.

### 5.4.3. Compressors

This object models a compressor using interpolated and extrapolated mapping. Typical uses are for modelling a compressor in a turbocharged or supercharged engine. Predictions of mass flow rate, outlet temperature and absorbed power are calculated by the use of a map that is made by the CompressorMap reference object.

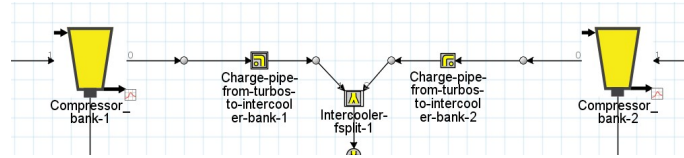
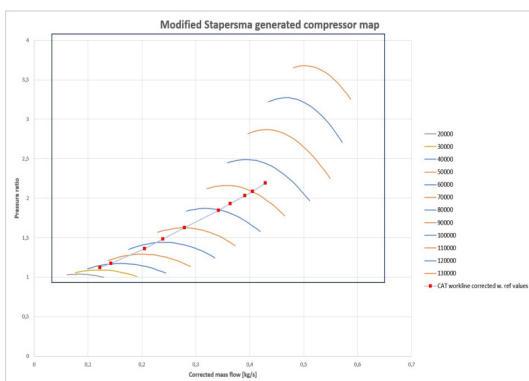


Figure 5.9: GT-ISE compressor layout

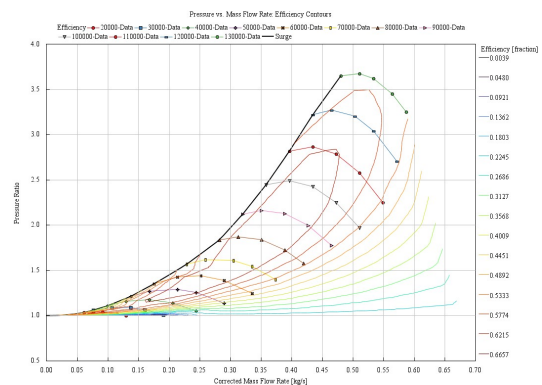
The CompressorMap template in GT-ISE processes compressor map data and generates a version of the map by interpolating and extrapolating to a minimal pressure ratio of 1.0 and a speed of 0.0 RPM. This pre-processed map allows the Compressor object to more accurately simulate compressor performance. Data entry requires a minimum of two speeds, with at least four speeds recommended for accuracy. Each speed line must include multiple data points, with, critically for this study, the lowest mass flow rate defining the surge (stall) line. The map can handle up to 300 rows and 60 speed lines, allowing detailed modelling across a wide range of operating conditions. Each speed line contains four columns: corrected RPM, corrected mass flow, pressure ratio, and efficiency. These values are corrected using reference conditions for pressure, temperature, and gas constant.

However, the exact compressor map of the Garrett TW6146 turbochargers outside the operational range of the CAT G3508a is still unknown. During measurements its only been possible to determine only one operational line. By using Stapersma method [40], which is based on Euler turbomachinery theory, it's possible to generate a set of raw data that approximates a compressor map of constant speed lines over a large unbound range of corrected mass flows and pressure ratios. Meaning, the generated mapping doesn't include limitations like surge or choke. For this study a Stapersma generated compressor map has been used and modified to include those limitations. Within this generated compressor map the known operational line has been plotted after being altered with corrected mass flows, using the same reference pressure and temperature as the generated map.

The generated mapping has been converted to the template of GT-ISE. The data is comprised of 12 individual speed lines, of each line 5 points have been taken. The range of the 5 points of each speed line has been taken wide enough to include intersection with the work line, with the lowest mass flow rate defining the surge line. As previous measurements or studies have not yet yielded methods to determine the surge limit of these specific turbochargers, definition of the location of the surge limit on the compressor map is quite arbitrary. With basically the only knowledge being that the phenomenon surge isn't detected while operating the engine. Meaning the operational work line of the compressor on the CAT G3508a doesn't intersect the surge line.



(a) Modified Stapersma generated input compressor map.

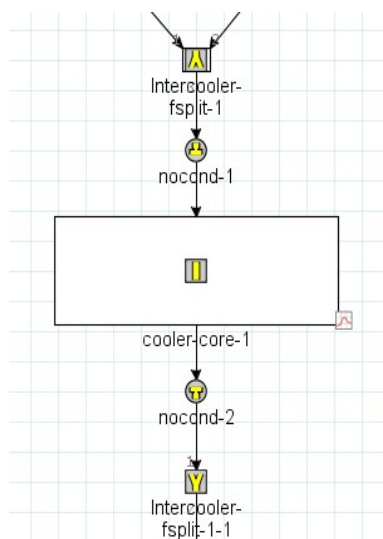


(b) GT-ISE pre-plot compressor map using data from image (a).

#### 5.4.4. Aftercooler

The CAT G3508a is equipped with an air to water charge air cooler that is being cooled by a secondary cooling water circuit. However, the CAT G3508a in Den Helder has been fitted with modifications to the secondary cooling water circuit. A controller regulates the amount of cooling water flow through the core by means of a three-way valve that can bypass the core. The PID controller is able to manage a constant targeted air cooler air exit temperature of approximately 303 [K]. This modification has been fitted for a constant and more predictable behaviour of the engine during experiments.

The charge air cooler is simulated in GT-ISE by means of a pack of small parallel air channels. The exact geometry of the charge air cooler core and its internals is not precisely known as it's not possible to see its insides completely. Additionally, the dynamics of its thermal behaviour are hard to predict precisely. However, simulation of the charge air cooler gets simplified due to the modifications to the CAT G3508a. As the real system is able to reach the targeted temperature value, it is possible to manipulate the model by means of the 'Imposed Wall Temperature' and a 'Heat Transfer Multiplier'. The imposed wall temperature of the core in the model is set to the same target value as the real system and the heat transfer multiplier forces the heat flow such that the wall temperature becomes the targeted air cooler air exit temperature.



(a) The aftercooler assembly in GT-ISE.

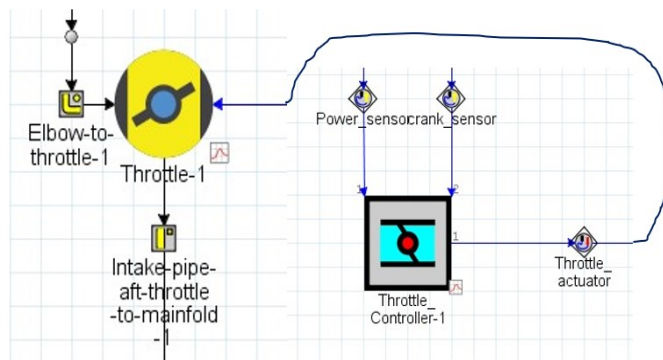


(b) View from the aftercooler core from downstream.

#### 5.4.5. Throttle

The CAT G3508a is equipped with a hydraulically powered electric controller for the butterfly throttle valve. The physical throttle is peculiar because it has a stroke of 75 degrees, because of its oval shaped plate in a round housing, that shuts at 15 degrees. No template object in GT-ISE has been found that simulates a butterfly throttle with a stroke other than 90 degrees. Additionally, the flow characteristic of the throttle valve is not known to very large detail. The ThrottleCon object in GT-ISE needs flow specifications of the forward and reverse 'Discharge coefficient'. In the Performance Tutorial some standard values for these coefficients are available, which are used for this model.

The ControllerThrottle object is designed for precise control of engine performance parameters during part-load operation in SI engines, a target break power in the case of this study. By adjusting the throttle angle, it manages engine dynamics without the need for manual tuning of a PID controller. The controller integrates a model-based feed-forward controller with a continuous feedback controller. Additionally, it features anti-windup protection to ensure stability and reliability during operation. This controller is optimized for engines where the throttle body feeds directly into a plenum that supplies air to the cylinders, with the possibility of a compressor upstream of the throttle, making it suitable for use in this model.



(a) The throttle assembly in GT-ISE.



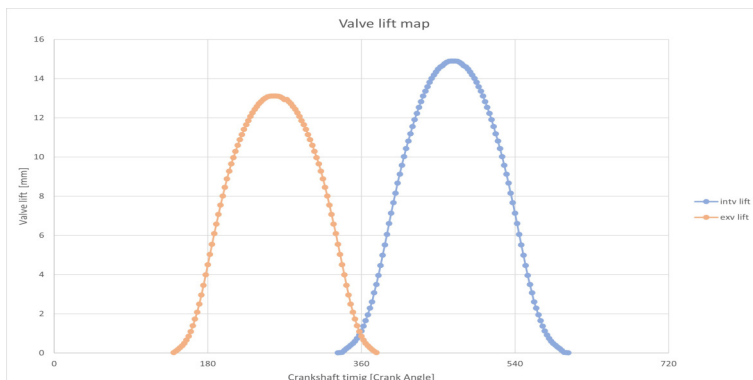
(b) View from the throttle from upstream, notice valve sitting shut at 15[°] due to its oval shape.

### 5.4.6. Valves

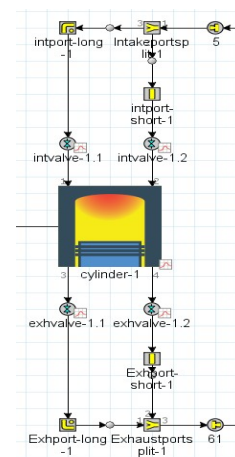
The ValveCamConn object defines the characteristics of a cam-driven valve, intake and exhaust, by specifying its geometry, lift profile, and flow characteristics. It operates by imposing a lift profile as a function of cam angle, with the option to allow the valve’s behaviour to adapt dynamically to different operating conditions. However, in the case of the CAT G3508a this isn’t needed as it doesn’t feature any dynamic variable in its valve actuation, like for example VVT. A nominal lift curve serves as the baseline for variable lift profiles. Additional features, such as valve lash, are incorporated to refine the relationship between cam angle and lift.

The template also incorporates aerodynamic characteristics by modelling flow coefficients and reference areas via the ‘Discharge Coefficient’, as is similar to the throttle body, which is described earlier. As with the throttle body are the real discharge coefficients not known precisely. However, in the Performance Tutorial some standard values for these coefficients are available, which are used for this model, as done similarly with the throttle body.

The valve lift of the CAT G3508a has been measured for both the intake and exhaust valve and logged per half crank angle. The measurement has been done on the end of the valve stem, so the measured values are the actual valve actuation. This means that the option for valve lash in GT-ISE is ignored, unlike when the valve lift would be measured directly from the camshaft or pushrod. The measured values have been modified to fit the template of the ValveCamConn object, which needs the reference crank angle to be at maximum lift, after which they have been put into the model.



(a) Valve map of the G3508a.



(b) View of the cylinder, cylinder head and valves of cylinder 1 in GT-ISE

### 5.4.7. Cylinder

The Cylinder object itself is comprised out of several separate templates that define the initial state, wall temperature, heat transfer and combustion model among others. The most noteworthy are being elaborated in this subsection. As the purpose of this study is focussed towards the gas exchange of the engine, means that what happens inside the combustion chamber between intake valve closing and exhaust valve opening is of less importance, so long the conditions outside the cylinder are accurate. However, the power production and combustion efficiency are significant factors that need to be considered for validation of the model.

The WoschniGT model in GT-ISE calculates in-cylinder heat transfer based on the classical Woschni. It improves heat transfer predictions by considering inflow through intake valves and backflow through exhaust valves during valve overlap. This model is recommended by GT-ISE when swirl data is unavailable, as it provides a practical and accurate solution for engine simulations across various operating conditions.

In a combustion model with multiple temperature zones, such as the Double Zone Wiebe combustion model used here, this attribute determines the weighting of convective heat transfer between the unburned and burned zones. The convective heat transfer rate for each surface within the combustion chamber can be expressed in terms of an effective gas temperature as follows:

$$Q = Ah(T_g - T_w)$$

$$T_g = \alpha T_b + (1 - \alpha)T_u$$

with

Q	convective heat transfer rate [W]
A	surface area [ $m^2$ ]
h	convective heat transfer coefficient [ $W/m^2K$ ]
$T_w$	wall temperature [K]
$T_g$	effective gas temperature [K]
$T_b$	burned zone temperature [K]
$T_u$	unburned zone temperature [K]
$\alpha$	weighting coefficient

The convective heat transfer rate is distributed to the burned and unburned zones as:

$$Q_b = \alpha Ah(T_b - T_w)$$

$$Q_u = (1 - \alpha)Ah(T_u - T_w)$$

The WoschniGT model doesn't require a lot of additional input data besides the combustion chamber temperatures apart from the piston to bore area ratio. The top area of the piston of the G3508a is significantly larger than the bore area as the piston features a significant bowl. The cylinder heads were disassembled from the engine block at some point during this study, giving the opportunity to measure the geometry of the pistons. These measurements have been used to model the top of the piston in CAD software, giving the ability to determine the area ratio of 1.33 [-] with high accuracy.

The double temperature zone Wiebe combustion model template in GT-ISE determines the combustion burn rate for spark-ignition engines, making it compatible with any type of fuel injection. The Wiebe function combustion model defines combustion timing using certain parameters: the Anchor Angle, which sets the crank angle for 50% fuel burn, the Duration, specifying the burn period between 10% and 90% completion, and the Wiebe Exponent, shaping the combustion curve with a default value of 2.0. These parameters have been determined using the Optimization tool that is included in the GT-ISE software. The very first functional draft of the model produced too much break power and too low exhaust gas temperature, while also having a specific fuel consumption that was too low. The optimization tool was set to a multi-objective to target a break power of 500 [kW] and an exhaust gas temperature (EGT) of 865 [K]. The Optimization tool, after 43 iterations, resulted in a break power of 496 [kW] and an EGT of 800 [K]. Putting priority more towards the power production as the determination of the EGT

have some uncertainties between reality and the model. The resulting values for the Anchor angle, Duration and Wiebe exponent were; 37.9 [ATDC], 45.8 [CA] and 2.24 [-] respectively. These values have been verified to be in a realistic and plausible range for the CAT G3508a, but a more precise method of determining the real values are still being studied. Additionally, the indicated specific fuel consumption came also in an acceptable range after the combustion model was updated with the new Wiebe parameters. In a later stage more Wiebe parameters were added for additional power levels, refer for this to Table 8.1.

### 5.4.8. Turbine

Naturally, the turbine shares a lot of similarities with the compressor object. Both, the object in GT-ISE as the methods of the data definition have parallels in both the compressor and turbine. The Turbine object models a turbine using interpolated and extrapolated mapping. Predictions of mass flow rate, outlet temperature and generated power are calculated by the use of a map that is made by the TurbineMap reference object.

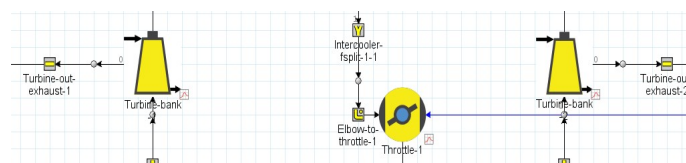
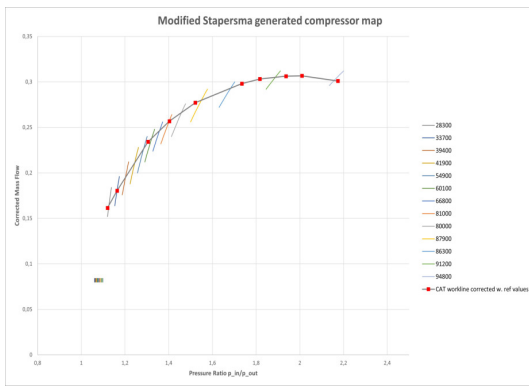


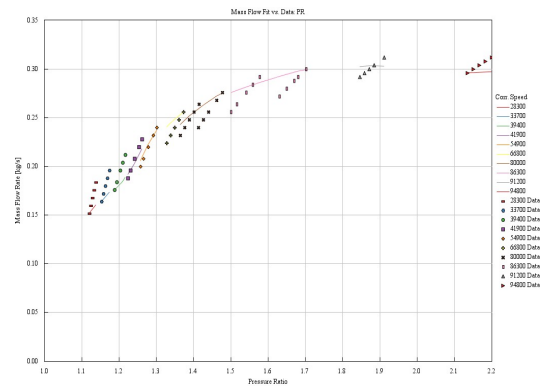
Figure 5.14: GT-ISE Turbine layout

The TurbineMap fitting template processes turbine map data by fitting it to proven equations and extrapolating it to cover a wider range of pressure ratios and speeds for simulation use. This process smooths measurement irregularities and extends the map to low speeds and pressure ratios, with the option to extrapolate beyond the original data range. Data entry requires a minimum of two speeds, with at least four speeds recommended for accuracy. Each speed line must include multiple data points. The map can handle up to 300 rows and 60 speed lines, allowing detailed modelling across a wide range of operating conditions. Each speed line contains four columns: corrected RPM, corrected mass flow, pressure ratio, and efficiency. These values are corrected using reference conditions for pressure, temperature, and gas constant.

However, as with the compressor data is the exact turbine map data of the Garrett TW6146 turbocharges outside the operational range of the CAT G3508a unknown. During measurements it's only been possible to determine only one operational line. Stapersma's method [40] is used again, making it possible to generate a set of raw data that approximates a turbine map of constant speed lines over a large unbound range of corrected mass flows and pressure ratios. Meaning the generated mapping doesn't include limitations like choke. For this study a Stapersma generated turbine map has been used and modified to include those limitations. Within this generated turbine map the known work line has been plotted after being altered with corrected mass flows, using the same reference pressure and temperature as the generated map. The generated mapping has been converted to the template of GT-ISE. The data is comprised of 13 individual speed lines, of each 5 points have been taken. The range of the 5 points of each speed line has been taken wide enough to include intersection with the work line. The generated mapping of the turbine has some particularities that stand out. Most importantly the vertical nature of the high-speed speed lines. The generated mappings are not very intuitive to read but the vertical nature of the speed lines indicate that the constant speed relation between the pressure ratio and the corrected mass flow is not as dependent on the mass air flow. Meaning that a small variance in mass air has relatively minor influence on the pressure ratio. The expected trend of the turbine mapping would be a more horizontal constant speed line, where a variance of mass air flow has a more effect on the pressure ratio, given a constant speed. Especially towards the higher mass flow region of the map is it more to be expected to see more horizontal speed lines. The pressure ratio, mass flow and speed are included in the validation.



(a) Modified Stapersma generated input turbine map.



(b) GT-ISE pre-plot turbine map using data from image (a).

### 5.4.9. Turboshaft

The ShaftTurbo object in GT-ISE links the whole model together and thus greatly increases the complexity of the differential equations. The connection between the conditions in the turbine and its power generation needs to be linked and balanced to the conditions and power absorption of the compressor. The object is used to model the dynamics of a turbocharger shaft, including speed, acceleration, and deceleration. It is specifically recommended for turbocharger applications and offers additional features compared to the standard Shaft object, such as an inertia multiplier and special initialization options.

The power balance between the generated power of the turbine and the absorbed power of the compressor at the same speed needs to be calibrated manually to make sure the model converges to a stable situation. This was done by first running the model with separate drivers on both the compressor and turbine set at the same speed. The simulation resulted in a power dissimilarity, where the turbine generated to little power. This has been resolved through the 'Efficiency Multiplier' by a factor of 1.12 [-], however the Performance Tutorial reports that the normal range should be between 0.95 [-] to 1.05 [-]. Identifying the source of the abnormal power unbalance is extremely complex as the amount of variables that influence the power balance is very large. The method as described in the Performance Tutorial has been closely followed, and it reports that identifying the root cause of performance issues in a complete engine model is very difficult. Adjusting an incorrect input could introduce additional errors, leading to further problems under different operating conditions. All input data has been compiled with the best available data and reasoning.

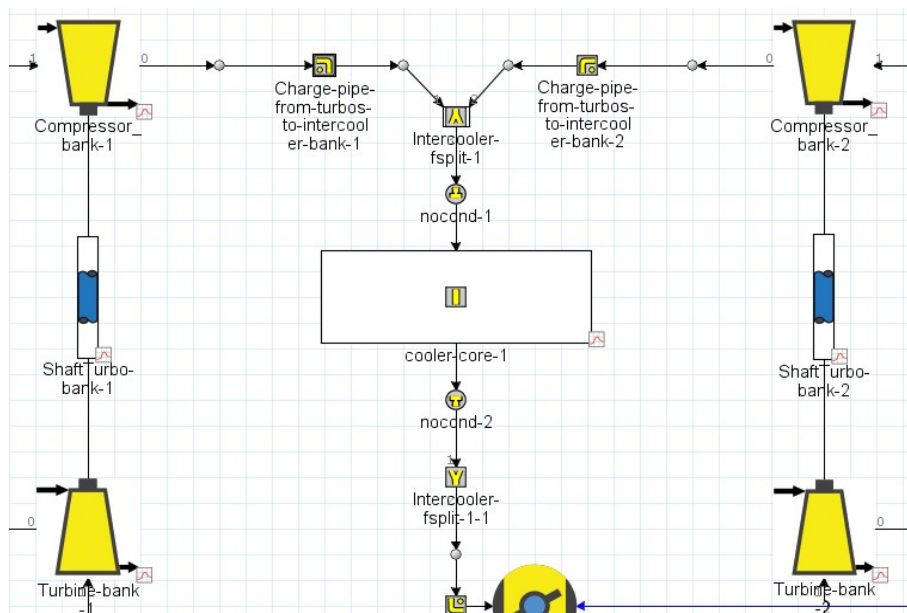


Figure 5.16: Complete turbocharger system in GT-ISE.

The quality of the estimation of the initial turbocharger rotational speed is very important for decreasing the time the model needs to converge . The best indication for this came directly from the measurements of the G3508a. The turbocharger starts the simulation at the specified initial rotational speed. However, the airflow is stationary at the initialization of the simulation. To not immediately stall the turbocharger speed a inertia multiplier profile was used. Initially, a high turbo inertia (multiplier = 1000) was applied for the first 30 'periods' or cycles to prevent speed drops while manifold air velocity developed from initial conditions before returning to its real value (multiplier = 1.0) for accurate modelling in the rest of the simulation.

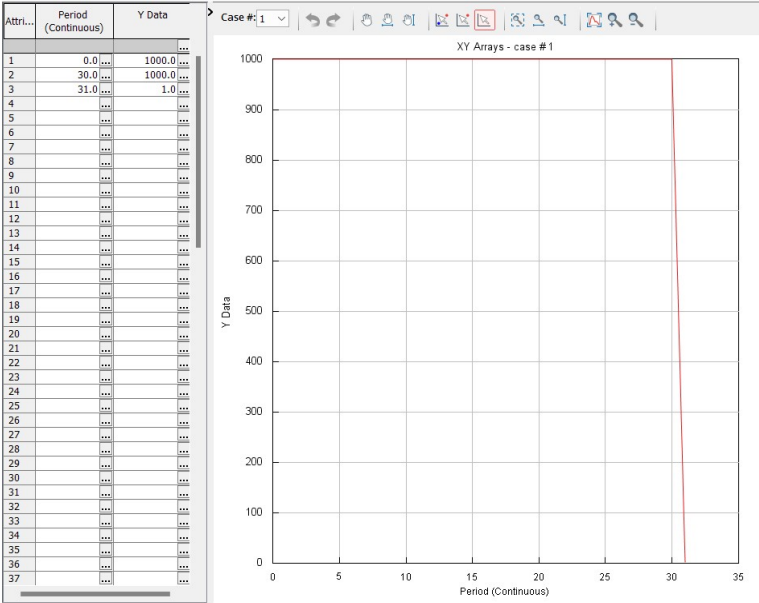


Figure 5.17: Inertia multiplier for the turbocharger assembly for first 30 cycles.

# 6

## Throttle Correlation Study

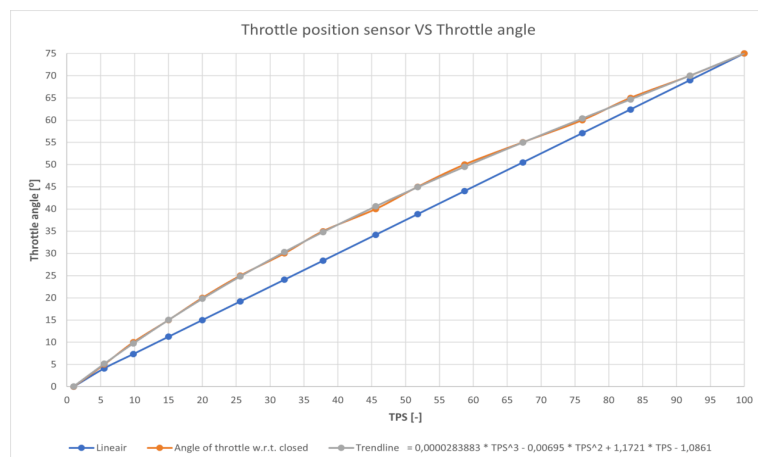
During the construction of the model it became clear that the setting of the throttle valve was uncertain. The CAT G3508a is equipped with a hydraulically powered electric controller for the butterfly throttle valve. The physical throttle is peculiar because it has a stroke of 75 degrees, because of its oval shaped plate in a round housing, that shuts at 15 degrees. Meanwhile, in GT-ISE has the throttle been modelled with a butterfly throttle with a stroke of 90 degrees, as explained in chapter 5. However, the throttle object in GT-ISE demands a throttle angle setting and the log files from the G3508a measurements only report a throttle actuator target signal ranging from 0 to 100 [%].

The correlation between actuator setting and throttle valve angle needed to be determined for correct operation or validation of the model. However, actuation of the throttle actuator of the G3508a is not possible with the engine turned off as it is powered hydraulically from the engines timing gear. Additionally, as the engine is running it continuously adjusts the throttle actuator as it continuously corrects the engines RPM to its set target. So measuring the throttle angle and referencing it to a actuator setting isn't simply done. An additional linear Throttle Position Sensor (TPS) was installed to get this connection between throttle angle and throttle actuator signal. The TPS was calibrated and zeroed at closed throttle and set to 100 [%] at full throttle. The system meant that a correlation between the newly installed TPS sensor and throttle angle could be made. A data set was logged at every 5 degrees by manually sweeping the throttle by its linkage through its entire range. This already showed non-linearities in its correlation. The function of the generated trendline that fitted the measured data to a high degree can be described as:

$$\text{Throttle angle (TPS)} = 0.000028883 \cdot \text{TPS}^3 - 0.00695 \cdot \text{TPS}^2 + 1.1721 \cdot \text{TPS} - 1.0861 \quad \text{for } \text{TPS} \in [0, 100]$$



(a) The installed throttle position sensor (TPS). Connected to the shaft of the throttle actuator that also actuates the throttle linkage



(b) The measured TPS data to throttle valve angle.

The correlation between the throttle angle and TPS was now known, the correlation between the actuator and TPS still needed to be investigated. This is only possible on a running engine. The newly installed TPS was also included into the logging system of the G3508a. So a record could be made where the signal of the actuator signal could be compared to the signal of the TPS. These signal values are recorded at 0.2 [s] interval at a constant load setting for the generator. However, the values of these signals need to be averaged as the engine is constantly over- or undershooting its target. Averages are taken over a 15 [s] timeframe. Using these values a correlation can now be made between the throttle actuator, TPS and throttle angle in the operational range of the engine. The operational range of the throttle is mainly focussed on the middle part of its complete range, as the controller can't control at either extremes. The highest recorded average throttle actuator signal therefor is 64.1 [%]. This correlates to a signal of 42.6 [%] TPS signal, which is 38.4 [°] throttle angle from closed, or just above half its range.

During operation the live readout of the data showed a similar trend between throttle actuator signal and TPS. However, the throttle actuator signal is a signal that is generated by the ECU's control algorithm based on the running conditions. The signal is then processed by the actuator to a physical position. On the contrary, the newly added TPS signal is a direct feed signal, so there will be latencies between both signals. Due to these latencies only constant load runs give the clearest relation between these signals. During constant load the ECU and throttle are designed to be constant and approximately in the middle of the range, so that they have capacity available for load steps. During load steps the throttle is opened, up to maximum, to reduce restrictions and transition time. For these reasons is all generated throttle data exclusively focussed on the limited range of constant load, outside this range no data has been generated. Extrapolating this data to outside the known range has proven to be difficult. Outside the operational range only limited data can be reasoned at the extremes. The throttle actuator signal is generated by the ECU's control algorithm, which is hard to predict. The assumption is made that 100 [%] throttle actuator signal corresponds to wide open throttle and 0 [%] throttle corresponds to closed throttle. Giving indication to the complete range and going from extrapolation to interpolation.

The generated quadratic trendline between the available TPS and actuator data for different load settings (0, 100, 200, 300, 450 and 500 [kW]) shows a high coefficient of determination ( $R^2$ ) and looks visually like a good fit.

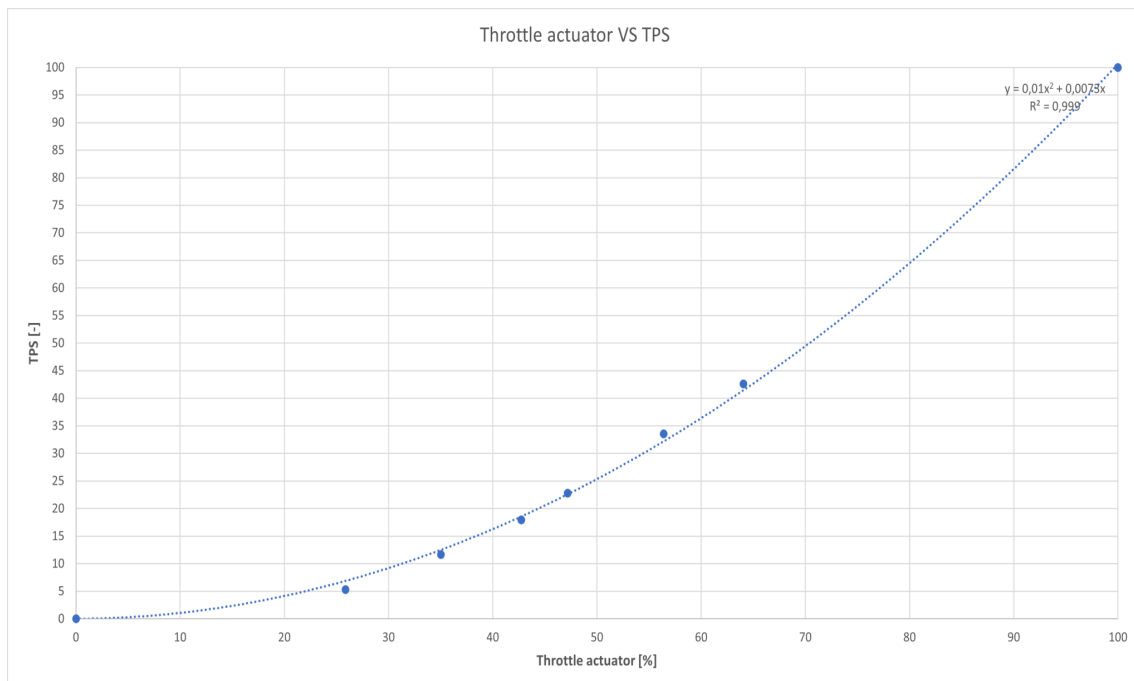


**Figure 6.2:** TPS against Throttle actuator signal.

So both the relations between the throttle valve angle to TPS and TPS to throttle actuator signal have been established. These relations can be combined to bypass the TPS and show the throttle valve angle to throttle actuator signal relation. This data can then be used in the validation phase as the model has been build using data that didn't include the TPS and only the throttle actuator signal. The combining of these relations did reduce the high coefficient of determination ( $R^2$ ) and visual fitment quality. However the throttle valve angle to TPS data is believed to be of higher quality as it is composed of more data over a wider range.

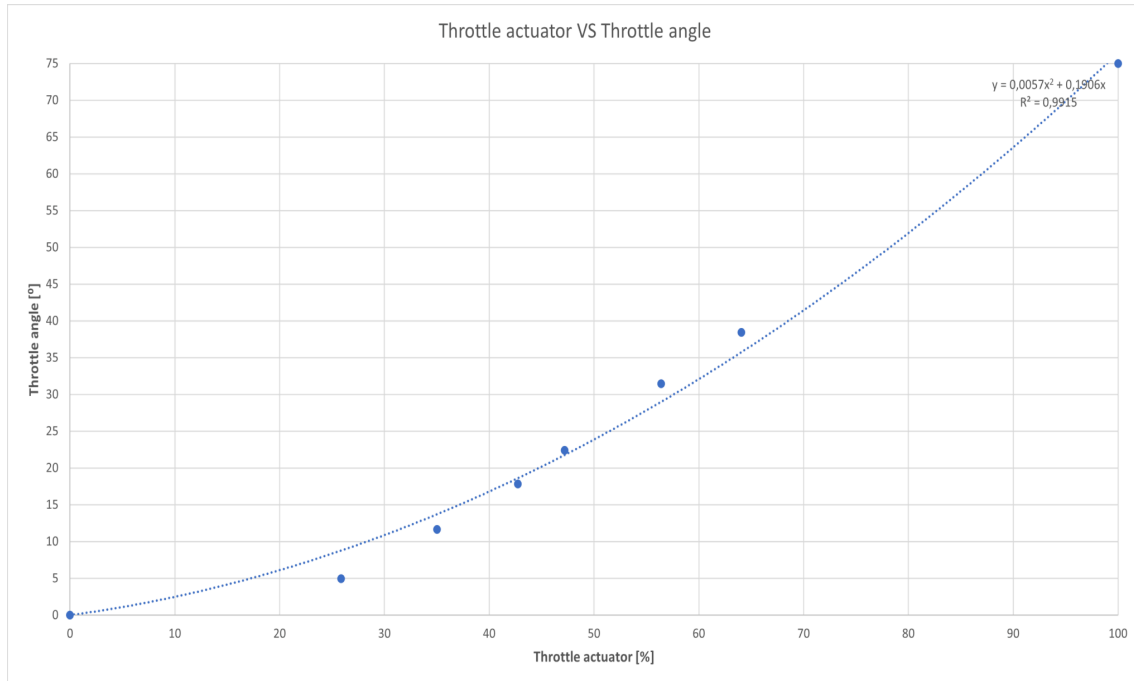


**Figure 6.3:** Angle of throttle against the Throttle actuator signal.

# 7

## Initial Validation Complete Model

### 7.1. Introduction

The methodology, as depicted in Figure 5.2, has been the main guideline for developing the model from scratch. The vast majority of data has been gathered by means of; geometric measurements, temperature readings, measurements of the stroke of moving parts, generated compressor maps, manufacturer specifications, and experimental data. Through this engine geometry, airpath design, fuel injection characteristics, turbocharger behaviour and combustion modelling have been implemented based on the best available data sources. Calibration efforts prioritized matching steady-state power output, mass flow rates, pressure ratios, and thermodynamic conditions within acceptable error tolerance of max.  $\pm 10$  [%].

During the building phase of the model a select amount of constant running conditions was used as a reference, namely the 500 [kW] and 300 [kW] run settings. The generated data from these measurements include the flow, pressure and temperature conditions in the air path on multiple crucial locations. These conditions have been used as a calibration target during the multiple stages of the model development, starting without turbocharger, only adding the turbocharger part by part. During each step the data from the aforementioned run settings was used as a reference to tweak certain parameters.

The empirical data of other constant run power settings is now added in the validation phase alongside the settings used during development. In total a number of six conditions are used, starting at 100 [kW] going up in increments of 100 [kW] to max power of 500 [kW] with an additional 250 [kW] as halfway point. These settings have been used as target input for both the control system of the CAT G3508a as the GT-ISE throttle controller in the model.

Data of multiple relevant condition parameters have been put together in a variety of parity plots. Ideally, all points should fall along the  $y = x$  diagonal line, which represents perfect agreement. The deviation from this line indicates the accuracy or error of the model. The additional error bands,  $\pm 10$  [%], are included to visualize deviations and to set an acceptable tolerance to the results. The dots represent each subsequent running condition, starting at 100 [kW], which is made red across all graphs for reference.

## 7.2. Steady state power

The steady state power indicates a nicely matching graph, as is expected. The control systems are using the same set power settings as target points, and thus both systems are able to produce comparable data. The exception here is that the GT-ISE model is not capable of producing 500 [kW] at max power setting. The controller is targeting for 500 [kW] and is only able to adjust the throttle valve. And as it undershoots its steady target it maxes the throttle to wide open throttle (WOT). The model is limited in other areas with regards to air flow and isn't regulated by the throttle at that moment, this leads to a reduced maximum power of the model. The predicted values are improved later on in chapter 8, please refer to Figure 8.1 for the updated version.

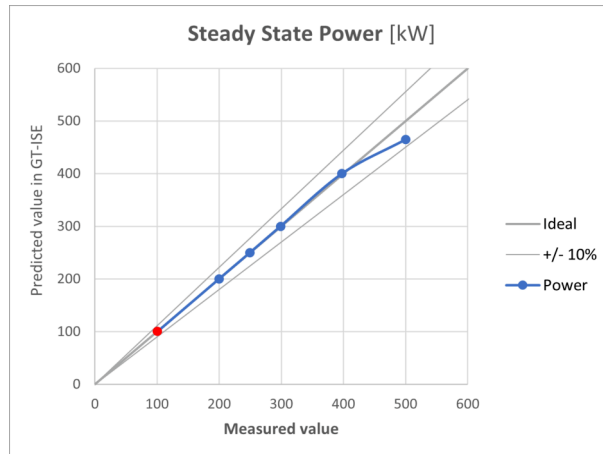


Figure 7.1: Steady state power, Predicted vs. Measured values.

## 7.3. Average turbocharger speed

The averaged speed of the shafts of both turbochargers of both engine banks is one of the last parameters that came available during the development. It was only during the last step that removed the fixed-speed drivers of the compressors and turbines for a floating turboshaft. Calibration of this parameter is very challenging as it is a circular dependant system, adjusting an incorrect input could introduce additional errors, leading to further problems under different operating conditions, as explained earlier. The predicted values are improved later on in chapter 8, please refer to Figure 8.2 for the updated version.

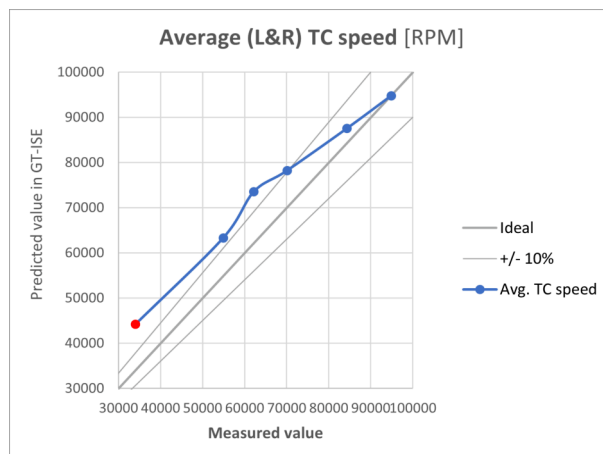
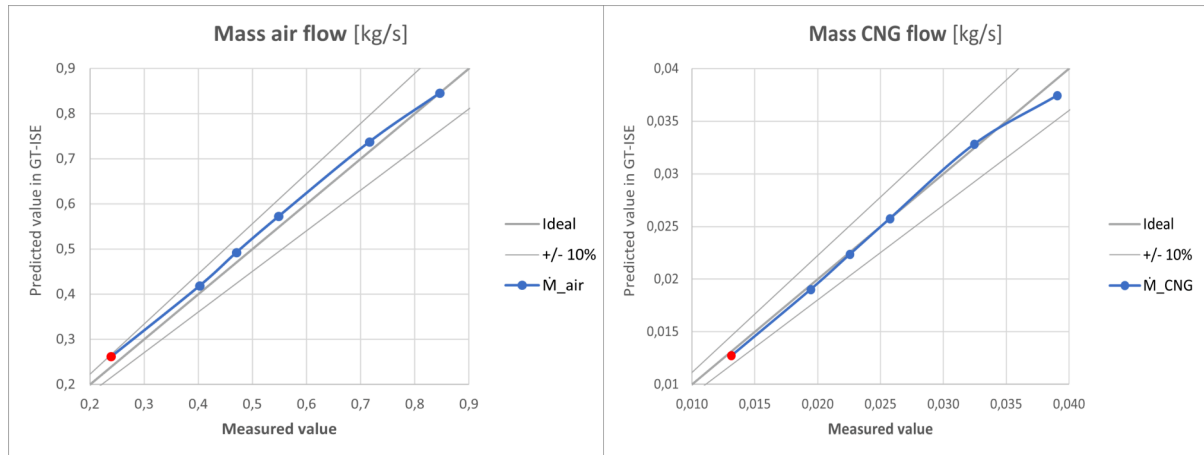


Figure 7.2: Average turbocharger speed, Predicted vs. Measured values.

## 7.4. Mass air flow and mass CNG flow

The mass flows of both air and CNG are in direct correlation with the power production as they define the energy flow in a similar way. The flows from the model both have a good match with the G3508a, with again the exception at max power. Where one can see that at max power the air flow of the model doesn't match the G3508a due to some restriction, more on that later. One can also see that the airflow of the model is slightly above ideal, where the CNG-flow is almost accurate, so the model would be running slightly leaner than the G3508a. Some additional tweaking of the fuel map might solve this. However, internal combustion engines are not very sensitive to slight AFR changes with regard to power production. Also it must be noted that the fuel injection is of the G3508a is based on MAP (Manifold Absolute Pressure) conditions in the inlet manifold, where as the model uses a MAF (Mass Air Flow) based injection based on flow condition at the injector, as explained in chapter 5. The predicted values are improved later on in chapter 8, please refer to Figure 8.3a for the updated version.



(a) Mass air flow, Predicted vs. Measured values.

(b) Mass CNG flow, Predicted vs. Measured values.

## 7.5. Pressure compressor in

The left and right averaged pressure that enters the compressors is very similar for both the model and G3508a. The model has a constant pressure that is a result of its boundary condition. The G3508a has some variance in its data as it is based on real sensors, hence its horizontal graph. Overall a maximum fault that is negligible.

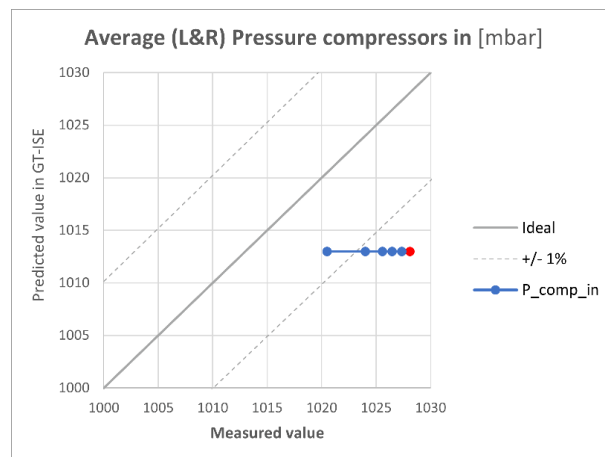


Figure 7.4: Pressure compressor in, Predicted vs. Measured values.

## 7.6. Pressure compressor out

The left and right averaged charge pressure that is produced by the compressors follows a similar trend for both the model and G3508a. The definition of the charge pressure that gets generated in the model is done by the compressor map, which is calibrated in the model on the 500 [kW] power setting. Overall an expected result when one also considers the mass flow and turbocharger speed charts. The generated pressure grows in error as on lower power settings, the origin of this error is likely found in the compressor map data.

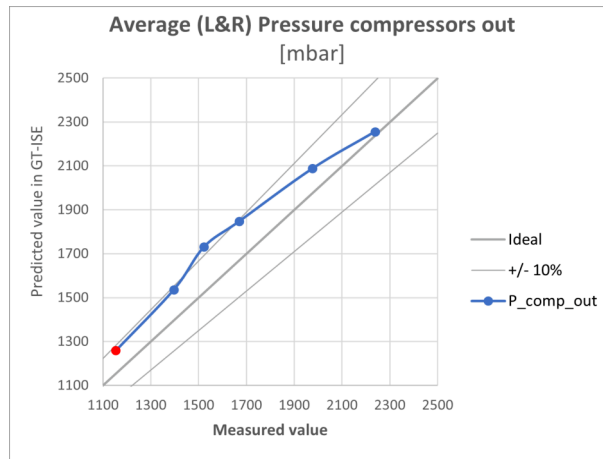


Figure 7.5: Pressure compressor out, Predicted vs. Measured values.

## 7.7. Pressure ratio compressors

This graph is a result of both graphs that are shown above, thus it follows a similar trend. As the error of the pressure that enters the compressors is small, only minor changes can be seen when compared to the compressor out graph.

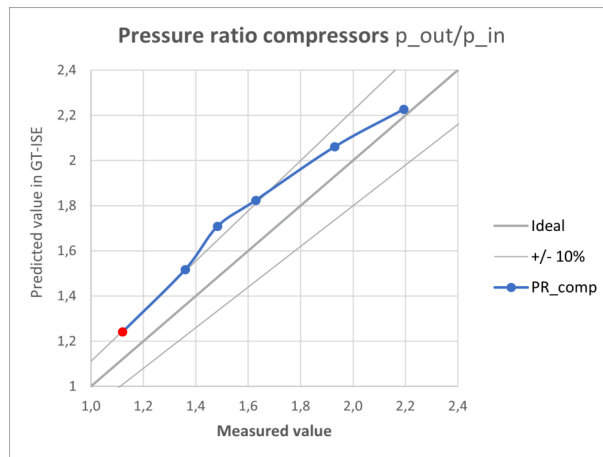


Figure 7.6: Pressure ratio compressor, Predicted vs. Measured values.

## 7.8. Temperature compressor in

The left and right averaged temperature that enters the compressors is very similar for both the model and G3508a. The model has a constant temperature that is a result of its boundary condition. The G3508a has some variance in its data as it is based on real sensors, hence its horizontal graph. Overall a maximum fault that is negligible.

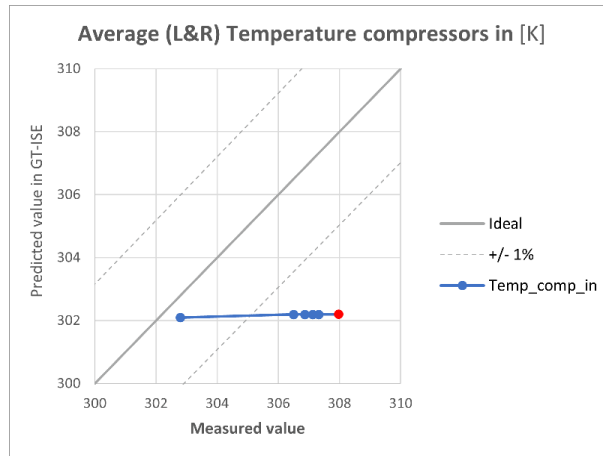


Figure 7.7: Temperature compressor in, Predicted vs. Measured values.

## 7.9. Temperature compressor out

The left and right averaged temperature that is produced by the compressors follows a similar trend for both the model and G3508a. The temperature takes on a similar trend as the generated pressure coming out of the compressors, this is to be expected as per ideal gas law.

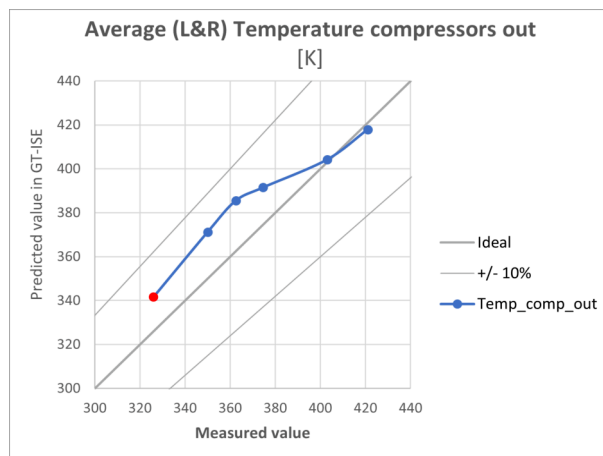


Figure 7.8: Temperature compressor out, Predicted vs. Measured values.

## 7.10. Pressure ratio aftercooler

The aftercooler part was created in an early stage of the development process of the model. The pressure differential over the aftercooler is relatively minor. However, a lot of care was taken to replicate reality as close as possible as the core is modelled using similar internal piping, as far as it is possible to see the core. Furthermore, the temperature differential over the aftercooler isn't graphed as there isn't a temperature sensor mounted directly after the aftercooler before the throttle. However, the modelled aftercooler is very effective in reducing the temperature of the charge air to the targeted 303 [K]. Too effective is concluded later, this is corrected in chapter 8.

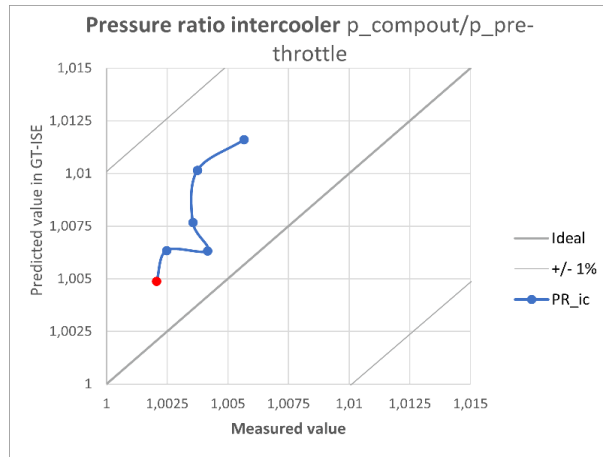


Figure 7.9: Pressure ratio aftercooler, Predicted vs. Measured values.

## 7.11. Pressure pre-throttle

The pressure directly after the aftercooler follows a similar trend for both the model as the G3508a. This is mainly a factor of the pressure generated by the compressors but is also altered by the reduced temperature after the aftercooler. Again it shows that the model was calibrated using the 500 [kW] setting.

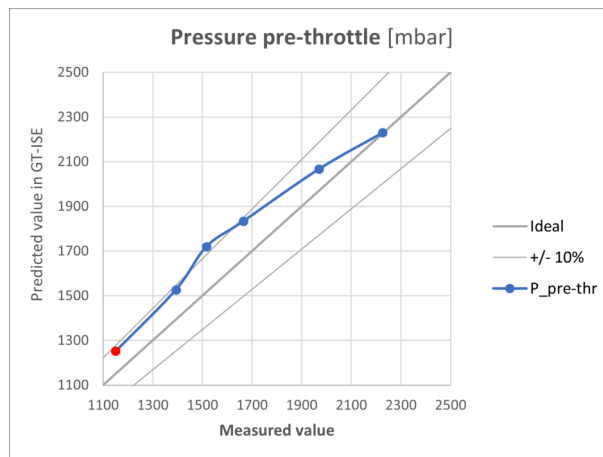


Figure 7.10: Pressure pre-throttle, Predicted vs. Measured values.

## 7.12. Pressure ratio throttle

The throttle's main objective is to be an adjustable restriction for the air path, thus regulate the mass air flow. The mass flow to the engine is within a satisfactory range due to the throttle setting. This is also depicted in the pressure ratio over the throttle. Which follows a similar trend for both the G3508a as the model. Notice here that the 100 [kW] setting (red dot) is in the top right, setting the highest pressure ratio, going down to lower ratios as the throttle opens for more flow and power. The modelled throttle being more restrictive in the lower power region and less restrictive towards max power, as the graph crosses the ideal diagonal.

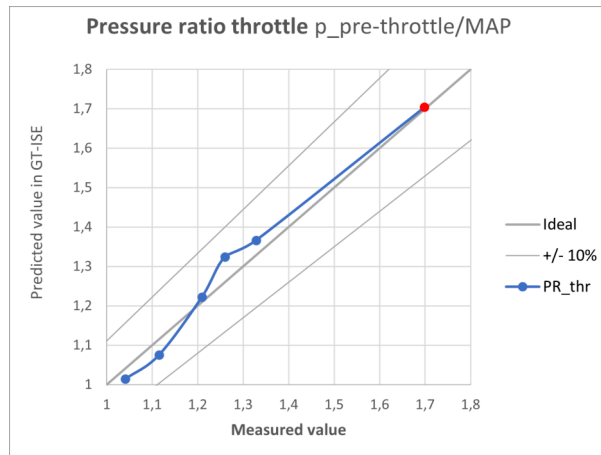


Figure 7.11: Pressure ratio throttle, Predicted vs. Measured values.

## 7.13. Manifold Absolute Pressure (MAP)

As the averaged generated pressure and all subsequent restrictions follow similar trends for both the model as the G3508a, it is to be expected that the resulting manifold absolute pressure would do the same. The model records show a MAP that is within a 10 [%] margin from the G3508a across the entire power sweep.

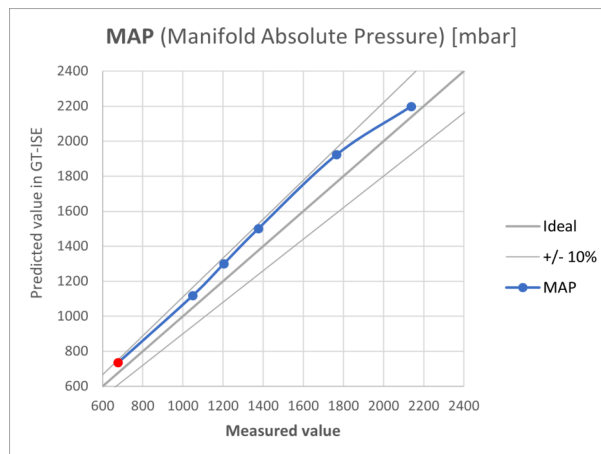


Figure 7.12: Manifold absolute pressure, Predicted vs. Measured values.

## 7.14. Manifold Air Temperature MAT

The charge temperature in the inlet manifold is close between the model and G3508a, differing by 2 to 8 degrees [K]. The model having a slightly cooler mixture than the reported MAT temperature in the G3508a. This could be explained by the fact that the modelled aftercooler is too effective. Or what could also play part in this is the fact that the inlet manifold is mounted inside the V-shaped engine block. The surface of the block at operating temperature will range from 80 to 90 degrees [C]. The increased temperature of the internal surface of the inlet manifold will increase the charge temperature through conduction and convection. This increased temperature of the inlet manifolds surface is included in the model, however the thermal behaviour of the inlet manifold can be manipulated through the 'Heat Transfer Multiplier' for further optimisation. The predicted values are improved later on in chapter 8, please refer to Figure 8.4 for the updated version.

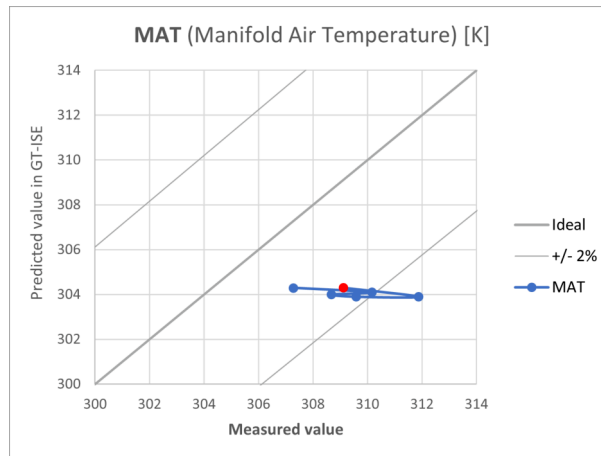


Figure 7.13: Manifold air temperature, Predicted vs. Measured values.

## 7.15. Pressure ratio cylinders

As the back pressure increases, the mass of the residual gas increases as well. And even though this engine can be classified as a non-overlap engine, the small overlapping of the valves will initiate negative scavaging of the cylinders and airpath. This will be very detrimental for the power development as the amount of fresh charge in the cylinders will be reduced. It can be seen that this effect is greatest going towards max power. The trend takes a turn and the pressure ratio over the cylinder in the model stagnates.

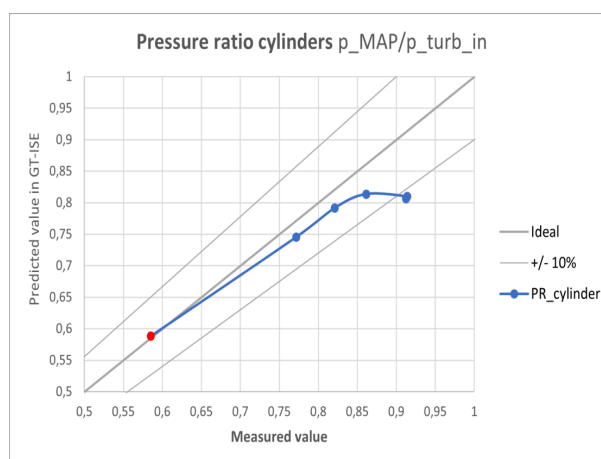


Figure 7.14: Pressure ratio cylinders, Predicted vs. Measured values.

## 7.16. Pressure turbines in

The left and right averaged back pressure that is produced by the turbines restriction follows a comparable trend for both the model and G3508a, yet it shows a growing error, deviating from the ideal towards the 500 [kW] mark. The definition of the back pressure that gets generated in the model is done by the turbine map. It is assumed that the turbine mapping and its subsequent back pressure is the origin of the restrictive nature of the model, thus the reason why it doesn't reach its target max power.

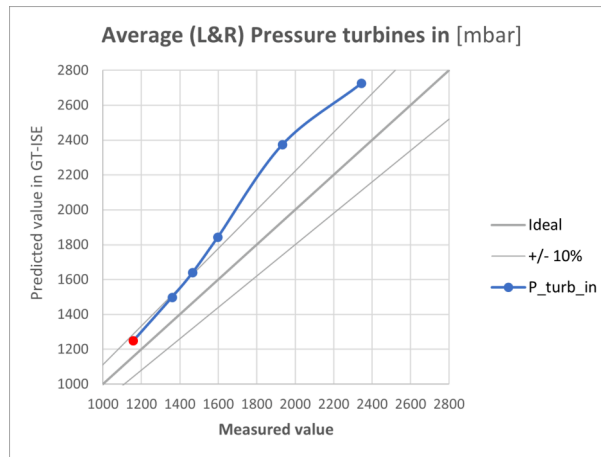


Figure 7.15: Pressure turbine in, Predicted vs. Measured values.

## 7.17. Pressure turbines out

The left and right averaged back pressure aft of the turbines is a result of the downstream exhaust system. The G3508a has an entire exhaust system that includes a heat recuperation system that may introduce restrictions that aren't taken into account in the GT-ISE model. The boundary conditions of the exhaust can however be adjusted to suit a higher back pressure. However, even after adjustment the nature of the modelled back pressure will be the same, showing a fairly constant value. That hasn't been done to not further deteriorate the power production, as the pressure gradient over the turbine would increase even further.

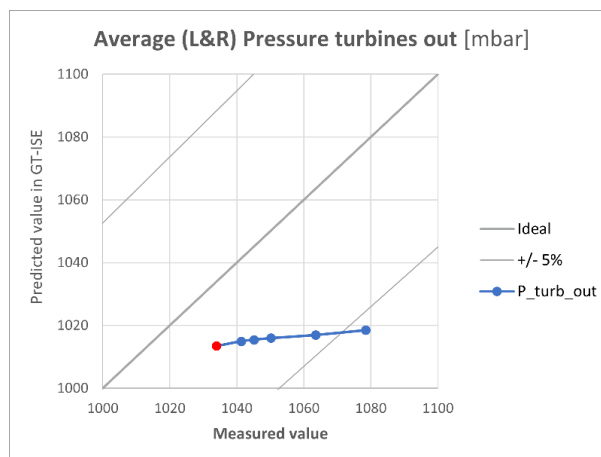


Figure 7.16: Pressure turbine out, Predicted vs. Measured values.

## 7.18. Pressure ratio turbines

This graph is a result of both turbine graphs that are shown above, thus it follows a similar trend. The error grows as the error of the pressure that enter and exits the turbines get added. Visually only minor changes can be seen when compared to the turbine-in graph, see Figure A.10. The trend is still similar. However, the error grows to proportions that need to be taken into consideration.

The deviation of the pressure ratio of the turbines is likely a direct result of the vertical nature of the speed lines of the turbine mapping. The vertical nature implies that a change of the mass air flow as a smaller effect on the pressure ratio when compared to a more horizontal nature. Both the turbocharger speed as the mass flow are within acceptable margins so the resulting deviation of the pressure ratio towards the higher mass flows through the turbines is seemingly a direct effect of the vertical nature in the turbine mapping. The predicted values are improved later on in chapter 8, please refer to Figure 8.5 for the updated version.

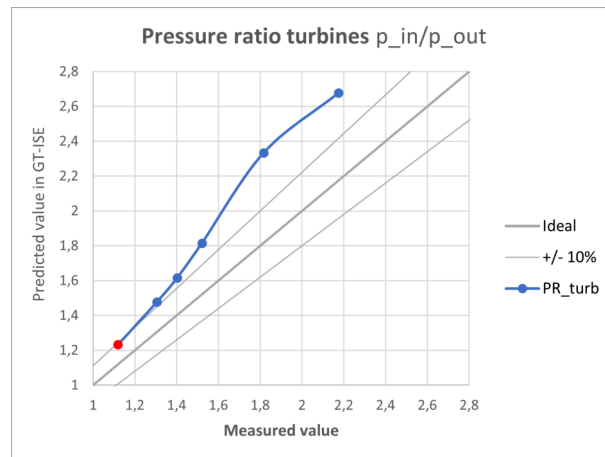


Figure 7.17: Pressure ratio turbine, Predicted vs. Measured values.

## 7.19. Temperature turbines in

The left and right averaged entry temperature of the turbines is directly correlated to the EGT. The optimization tool that was used for determination of the Wiebe parameters targeted the specific EGT for the max power setting. This seems to still be accurate for the final model after inclusion of the turbocharger. However, the error in EGT grows when going away from max power. It is challenging to diagnose the origin of this deviation accurately. The turbine mapping could be the source, or maybe it is beneficial to let the Wiebe parameters vary across the various power settings. The Wiebe parameters have been updated to vary across the various power settings, this is done in chapter 8 refer to Figure 8.6.

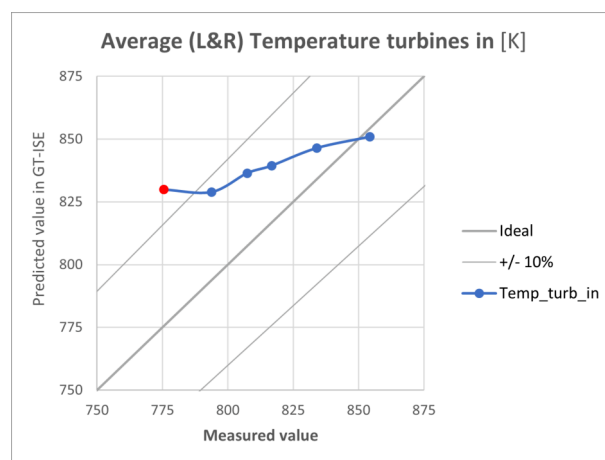


Figure 7.18: Temperature turbine in, Predicted vs. Measured values.

## 7.20. Temperature turbines out

The left and right averaged exit temperature of the turbines shows a trend that is almost tangential to the ideal diagonal, which is somewhat apprehensive. The error seems to decrease as the power setting is increased. However, a raised post turbine temperature indicates an excess in enthalpy that is wasted in the model. This could be a reason why the model requires the 'Efficiency Multiplier' in the turbine object for compensation of the lost power potential. Likewise with the entry temperature it is assumed that this is down to either the Wiebe parameters or the turbine mapping. The predicted values are improved later on in chapter 8, please refer to Figure 8.7 for the updated version.

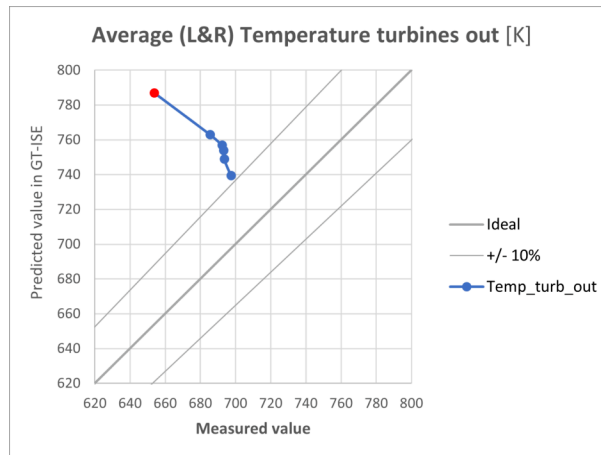
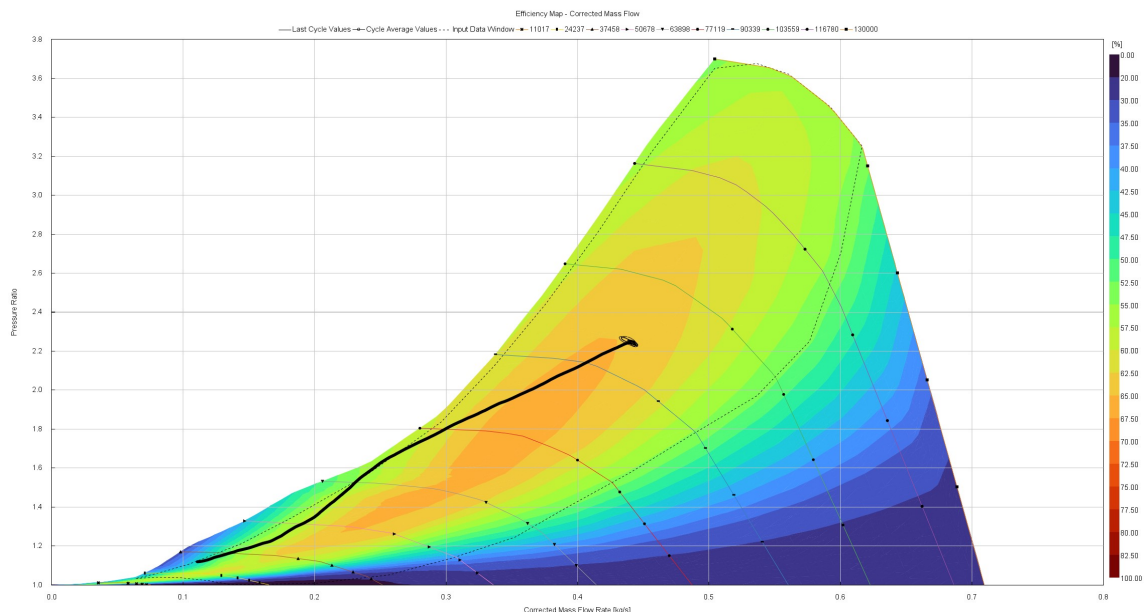


Figure 7.19: Temperature turbine out, Predicted vs. Measured values.

## 7.21. Compressor maps

The compressor maps below show the generated efficiency map with pressure ratio plotted over corrected mass flow [kg/s] with constant speed lines included. Included is the workline in black that indicates every static running condition (dynamic conditions may deviate from the workline). The exact behaviour of the compressor on bank 1 is differing from bank 2, which is remarkable. Both have compressors share extremely similar running conditions, geometrically the only difference being the length and bend radius of the charge pipes down to the aftercooler, aside from each of them being powered by their individual turbine. But, the conditions just before the turbines are equalized as there is a pipe that joins both exhaust manifolds. Reason for concern is the fact that the workline edges or ever so slightly crosses the stall or surge line. The work line as measured from the G3508a doesn't intersect the plotted input data, as explained in subsection 5.4.3. This could be due to the fact that the Stapersma generated compressor maps are differing from reality. This presumably is the main reason for the differing worklines between measured and predicted. However, the positioning of the stall or surge line has been chosen arbitrarily, also explained in subsection 5.4.3.



**Figure 7.20:** Resulting operational line plotted on the compressor map of bank 1 in GT-ISE.

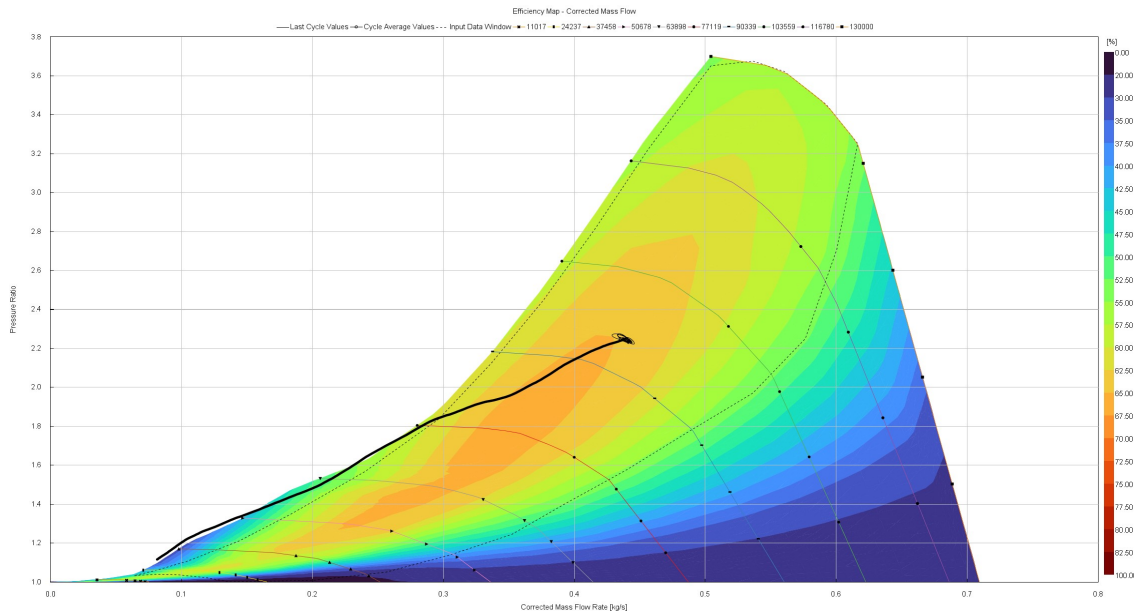


Figure 7.21: Resulting operational line plotted on the compressor map of bank 2 in GT-ISE.

## 7.22. Turbine maps

Taking any conclusions from the turbine maps has turned out to be challenging. The turbine mapping shows a fairly slim range and the traces of the steady state operational point of just one power setting cover a wide range. Both turbine reports display this behaviour for the entire range of power settings. The generated efficiency maps show mass flow [kg/s] plotted over a wide extrapolated range of pressure ratios. Still, the back pressure generated by the turbines is excessive and the resulting exit temperature of the exhaust gas indicate that the available exergy isn't as effectively captured by the modelled turbines as the G3508a turbines.

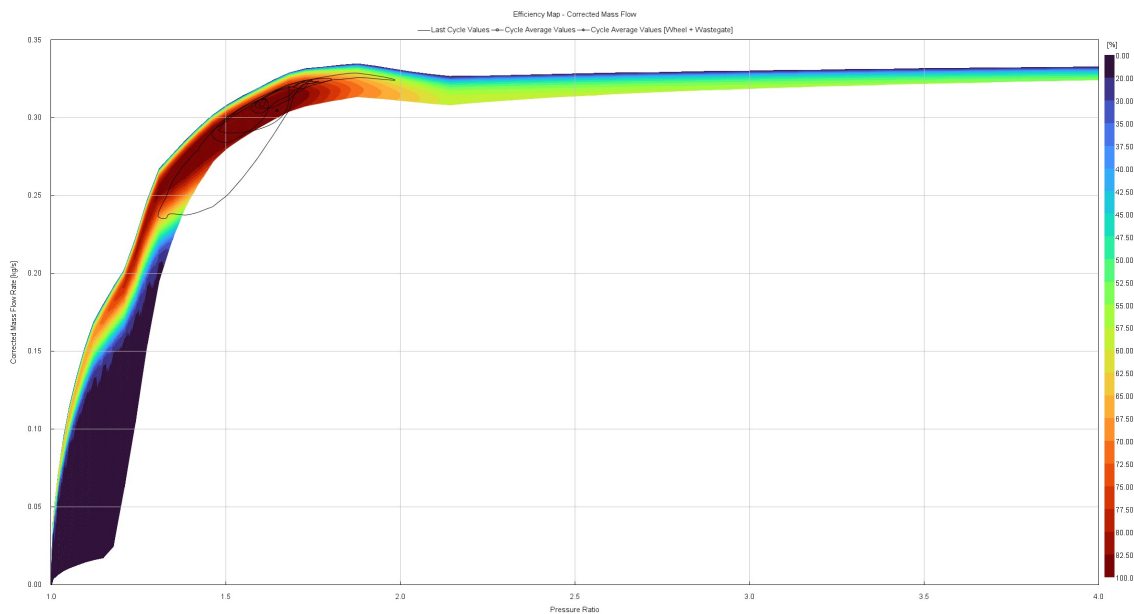


Figure 7.22: Turbine map map of bank 1 in 250 [kW] setting in GT-ISE.

## 7.23. Turbocharger speed

Shown in Figure 7.23 is the recorded speed of the turbocharger of bank 2 as the engine performs a load step from 450 [kW] to 500 [kW], depicted is speed in [RPM] vs time in [sec]. What is interesting here is the oscillating nature of the speed line. The hypothesis here is that this is due to the fact that the engine has a crossplane crankshaft. The speed line has approximately 12.5 peaks in every second, this works out to 750 every minute. As the engine runs it cycles its combustion cycle 750 times each minute because it's a 4-stroke engine running at 1500 [RPM]. So every two rotations of the crankshaft the turbocharger peaks in its speed. This is likely due to the unequal spreading of the exhaust pulses of the cylinders that are mounted in one single bank. As the engine runs it fires its cylinders with a firing order of 1-2-7-3-4-5-6-8. And as the cylinder count order alternates between each bank, having the odd cylinders on one bank and the even on the other bank, it doesn't alternate firing evenly from bank to bank. It fires cylinder 7 and 3 sequentially on bank 1 (L or left), same for cylinder 6 and 8 on bank 2 (R or right). So the engine fires the banks in order of L-R-L-L-R-L-R-R. This means an unequal spacing of the exhaust pulses. Thus consequently of the crossplane firing order receives each exhaust manifold of each bank thus an unequal exhaust pulsing of 180-90-180-270 crank angle. It's this short phase pulse of 90 [CA] followed by a longer phase pulse of 270 [CA] that is likely the origin of the speed variance. Whether the amplitude of each peak is accurate is questionable. The model does take the inertia of the rotating assembly of the turbocharger into account. If this oscillating behaviour would occur on the CAT G3508a it would certainly be very difficult to measure, since getting average speed indication of the turbochargers was quite a challenge, let alone variations of the speed over a single cycle. Additionally, the exhaust manifolds are linked together by a small pipe, whether that is entirely effective in equalizing the conditions between each bank seems questionable (at least in the model). If it would be fully effective in equalizing the conditions then the speed line should probably not show this oscillating nature, and also then would both compressors probably show more equal behaviour.

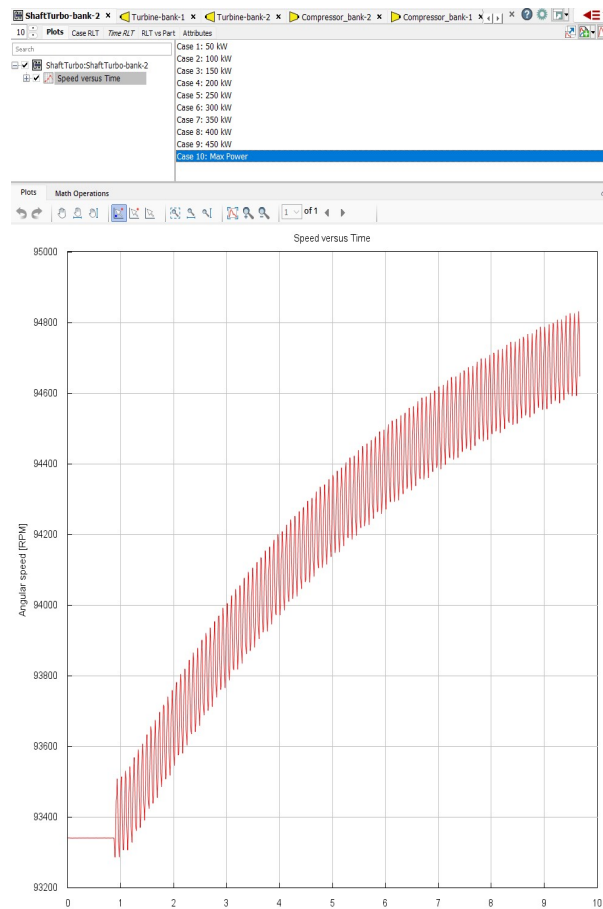
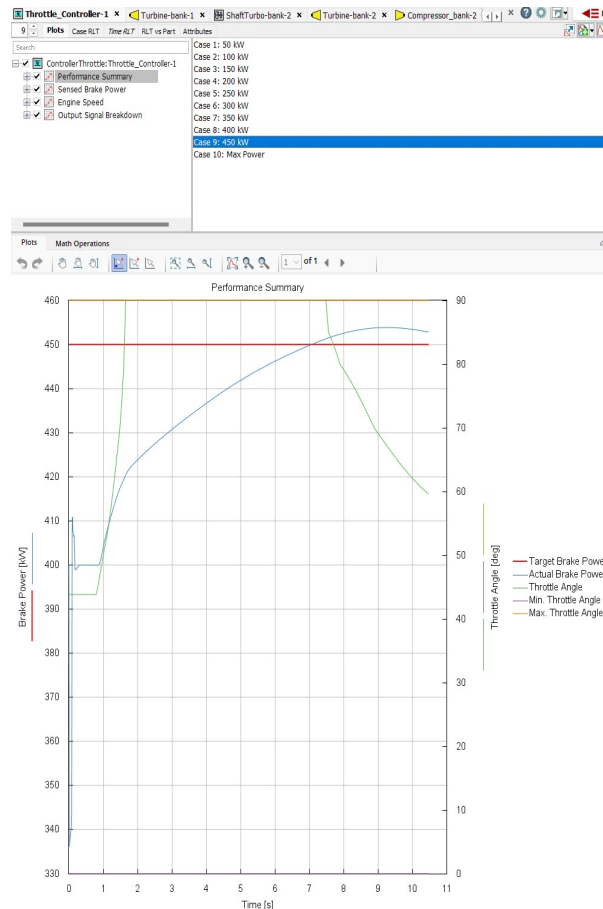


Figure 7.23: Turbocharger shaft speed during transient operation to 500 [kW] setting in GT-ISE.

## 7.24. Validation and connection of throttle theory.

Shown below is the performance summary of the throttle controller object in GT-ISE. The controller integrates a model-based feed-forward controller with a continuous feedback controller. Some relevant data of the controller is displayed, data it uses to determine its action. What is of interest with regards to the throttle theory is the final valve angle, which is the end point of the green line.



**Figure 7.24:** Readout of the throttle controller during transient operation to 450 [kW] in GT-ISE

The final valve angle of its stable running condition has been put together for various running conditions of the model. Same has been done for a data set from measurements of the G3508a that includes the new TPS sensor. This is a different measurement data set when compared to the one used earlier in the validation, as this new differing set includes the TPS data. This data set has been generated on power settings 100, 200, 300, 450 and 500 [kW]. The resulting throttle valve angle data has been put together in a parity plot. In this parity plot is the diagonal not equal to  $y = x$ . Due to the fact that the throttle on the G3508a has a stroke of 75 degrees and the model uses a throttle that has a 90 degree domain. Still when assuming a throttle with a smaller domain scales linearly the resulting graph should fall on the ideal diagonal.

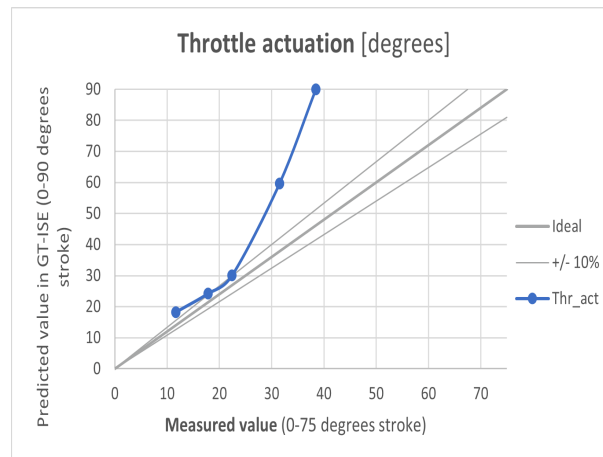


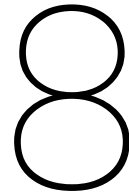
Figure 7.25: Throttle actuation, Predicted vs. Measured values

Drawing conclusions from this diverging behaviour is challenging. During the throttle correlation study chapter 6 it has been discovered that there are certain non-linearities between the strokes of the installed TPS and throttle valve angle. These non-linearities could likely mainly be attributed to the throttle actuation mechanism itself and partly to the mounting of a linear positions sensor on a part that follows a circular trajectory.

However, the throttle of the G35508a actuates to just above half its stroke where the model needs wide open throttle (WOT). This could be for several reasons; firstly, the discharge coefficients could be differing. Secondly, the assumption of linear scaling from 75 degrees to 90 degrees could be faulty. Thirdly, the throttle of the G3508a is mounted directly after a 90 degree elbow in the airpath. It is likely that this introduces a lot of turbulence in the airflow. These by definition are 3-dimensional effects, GT-ISE is only capable of modelling a single dimension, thus purely neglecting the possibility of turbulence.

The main takeaway of this is that the main objective of the throttle is still achieved as both the model as the G3508a have very similar mass flows and pressure gradients over the throttle valve. This is effectively regulated by throttle controllers, the fact that the resulting valve angle differs might not be a factor of great relevance. With regards to the model maxing out the throttle to WOT; when restrictions are eliminated that prevent the simulation of achieving its target max power of 500 [kW], it is likely to assume that the throttle controller object can successfully regulate the throttle to maintain this target.

Another takeaway from this study is probably the method to go about determining the throttle angle. The double conversion from throttle angle to TPS and subsequently from TPS to actuator gives room for error and is based on a relative narrow operational domain of data. A much more accurate way to determine the throttle angle is to measure the throttle angle directly. There are many circular potentiometers available on the market that are capable of connecting to the throttle assembly. This takes away all conversion errors. Additionally, this would make it possible to view a live readout of the throttle angle without the need of time averaging the data. These type of sensors are typically plenty quick enough to keep up with the 0.2 [sec] data monitoring interval of the system.



## Last Iteration And Re-validation

During the development and validation stage some aspects came to light that showed there was still room for further advancement of the calibration. Certain parameters were determined early-on in the model design process and it is deemed beneficial to revise them for two reasons. Firstly, the variance of parameters can give an indication of the robustness or delicateness of the model. When a certain variable is altered in a complex model, like build here, it will undoubtedly have secondary effects on numerous other parameters. The resulting secondary change gives an indication on the robustness. Secondly, some of the models assumptions can be tweaked as the model has gotten more and more complete and more and more resulting data can be assumed as stable, thus the comparison between real and model data can be validated and assumed reliable.

Still, when looking at the data of the turbine entry temperature the interest for a better quality match couldn't be ignored. During the development of the incylinder model the assumption was made that the Wiebe parameters could stay constant across the entire load setting range. This seemed reasonable during the development stage as the non-turbocharged 500 [kW] and 300 [kW] models that were used for development and calibration did seem reliable and consistent with constant Wiebe parameters. The turbine entry temperature for low load settings diverged as the model developed, showing raised values in the model when compared with the measured value. This is the case even though the air-fuel-mixture-flow and break-power figures were seemingly quite accurate. So the chemical energy flow in the intake and the mechanical energy flow are corresponding and proportioned correctly, the available exergy in the exhaust flow was not following the same trend.

The exhaust exit temperature is also indicating a miscorrelation between the model and reality. The entry temperature shows a trend that deviates from the desired measured values. The exhaust gasses are expanded in the turbine and the available exergy should be recuperated as mechanical energy. Naturally, the turbines exit temperature very reliant on the entry temperature. However, the turbine exit temperature shows an even greater deviation when compared to the entry temperature, indicating that the turbine mapping is differing from reality. This can be proven by improving the quality of the turbine in temperatures. The increase in the deviation indicates that the turbine in the model doesn't adequately capture the exergy, so energy is lost in the exhaust gases that exit the model. This raised exit temperature and its increased error when compared to the entry temperature could be an explanation for the abnormal 'Efficiency Multiplier'. The tutorial mentions that a normal range for this factor should be from 0.95 to 1.05 [-], but during the development a value of 1.12 [-] has been selected. The 'Efficiency Multiplier' of 1.12 [-] indicates a measure to compensate for this inaccuracy.

To remedy this the model in the previous validation has been revisited and the Wiebe parameters have been adjusted. The method for the determination of the Wiebe parameters has been done with largely the same method as earlier. The optimizer in GT-ISE was utilized to determine the correct set of Wiebe parameters for each load setting where possible. To do this the throttle controller in the model was modified. The controller was changed to be regulated by mass air flow based on validated flow data from the previous latest measurement. This flow data was within satisfactory margins and

mass air flow in SI engines is naturally directly related to power production. The mass flow throttle was verified to produce the same results as the power throttle. This modification was done to exclude the throttle actuator from interfering with the optimizer as the controller was originally power regulated and the optimizer is altering values to target a certain power figure, thus the controller and optimizer would interfere with each other. Then the optimizer was run to optimize the Wiebe parameters for power settings 100, 200, 250, 300, 400 and 500 [kW]. Targeting for the measured values of the turbine entry temperature on bank 1 and the desired break power. As the throttle is now mass air flow regulated not much should change on the intake side and the energy flow in the mass air-fuel-mixture flow should be very similar. The Wiebe parameters then determine how the energy flows from the cylinder onwards, to either mechanical power or to the available exergy for the turbine in the exhaust flow.

The optimizer was able to find better Wiebe parameter values for all power settings except the 300 and 500 [kW] settings. For these the optimizer converged to the same values as earlier after numerous iterations; 37.9, 45.8 and 2.24 for the 'anchor angle', 'duration' and 'Wiebe exponent' respectively. For all other power settings the optimizer was able to find new parameters that were able to match the desired target turbine entry to a better degree. Varying the 'anchor angle' down to 27.75 [ATDC], the 'duration' down to 36.47 [CA], and the 'Wiebe exponent' to 2.11 [-], all relative to the initial values mentioned earlier, with some values in-between.

Power target [kW]	100	200	250	300	400	500
Actual power [kW]	101,00	200,00	249,64	298,87	397,67	500,43
Anchor angle [ATDC]	27,75	34,21	34,20	37,90	35,00	37,90
Duration [CA]	36,47	39,47	42,20	45,80	37,60	45,80
Exponent [-]	2,17	2,14	2,24	2,24	2,11	2,24

**Table 8.1:** Wiebe parameters for all load cases

The Wiebe parameters vary a bit for all power settings. With these parameters the model is better able to target the specified turbine entry temperature, while producing similar power figures and not deviating other measures significantly. These Wiebe parameters have been put into the model in the 'Case setup' and are now varied by the cases for load setting. Afterwards the throttle has been remodified to be regulated by power like it was previously. The correlation between power-regulated throttle and mass-air-flow-regulated throttle has also proven to be reliable in this instance as even the mass air flow shows a better match between the newly predicted and original measured values. The variance of these parameters have shown that the model does in fact run robust on multiple set parameters and doesn't show unstable behaviour that was seen during development, like run-away turbochargers speeds.

Other specifications and settings have also been adjusted additional to the optimization of the Wiebe parameters. This was done separately after the results of the Wiebe parameters were assessed and validated, to keep track of the influence of each alteration. The manifold air temperature was deemed sub-standard. The absolute error was only within a couple degrees and the targeted temperature was set to the same target as the G3508a's aftercooler system. The adjustment of this value is of relative ease that a better match could easily be realised. Additionally, during this study it became clear that the accepted conrod length was in-fact faulty. The accepted conrod length of 861 [mm] was incorporated into multiple studies and was also used a setting in the 'MCAT' system that controls the G3580a behaviour. This length has been reevaluated and estimated to be approximately 380 [mm] after some suspicions on its length were raised. This adaptation has been incorporated into the model. However, this adaptation is expected to have very minimal effect on the operational quality of the model. The conrod length is primarily related to the in-cylinder model. Specifics of this level of the in-cylinder process are not within the main focus of this study, so alterations are expected to have minimal impact. It would change the in-cylinder volume to crank angle relation, also changing the PV-diagram. It would also change the secondary balance character of the engine as the piston moves in a less harmonic manner as the conrod length comes down from infinity. Again, these conrod related aspects are not the primary focus of this study, still it is corrected.

## 8.1. Re-validation

Afterwards, the model has been re-validated and shows improved turbine entry temperatures at the targeted power settings. The graphs with the most notable change are briefly covered below. All graphs that aren't covered showed aren't relevant for this change or showed too little change to be of any significant interest, they are however included in the appendix. The orange line displays the latest iteration with the 'name3' reference. The power settings are identical as the initial validation, starting with the red dot at 100 [kW], increasing to 200, 250, 300, 400 [kW] and finalizing at max power (=500 [kW]).

### 8.1.1. Updated steady state power

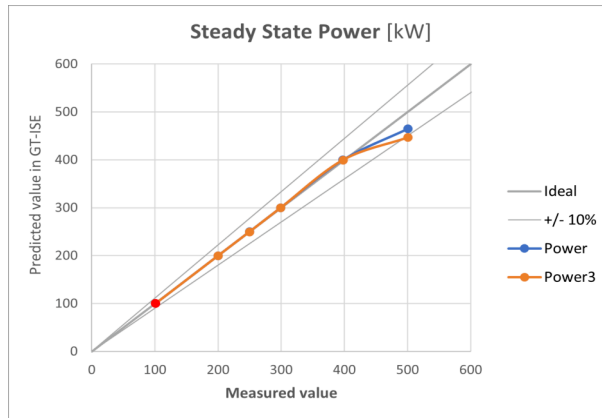


Figure 8.1: Steady state power of previous (blue) and latest iteration (orange), Predicted vs. Measured values.

Steady state power doesn't change much as would be expected since both iterations were run with a throttle controller that targeted a specified power output. The notable difference happens at max power, where both iterations max out at WOT. However, both iterations share the same Wiebe parameters, so the differing factor here is the risen MAT. A lower power as a consequence of a higher MAT makes sense. A rise in temperature lowers the air density, decreasing the energy flow, thus the power goes down.

### 8.1.2. Updated average turbocharger speed

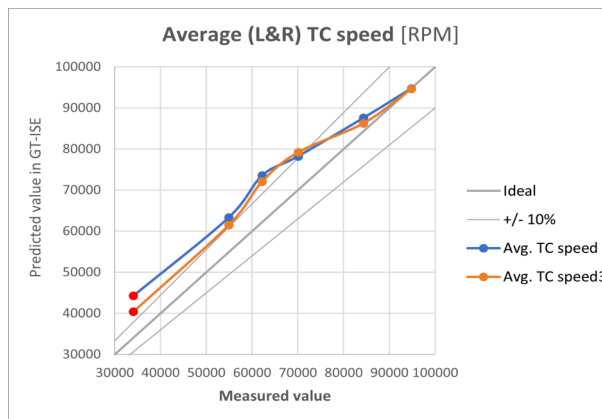


Figure 8.2: Average turbocharger speed of previous (blue) and latest iteration (orange), Predicted vs. Measured values.

The turbocharger speed beautifully displays the effect of what the recalibration of Wiebe parameters has done. The target was to reduce the turbine entry temperature, thus reduce the available exergy for the turbine to recuperate. It is within expectations that a better matching exhaust gas exergy would reduce the overshoot of the turbocharger speed. This is achieved for all power settings except the 300

and 500 [kW] mark, where the optimizer was unable to find a better solution than the first iteration. On the 300 [kW] mark it can be seen that it even displays a higher overshoot, as a consequence of the risen MAT.

### 8.1.3. Updated Mass air flow and mass CNG flow

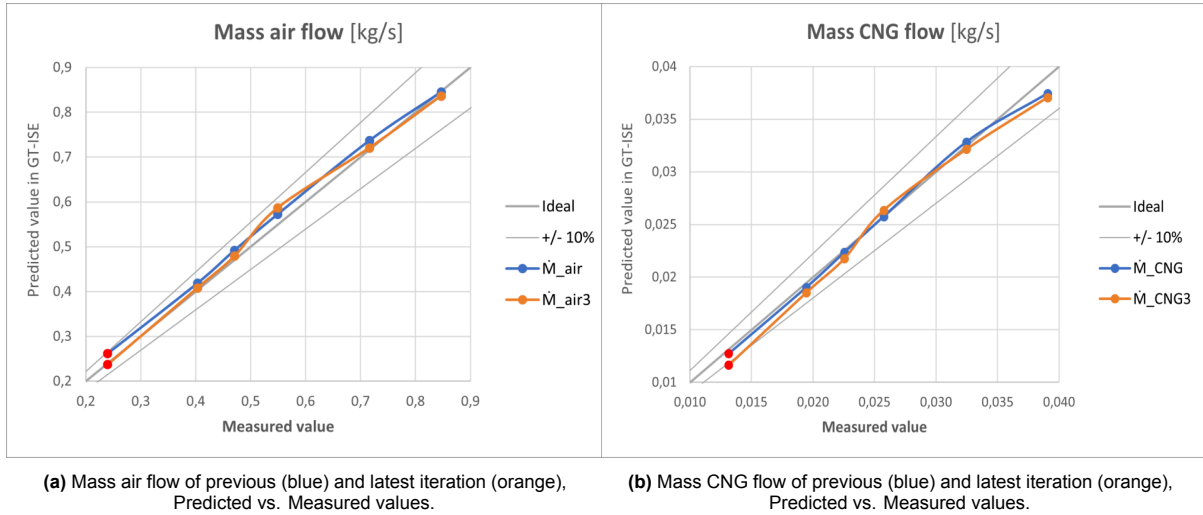


Figure 8.3: Updated mass flows.

The mass air flow shows similar behaviour. Presumably as a consequence of rebuilding the model to be throttled by mass air flow during the optimization, makes it an almost perfect match. Again with the exception of the 300 [kW] mark, which suffers from a risen MAT at the initial Wiebe parameters. The CNG mass flow is offset with the same proportion as it is directly related to the mass air flow in the fuel mapping. The error could be a result of errors in fuel mapping or measurement accuracy for example

### 8.1.4. Updated Manifold Air Temperature MAT

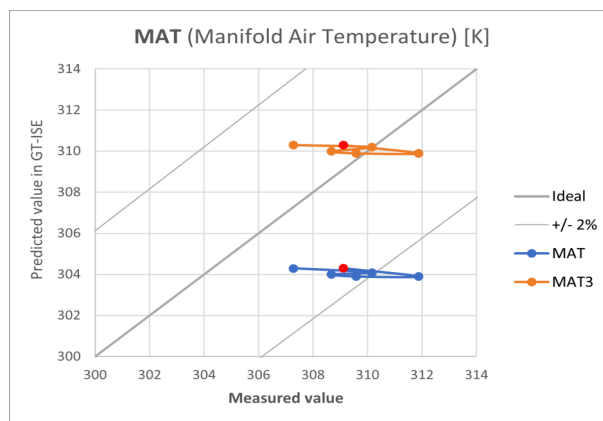
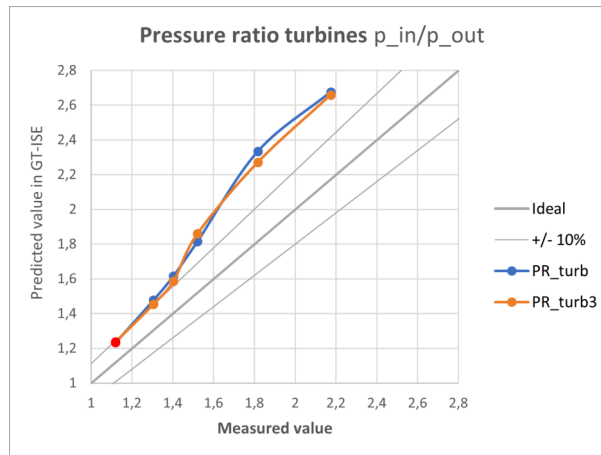


Figure 8.4: Manifold air temperature of previous (blue) and latest iteration (orange), Predicted vs. Measured values.

The MAT shows behaviour that is to be expected as it is manually corrected. The horizontal nature of the line is a result of the model being more stable in forcing the MAT to its targeted set point. The measured value still varies in an acceptable region, but is not predictable. This is presumably a consequence of hysteresis in the electrical control system of the G3508a's aftercooler system.

### 8.1.5. Updated average pressure ratio turbines



**Figure 8.5:** Pressure ratio turbine of previous (blue) and latest iteration (orange), Predicted vs. Measured values.

The pressure ratio over the turbine displays similar behaviour, although the effect isn't as profound as one might expect. The calibration of the Wiebe parameters for all power settings except 300 and 500 [kW]. The limited effect the recalibration had on the pressure ratio is confirmation for the suspicion that the turbine mapping isn't reliably accurate.

### 8.1.6. Updated average temperature turbine in

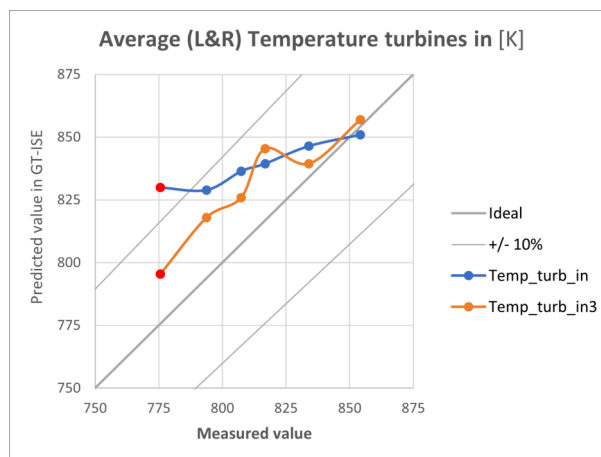


**Figure 8.6:** Temperature turbine in of previous (blue) and latest iteration (orange), Predicted vs. Measured values.

The turbine entry temperature best shows the effectiveness of the new calibration, again with the exception of the 300 and 500 [kW] marks. The new iteration show a much improved trend, indicating how effective the Wiebe parameter recalibration was. Making the model more reliable and better fit for purpose.

### 8.1.7. Updated average temperature turbine out

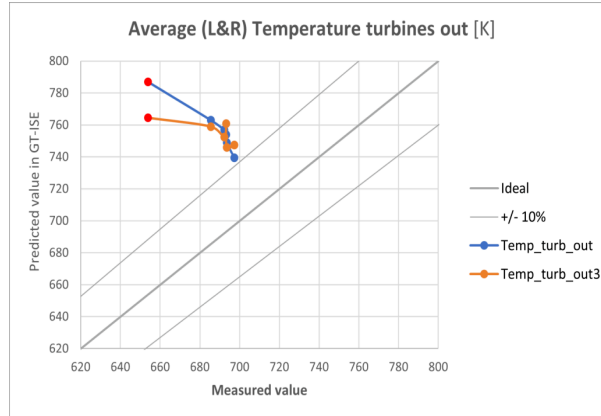


**Figure 8.7:** Temperature turbine out of previous (blue) and latest iteration (orange), Predicted vs. Measured values.

The turbine exit temperature doesn't show as great effect as one might expect. This again is presumably due to the turbine mapping. There are seemingly very little alternatives to correct the turbine exit temperature drastically other than a revision of the turbine mapping.

Generally, the optimized Wiebe parameters have had an advantageous effect on nearly all measures that are used in the validation. Nearly all measures improved in trend and/or accuracy, although these changes are mostly marginal. The MAT had an opposing effect, some measures diverging from the ideal diagonal. This is to be expected as the increased temperature also increases the respective pressures. An increased MAT also translates to an increased in-cylinder temperature and increased exhaust gas temperature. Additionally, an increase in temperature in the intake air decreases the air density and thus lowers the maximum power of the engine as it maxes out at WOT. Finally, the deviation of the exhaust exit temperature mostly remains after correction of the entry temperature by the Wiebe parameters iteration. Indicating at a turbine mapping that is insufficient in accurately capturing the correct turbine behaviour.

## 8.2. Validation conclusion and model assessment

During the development of the model a lot of effort was put in to make the model as complete, versatile and accurate as possible. The engine has been piecewise evaluated and remodelled in the GT-ISE software, focussing mainly on the air path. Inspiration on the building method was taken from the GT-ISE tutorial. However, naturally the tutorial itself does not describe how to model the G3508a specifically. The vast amount of data that was needed to make up the model was gathered via numerous methods, including but not limited to; physical (geometric and thermal) measurements, product guide, engine manuals, GT-ISE tutorials[37], cross-sectional drawings, MCAT control system, GT-ISE optimizer, Stapersma compressor and turbine flow theory, and G3508a operational measurements. These data inputs have been put together to be able to model the conditions and behaviour of the flowing gaseous media through the engines entire airpath, with the exception of blind ends of the vacuum system like the crankcase ventilation or similar.

During the validation it became clear that the calibrated settings are generally the best match and by far most measures are within an acceptable margin of the desired values. The measured values are accepted as reliable but also these systems have discrepancies. Still, after the addition of the further power settings a supplementary revision of the Wiebe parameters ensured the best possible match for all power settings, given the available data and reasoning. In the literature review it became evident that the GT-POWER suite has respectable potential in accurate predictions of engine parameters. In the paper of Dong et al. [34] it is reported that the fuel consumption only deviated 0.7 [%] between measured and predicted values. That astonishing accuracy isn't achieved here. However, the model is now optimized for acceptable margins of max. +/- 10 [%] for all measures possible, with the vast majority parameters being more accurate for most cases being +/- 5 [%]. The select few measures that show diverged trends with an error that is above that tolerance of max. +/- 10 [%] can be reasoned by

the lack of higher quality data, like the unnatural vertical speed lines in the turbine mapping for example. Additionally, the variance of the Wiebe parameters has shown that the model can run consistently stable with differing engine parameters, indicating that the model is robust.

The final version of the model represents the air path of the CAT G3508a by dividing it in 283 separating flow volumes. An order of magnitude higher when compared to more common mean value models. This increase in flow volumes increases the resolution of the physical aspect of the engine over other engine model types; like MAP-based and Mean-Value models.

MAP-based models rely on pre-measured data stored in look-up tables and sensors data (I.E. throttle position, manifold pressure, engine speed), and the model then interpolates values from these tables. The benefit of these models is that they are fast, computationally efficient, and widely used in engine control units (ECUs). The drawback is mainly that they lack physical insight and don't adapt well to changes in engine conditions, and requires extensive experimental data.

Mean-Value models rely on an approach that is more physics based and captures the average behaviour of engine subsystems over a cycle. Typically Mean Value models predict air and fuel flow, pressure dynamics, and thermal effects using differential equations. These models typically work at a lower time resolution that is cycle averaged instead of at crank-angle resolution. The benefit of these models is that they provide a good balance between computational speed and accuracy, useful for system optimization. They are however less detailed than CFD and may not capture transient effects at high resolution.

CFD models feature a great increase in resolution, as they are based on up to three dimensional high-fidelity numerical simulations that solve the fundamental equations of fluid motion (I.E. Navier-Stokes equations). These CFD models are suited to analyse in-cylinder combustion, fuel-air mixing, heat transfer, and emissions formation in great detail. CFD models are known for high accuracy and deep insights into local flow fields, combustion, and heat transfer. They are however; computationally expensive, not suitable for real-time applications.

The developed GT-ISE model is positioned between the Mean-Value and CFD type models. The GT-ISE model relies on a physics based approach and captures behaviour like; air and fuel flow, pressure dynamics, and thermal effects that is at crank angle resolution. It models these parameters in a one-dimensional model for the airpath and at a zero-dimensional level for the in-cylinder process. The increase of the separate flow volume of 283 is orders of magnitude greater than Mean-Value models, this is especially beneficial for transient behaviour modelling. Additionally, the non-cycle averaged but rather crank angle level resolution adds to this aspect. The GT-ISE model models these aspects with improved resolution without being over computationally intensive. This relative ease of computation can be attributed to the efficiency of the internals of the commercial GT-ISE software. The steady state simulation of a given power level takes approximately 10 minutes or less when running on a regular computer, the stated runtime depends mostly on the quality of the initial turbocharger speed estimation. The development process and approximated runtime of 10 minutes for a steady state simulation is considerably less intensive than what a CFD model would require. Therefore the GT-ISE is nicely positioned between the Mean-Value and CFD models, improving the physical and time resolution without the need for excessive computational investments. For these reasons it is concluded that the model represents the CAT G3508a to a satisfactory qualitative scientific level and is therefore fit for purpose to be used for research.

# 9

## Hybrid Electric Turbocharging Compounding

### 9.1. Method

After validation, the model replicates the behaviour of the CAT G3508a and therefore represents it to a satisfactory level. The majority of relevant parameters are within acceptable margins, the select few that are out of this specified tolerance of  $\pm 10$  [%] have plausible reasoning why that is the case, mainly caused by lack of higher quality input data. Moreover, still remaining discrepancies are between the GT-ISE model and the G3508a. The model now serves as a new base in this research, any error that remains in the nature of the model will also be affecting all modified models that feature additional parts or objects to the existing assembly. The error between the G3508a and the modified models will remain, so a direct comparison between non-modified models and modified models can be made. Conclusions of general behaviour and qualitative results based on these modified models can then be drawn in reference to the non-modified model and subsequently to the G3508a, as the non-modified model is accepted to represent the G3508a to a satisfactory level. However, some discrepancies between the model and real engine must be kept in mind.

The model is now ready and fit for purpose for modification of the turbocharger system to include simulation of an electric machine of some sort, such that it is converted to hybrid electric turbocharging. The modification will be done by inspecting numerous example models in the GT-ISE catalog. From these examples inspiration for relevant parts and methods will be taken that is needed to convert the model. When the modification is successfully done several compounding cases will be added alongside the non-compounding cases which are used in the final iteration from the validation. This method gives a clear indication which factors differ between these cases that keep the output of the system equal for both compounding and non-compounding. Finally the interesting findings will be elaborated in various sections.

### 9.2. Modification

The research topic for this study is regarding the electric hybridization of the turbocharger system and what implications this has on the behaviour of a throttle controlled large SI gas engine. The build model of the CAT G3508a is a direct replication of the existing system which uses a common free floating turbocharger system. The model therefore needs to be modified to replicate the integration of some electric machine on the rotating turbocharger assemblies.

The GT-ISE catalog is very extensive and includes numerous parts that are able to model an electric machine of various types. The targeted modification is to include a machine that is able to add and/or subtract a specified torque from the rotating turbocharger shaft. When it is used to add torque it would assist the turbine in providing power for the compressor, assisting in the transient response and boost profile. When it is used to subtract torque it takes away power that is being generated by the turbine, reducing the available power for the compressor. It is expected that the steady state rotational speed of the turbocharger assembly is differing when torque is added or subtracted. The steady state speed requires an equilibrium between generated and consumed power. Because of the unpredictable nature

of this steady state speed it is difficult to predict what power the electric machine can generate, hence the decision for a torque regulated machine.

The model has been modified by including a series of objects that link the ‘ShaftTurbo’ object to a ‘Torque’ object. The ‘Torque’ object is relatively simple and is only able to apply a specified mechanical torque to a newly added ‘Shaft’ object. The ‘Shaft’ object is differing from the ‘ShaftTurbo’ object as it doesn’t include the inertia multiplier mentioned earlier. The ‘Shaft’ object is set to match the ‘ShaftTurbo’ object in initial speed and has the option for a specified moment of inertia for the added assembly. The moment of inertia is chosen to be minimized to the minimum of  $1e-9 [kg * m^2]$ , as the inertia is not of great relevance in static modelling and only elongates the computational time the model requires for convergence. The ‘Turboshaft’ and ‘Shaft’ objects are connected by use of a ‘GearConn’ object with a gear ratio of 1:1 and a mechanical efficiency factor of 1 to not over complicate the model. In reality most turbochargers that include an electric machine utilize one common shaft for both the turbochargers assembly as the electric machine, similar to image [Figure 3.2]. This implies very little additional mechanical losses as no gearing is used, the added mechanical losses would most likely exclusively result from the additional bearing loading.

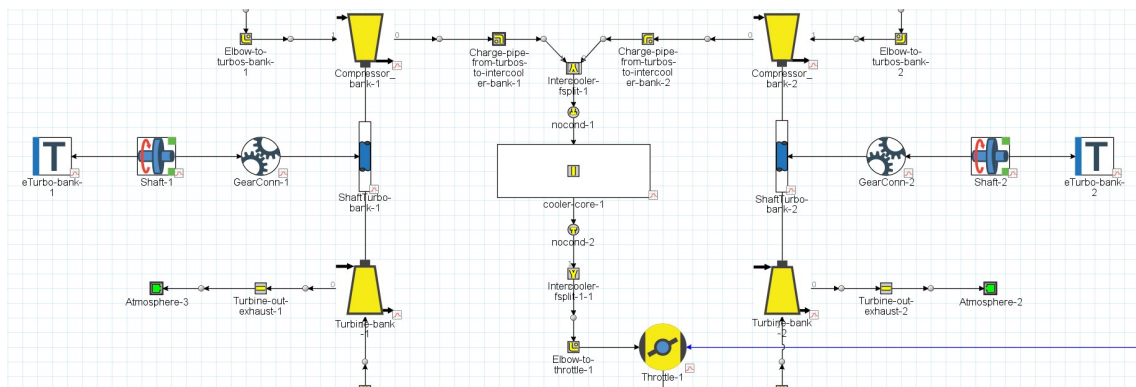


**Figure 9.1:** The modified turbocharger system to include objects that simulate electric machines for hybrid electric turbocharging.

The study of an e-compounding system also requires corresponding modifications to the throttle controller to now be targeting a system power. The controller initially was designed to be targeting a specified crank break power, similar to the loadbank control of the generator connected to the G3508a. Additional power is now generated with the inclusion of electric machines on the turbochargers. The model is set up to calculate the generated mechanical power from the ‘Torque’ objects and add it to the crank break power. Resulting in a total mechanical break power without considering electric conversion losses for both crank power as turbocharger power. This total mechanical break power is included in the throttle controller through the use of a ‘RLTCreatorSuper’ object, such that it targets for a desired total system break power.

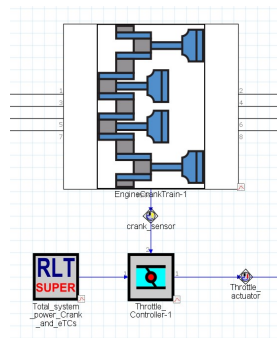
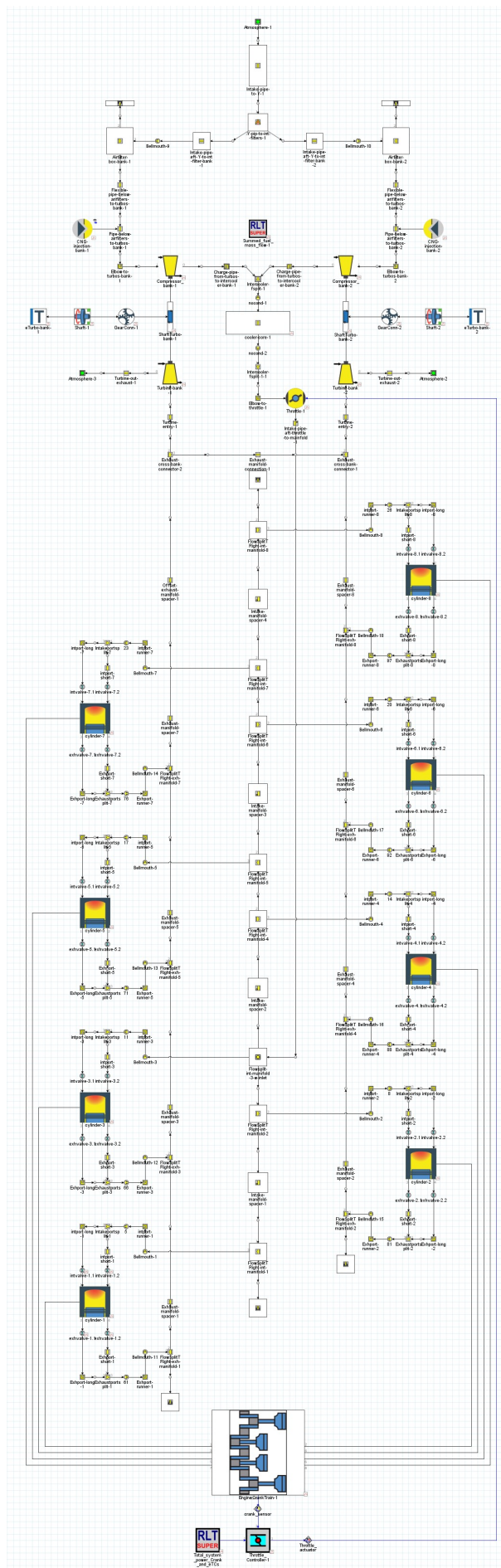
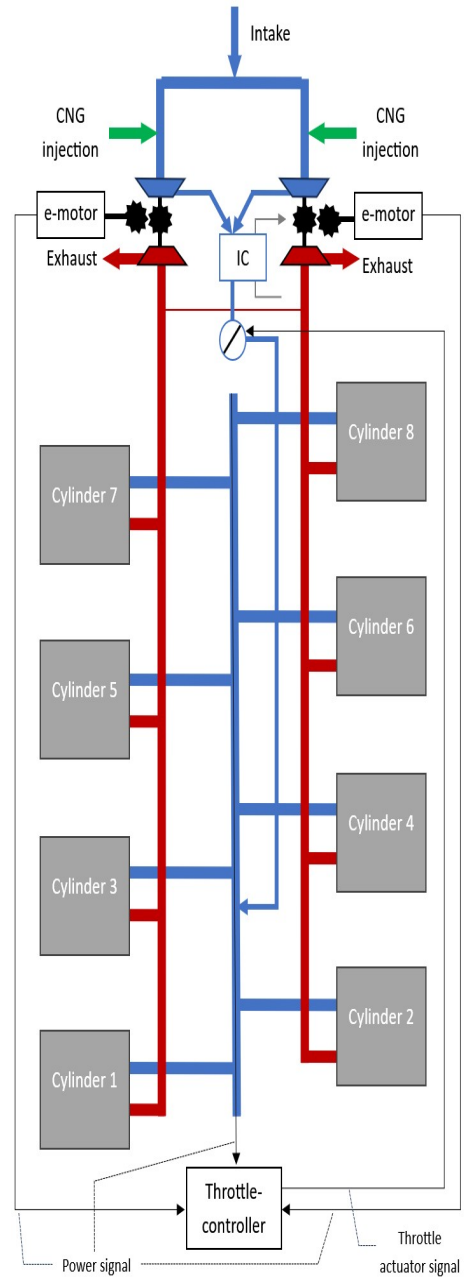


**Figure 9.2:** The modified throttle controller that uses system power as input signal.



(a) Complete overview of the graphical user interface of the GT-ISE model of the CAT G3508a including the e-turbo components.



(b) Schematic overview of the airpath of the CAT G3508a including the e-turbo components.

After the complete modification the model was verified to be functioning as expected. When an arbitrary torque is subtracted from the turbocharger shaft the system now converges to a stable steady state that reduces the rotational speed of the turbocharger system. When torque is added to the turbocharger assembly the steady speed is raised accordingly. This is similar to significant alterations of the mechanical efficiency of the turbocharger.

### 9.3. Cases

For system compounding, a static simulation is required as compounding is utilized for system efficiency enhancing, which is desired for a prolonged amount of time running a constant loading. The current setup of the model is perfectly viable for a static simulation, even with the new addition of the 'Torque' objects on the turbocharger assembly. The goal for compounding is to extract mechanical energy from the turbocharger shaft. This can now be done by applying a resistive torque, called 'eturbo torque' from now on, on the turbocharger shaft and calculate the generated power by multiplying it with the monitored steady state rotational speed. The model now automatically adds the generated power by the turbochargers to the crank power for a total mechanical system power. By varying the applied torque, the effect and behavioural changes can be monitored with the objective to maximize efficiency.

For this objective the services of GT-ISE's optimizer are again utilized. As the throttle is now regulated by system power a variance in eturbo torque will result in the same total output power, if set within certain limits. The optimizer is set to vary the eturbo torque to target an equal system power output as the 'case setup' for throttle controller and to minimize the total injected fuel flow mass. The fuel flow mass can now be an indication of system efficiency as system output is kept constant. Basically keeping output constant while minimizing the input.

This optimization is done for a similar set of cases that are used earlier. Earlier 100, 200, 250, 300, 400 and 500 [kW] were used without eturbo compounding. Now new eturbo e-compounding cases are joined, the 100 [kW] is also joined by a 100 [kW] e-compounding case, the 200 [kW] by a 200 [kW] e-compounding case, and so on. This for all cases except the 500 [kW] setting. The validation has proven that the model is restricted in air flow, most likely by the integration of the turbine mapping. The model requires WOT for 446 [kW] and has consequently no room for the introduction of other restrictions. The 500 [kW] e-compounding case is therefore exempt from this study, it would need a revision of the turbine mapping first.

A total of 11 cases is now used for simulation of the differing power levels with and without e-compounding:

Case nr.	1	2	3	4	5	6
Case name	100 [kW]	100 [kW] e-compounding	200 [kW]	200 [kW] e-compounding	250 [kW]	250 [kW] e-compounding
Case nr.	7	8	9	10	11	
Case name	300 [kW]	300 [kW] e-compounding	400 [kW]	400 [kW] e-compounding	500 [kW]	

Table 9.1: Case overview

### 9.4. Results of optimization

The optimizer algorithm was set to use a multi-objective Pareto function. This algorithm identifies multiple optimal solutions that are considered to be equally 'valid'. From the reported results a selection was later made as not all results are considered to be as valid as others. The optimizer set to vary the eturbo torque between two limits for each case, 0 and 0.5 [Nm] for the 400 [kW] for example. Most optimization taking approximately 60 iterations and often well over 1000 minutes for a 2d Pareto graph that contains sufficient data. The results of the 400 [kW] e-compounding optimization are discussed below, the method is equal for all e-compounding cases.

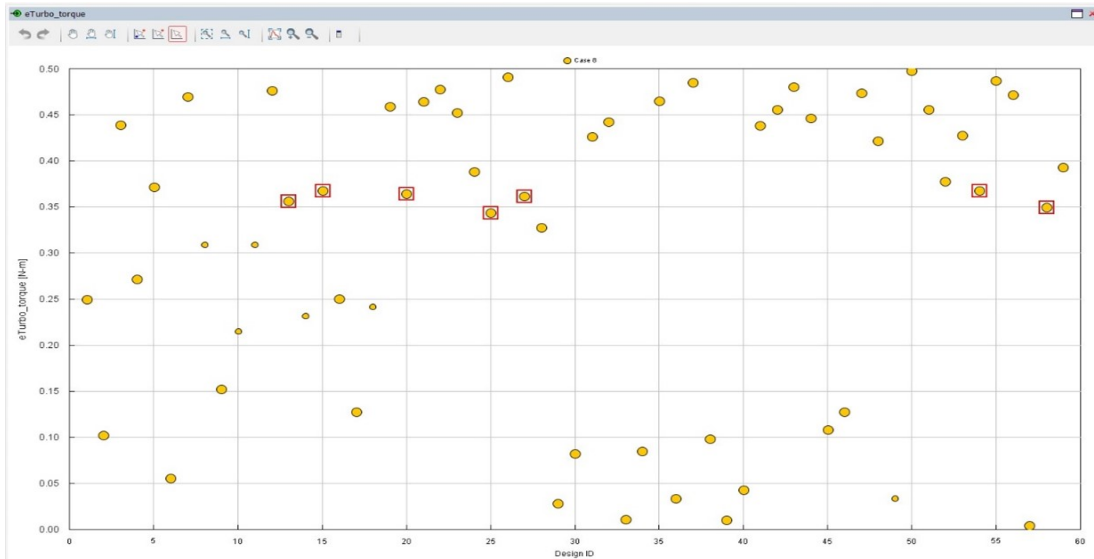


Figure 9.4: View of the GT-ISE optimizer interface, varying the eturbo torque case by case.

Here it can be seen how the optimizer is varying resistive eturbo torque as it iterates through differing versions. The algorithm seemingly prefers results towards either extremes as it runs, allowing for concessions in system power. The versions with a eturbo torque above the red box marked versions in Figure 9.5 are the ones that corresponding to ones that diverge from the targeted system power in Figure 9.5.

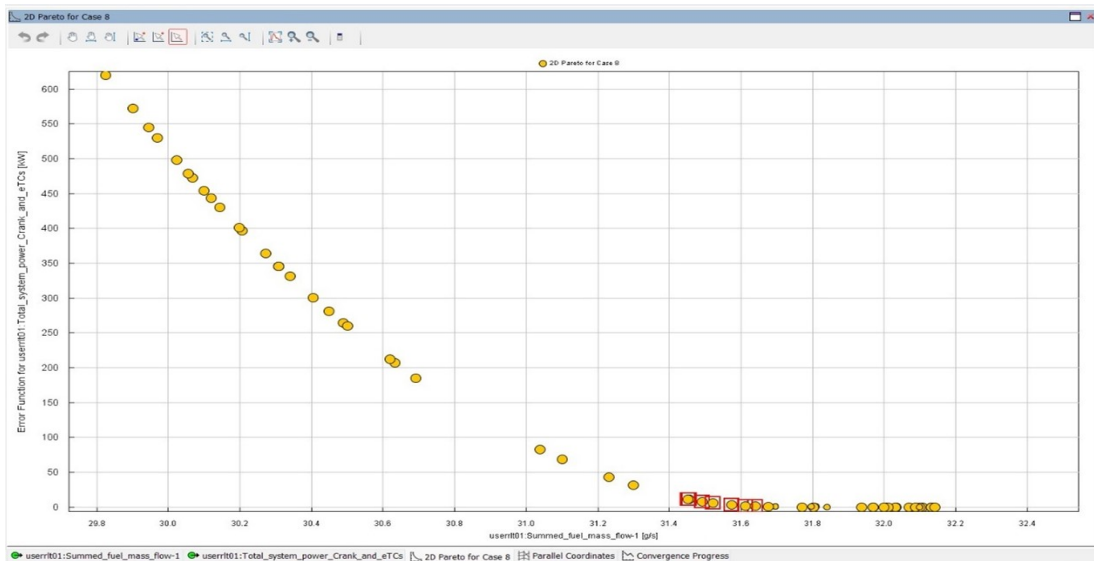


Figure 9.5: View of the GT-ISE optimizer pareto graph interface, increasing in power 'error function' along the y-axis dimension.

The resulting Pareto graph is composed of an Error Function of Total system power on the y-axis as a function of Summed fuel mass flow on the x-axis. As long as the Error Function remains converged to the x-axis or 0 the produced power is at its targeted value of 400 [kW]. Some cases at 400 [kW] require a higher injected mass flow, varying by approximately 0.6 [g/s]. Cases that show an increased Error Function of Total system power require even less fuel mass flow, however reductions in the targeted total system power are very undesired. These cases with reduced system power are therefore not 'valid'. Additionally, the cases that require a higher fuel flow aren't as efficient as possible.

The optimizer is run for all cases and the resulting eturbo torque setting is selected where the system still produces at least 99 [%] of targeted system power, resulting in the lowest system Break Specific Fuel Consumption (BSFC) for each case for those system requirements.

From this can be concluded that the system increases in efficiency as the applied eturbo torque raises from 0 up to an optimal eturbo torque. At optimal torque the system is still able to produce a targeted system power within acceptable tolerance while reducing the required fuel mass flow, thus minimizing the system BSFC and maximizing efficiency. A brief overview of the results of the optimized cases is given in Table 9.2.

System target power	100 [kW] e-compounding	200 [kW] e-compounding	250 [kW] e-compounding	300 [kW] e-compounding	400 [kW] e-compounding
eturbo torque [Nm]	1.40	1.78	1.57	1.22	0.35
System power [kW]	99.85 (99.9%)	198.03 (99.0%)	247.94 (99.2%)	298.00 (99.3%)	397.93 (99.5%)
Crank power [kW]	94.81	18.04	232.28	281.62	391.91
Cumulative eturbo power [kW]	5.04	11.99	15.66	16.38	6.02
Fuel flow relative to non-compounding system [%]	97.6	95.5	94.5	94.8	98.2

**Table 9.2:** Brief fuel consumption and efficiency overview of e-compounding cases

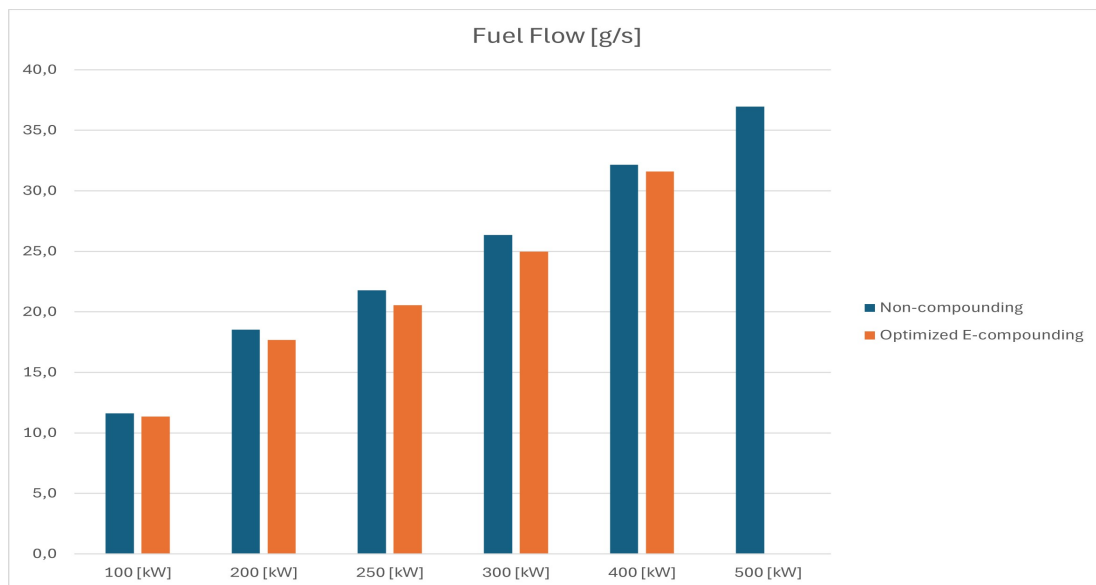


**Figure 9.6:** Cumulative injected mass flow for all cases.

## 9.5. Constant power production

The system is able to reach the targeted system power for a select range of eturbo torque settings, as can be seen by the Pareto graph in Figure 9.5. The system power production is regulated and controlled by the throttle controller. By introducing a resistive torque on the turboshaft the steady state rotational speed of the turbocharger assembly is reduced (Figure 9.7), shifting its operational point in the efficiency map, more on that later. Additionally, the generated eturbo power is subtracted from the power that is generated by the turbine, leaving less power available for the compressor. Effectively lowering the turbochargers mechanical efficiency. Therefore, the lower powered compressor is not able to produce the same pre-throttle charge pressure as a non-compounding setup (Figure 9.8). This lowers the charge air density and mass air flow. The throttle controller compensates for this by opening the throttle further, up to WOT in all e-compounding cases that are optimized see Figure 9.9.

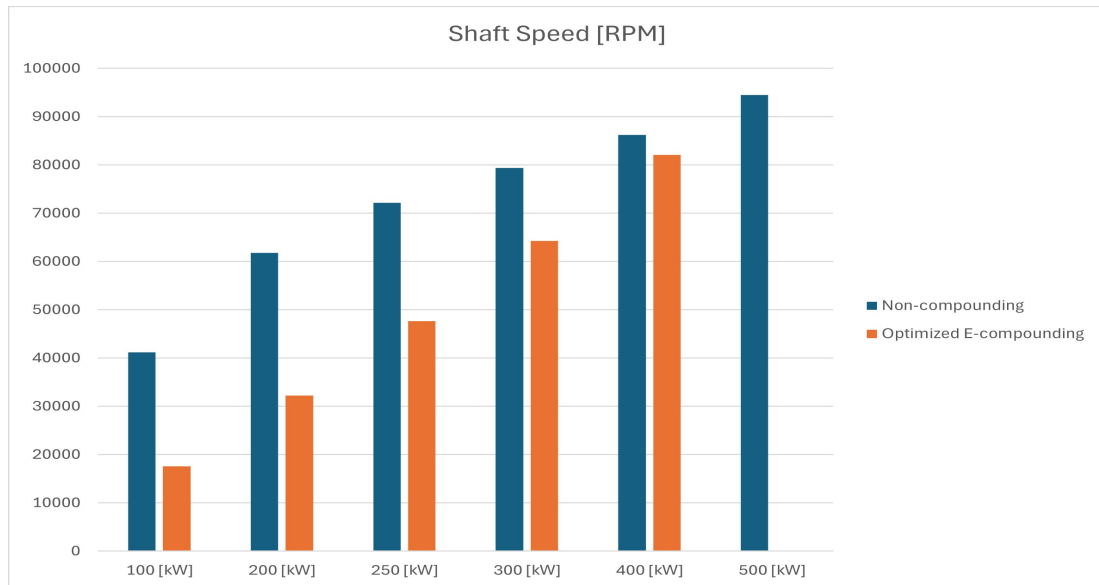


Figure 9.7: Average turbocharger speed for all cases.

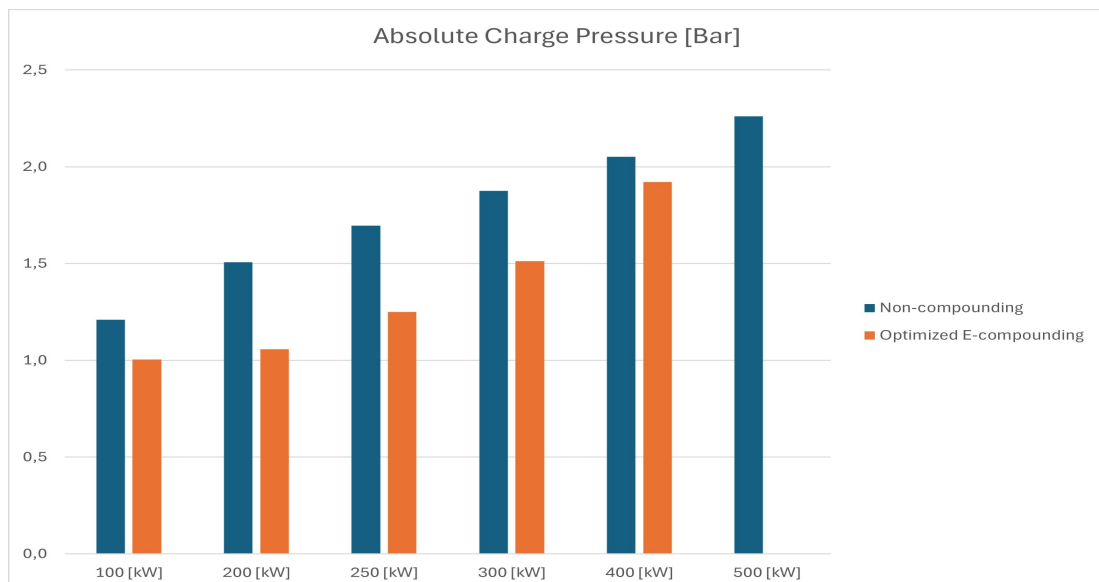


Figure 9.8: Charge pressure pre-throttle.

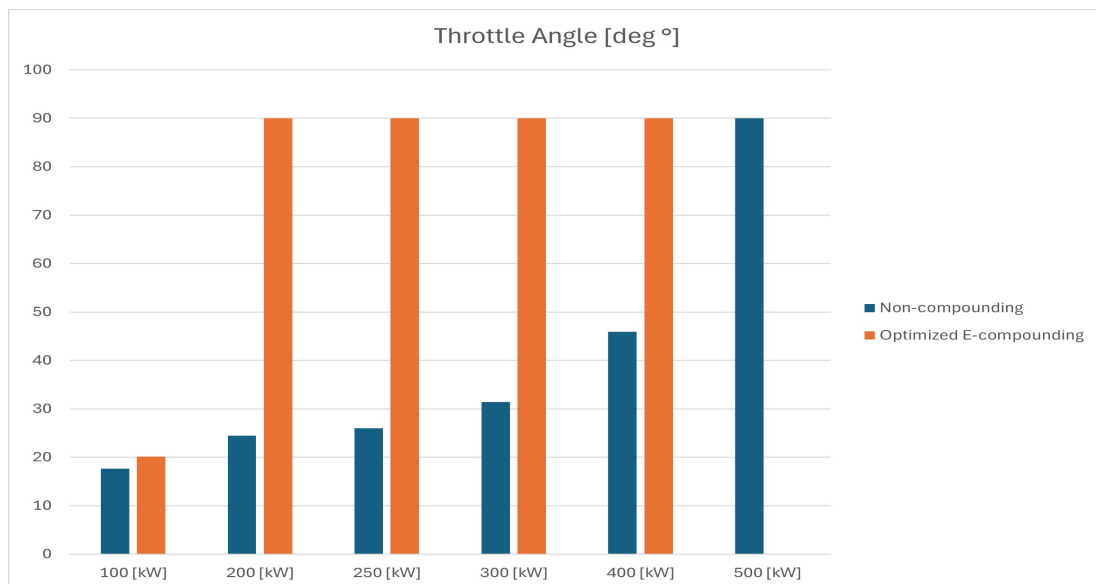


Figure 9.9: Throttle angle for all cases.

The throttle controller targets system power so it regulates the air flow to the engine such that the system produces within a  $\pm 1$  [%] tolerance. However, system power is of course an addition of crank and eturbo power, so it is reliant on a more complex system. Still the controller is able to reach target power up to the optimized eturbo torque figures. Increasing the eturbo torque any higher the system max power degrades, any lower the throttle controller will start closing the throttle to reduce the air flow and thus mainly decrease crank power.

The exception to the WOT statement is the lowest 100 [kW] e-compounding setting, see Figure 9.9. Here the resistive torque is maximized on basis that it runs consistently stable. The application of 1.40 [Nm] eturbo torque results in a desired system output power, increasing the eturbo torque by just 0.02 [Nm] stalls the model, producing negative power. At 1.40 [Nm] the throttle controller opens the throttle only partially further when compared to the non-compounding 100 [kW] case. This is contrary to all other cases where an additional increase in torque reduces maximum system power, because of the WOT. The cause for the stall is assumed to be rooted in the compressor behaviour, as the pressure ratio over the compressor becomes smaller than 1 [-] at higher torque settings, as can be seen by case 2 in Figure 9.8 or by the compressor map in Figure 9.18. The compressor map in GT-ISE doesn't extrapolate below a pressure ratio of 1 [-] by default, as it is very unnatural behaviour for a compressor to produce below atmospheric pressures. Whether this behaviour is caused by model limitations or a plausible real phenomena is not certain. A SI engine can run absolutely fine on below atmospheric pressures as that is exactly what a throttle does, so it seems unlikely that this would stall an engine.

### 9.5.1. Implications on dynamics

This study mainly focusses on the efficiency potential of hybrid electric turbocharger compounding in steady state operations. However, some hypotheses on transient performance can still be made. The compounding system reaches maximum efficiency at an optimized eturbo torque where the throttle controller compensates for the introduced restrictions by opening the throttle up to WOT. This introduces certain operational control peculiarities. A regular SI engine would open the throttle during a load step to a higher power setting, up to WOT in some cases. But when running in optimized eturbo compounding mode the system is already at WOT. This implies that when a load step is initiated, the system must respond via control of the eturbo torque, by reducing it. If it were set to zero [Nm] in an instant it would be similar to a regular non-compounding load step where the controller would reach WOT in the same instant. The differencing factor now is that the initial turbocharger speed at the begin of the load step is reduced considerably, see Figure 9.7, this increases the transient response time. If the eturbo system potential is utilized, this can be compensated; when the eturbo torque would be set to assisting mode rather than to zero the transient response time can potentially be reduced, possibly even when compared to initiating a load step in non-compounding mode without assist.

## 9.6. Impact on fuel consumption

The e-compounding system is able to realize noteworthy fuel consumption savings. This is in line with expectations as during the literature review research has been found that has set precedent for these fuel savings of compounding systems. Westhoeve (2018) [10] reported a nominal system efficiency increase of 2.3 [%] for a CI dual fuel engine using the Diesel B mean value model of a Wärtsilä 6L43DF. Rusman (2018) [11] reported a potential efficiency increase in part load of approximately 15 [%] for the Zr. Ms. De Ruyter 'LCF'-frigate, which is powered by a CODOG configuration partly consisting of 2 compounding Wärtsilä W26-STC. This is partly realized by shifting the operating point of the diesel engine. Figari et al. (2022) [31] report a maximum energy surplus of 2 to 3 [%] for a hybrid electric turbocharged large 9-cylinder 8775 [kW] dual fuel engine using the same GT-ISE software and similar 0-dimensional Wiebe combustion model. The study also reports that the optimal nominal motor size is 300 [kW] and NOx emissions increased 15 [%] in diesel mode. Another study by Dong et al. (2020) [34] focussed on automotive turbocharged 1.6 to 2 [L] displacement engines. These engines were also modified with hybrid electric turbochargers in the same GT-ISE software package. They report tank-to-wheel energy saving of 1 to 5 [%]. In literature an analogous consensus is set where various types of engines benefit of efficiency gains when they utilize a compounding hybrid electric turbocharging system. The findings of the e-compounding model of the CAT G3508a agrees with the consensus. The BSFC of the system does show a decrease in fuel consumption and consequently an increase in system efficiency across the entire range of part load settings, up to 5.5 [%] for the 250 [kW] e-compounding system. Refer also to Table 9.3 and Figure 9.6. Here it can also be seen that the apparent maximum power generated by the e-compounding system is approximately 8.19 [kW] per side. The maximum could be more, possibly between 250 and 300 [kW] system output. So exclusively for compounding an electric motor of 10 [kW] would likely be sufficient.

Target [kW]	100	200	250	300	400
Actual [kW]	99,85	198,03	247,94	298,00	397,93
Power target accuracy [%]	99,9	99,0	99,2	99,3	99,5
Crank break power [%]	94,81	186,04	232,28	281,62	391,91
Cum. Epower [kW]	5,04	11,99	15,66	16,38	6,02
Throttle angle [degrees]	20,14	90,00	90,00	90,00	90,00
eTurbo torque [Nm]	1,40	1,78	1,57	1,22	0,35
Fuel consumption CAT G3508a for reference for same power settings [g/s]	13,14	19,45	22,55	25,74	32,46
Fuel consumption model non-compounding [g/s]	11,63	18,51	21,76	26,35	32,16
Fuel consumption error in predicted values (non-compounding/CAT G3508a) [%]	11,5	4,8	3,5	2,4	0,9
Fuel consumption e-compounding [g/s]	11,35	17,67	20,56	24,98	31,58
Relative fuel consumption (e-compounding/non-compounding) [%]	97,6	95,5	94,5	94,8	98,2
Saved fuel fraction through e-compounding [%]	2,4	4,5	5,5	5,2	1,8

**Table 9.3:** Complete fuel consumption and efficiency overview of e-compounding cases

## 9.7. Efficiency gain cause

The goal of a 4-stroke engine is to produce a desired torque at a given rotational speed, the function of both resulting in power. A 4-stroke engine only produces positive torque and power on its power stroke, all other strokes require net negative torque and power. On the exhaust stroke the piston needs to force the residual gasses out of the cylinder along the valves and through the exhaust and turbine, this requires work. Similarly, on the compression stroke the piston needs to compress the charge mixture to a 12:1 ratio, this also requires work. Although it must be noted that most of this compression work is returned on the expanding power stroke. The intake stroke is also a stroke that requires work and thus sets a net negative torque on the crankshaft. This required work is taken from the available kinetic energy from the readily rotating assembly which has inertia. This phenomena of required work input in the movement of the working media through the engine is called 'pumping losses' and defined as the PMEP (Pumping Mean Effective Pressure) [bar] for the intake and exhaust stroke. The PMEP is one of the main contributors to the MMEP (Mechanical Mean Effective Pressure) [bar] in GT-ISE. Note that

the GT-Power convention is such that PMEP is negative and FMEP [bar] is positive. Therefore, the quantity FMEP-PMEP represents the total loss due to friction and pumping work.

$$\text{PMEP} = \frac{\sum_{i=1}^{\# \text{ Cylinders}} \int_{180}^{-180} \frac{P_i dV_i}{V_{\text{disp}_i}}}{\# \text{ Cylinders}} = \frac{\sum_{i=1}^{\# \text{ Cylinders}} \text{pmepc}_i}{\# \text{ Cylinders}}$$

with

PMEP	Pumping Mean Effective Pressure [bar]
$P_i$	Instantaneous cylinder pressure of cylinder [bar]
$V_i$	Displacement volume of cylinder [ $m^3$ ]
pmepc <sub>i</sub>	Cylinder pmepr RLT of cylinder (calculated in EngCylinder objects) [bar]

When the intake stroke starts, the intake valves lift and the piston moves away from TDC thus increasing the volume inside the combustion chamber. This volume needs to be filled by the desired charge mixture mass. This charge mixture needs to flow past all restrictions in the intake system into the combustion chamber, being forced by a pressure differential over these restrictions. These restrictions are a result of the design of the intake system, partially from the nature of the geometry, but mostly from engine components that serve a function in the management of the air. The intake valves are somewhat restrictive but are essential for correct operation. Likewise with the throttle valve, the function of the throttle is to regulate the mass flow rate of the charge mixture towards the combustion chamber. This is needed in SI engines as they require a specific AFR.

A throttle is effective when a SI engine is running at part load where the engine only requires a small charge mass flow. Thus the throttle is mostly closed for a large restriction and more moderation of the airflow. It is this restriction of the throttle however that also contributes to pumping losses and additional work that needs to be put in the intake stroke. CI engines like diesel engines don't suffer from this as they generally aren't throttle regulated. Partially for this reason are diesel engines considered as more efficient as they lack the restrictive nature of a throttle at part load. The goal for SI engines is to regulate flow at part load with as little pumping losses as possible.

There are systems available that regulate the mass flow without the need of a throttle, BMW's Valvetronic [41] for example. This system is used on both NA as turbocharged engines. Valvetronic regulates the intake mass flow by altering the intake valve lift which is made infinitely variable from almost 0 lift to regular full actuation. By altering the valve lift to regulate the mass flow, the requirement for a throttle was largely removed. During normal operation, the system is able to open the throttle further and reduce its pumping losses, increasing the engines efficiency, achieving a consumption reduction of 12 [%].

It is also this shift in engine power moderation method that is one of the main contributors for the efficiency gain of the e-compounding cases when compared to non-compounding. The withdrawal of energy from the turbocharger causes the operational point of the turbocharger system to shift as there is less power available for the compressor. By doing this the turbocharger acts like a throttle and is sufficient in moderating the engines system power. This implies that the throttle can be set to fully open. It is this wide open throttle that lowers the pumping losses of the e-compounding cases and therefore reduces the MMEP. This is supported by the pumping power indication in GT-ISE, see Figure 9.10. Here it can be seen that for all compounding cases that the negative pumping power decreases (notice the y-axis negative numbers). The effect isn't as significant at the 100 [kW] setting, as the throttle angle is only opened partially for e-compounding and non-compounding cases. The impact of WOT e-compounding increases as the mass air flow increases with the power settings for cases 200 to 400 [kW]. The effect decreases at the 400 [kW] cases as the throttle is opened relatively far for the default non-compounding 400 [kW] case. Refer to Figure 9.9 for the throttle angle. The trend of having more impact as the power settings and consequent mass air flow increases and decreases for the 400 [kW] is also noticeable in the fuel consumption, see Table 9.3. Additional to the WOT is also the factor that the engine crank power alone is lower due to the energy recuperation of the turbochargers, so the mass air flow is lower, additionally reducing pumping power. The system power output is equivalent between e-compounding and non-compounding, however the engine power is lower. This thus decreases overall mass air flows and thus also partly decreases the pumping losses.

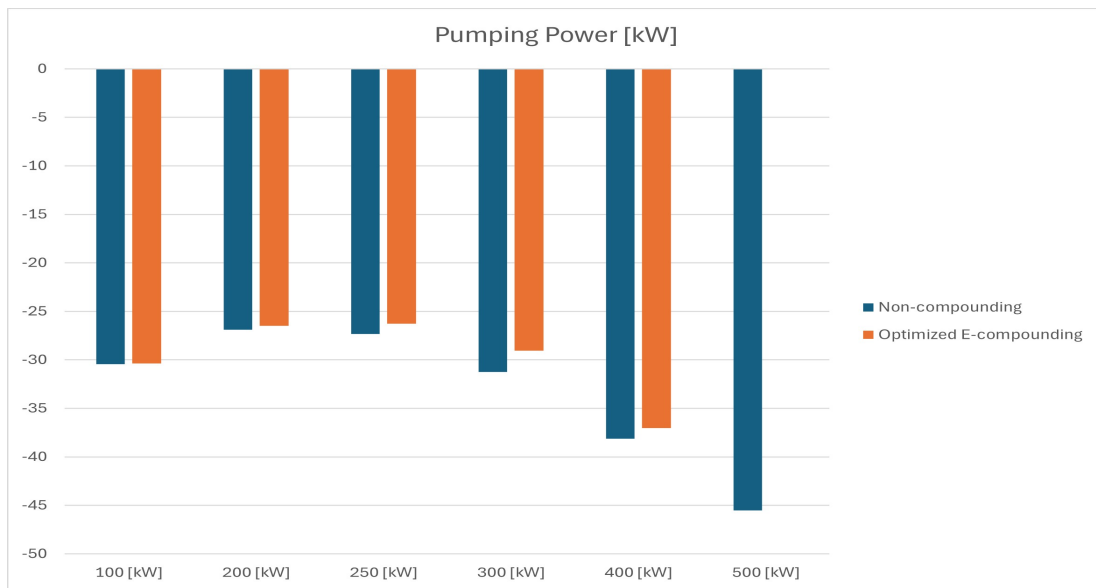


Figure 9.10: Pumping power for all cases, note the negative numbers on the y-axis.

Complementary to the decreased pumping losses is the decrease in friction of the rotating engine assembly. As the engine cranktrain produces lower power the IMEP and maximum cylinder pressure are also slightly reduced. The friction model in GT-ISE has the maximum cylinder pressure as a first order factor, so this will play a role in reducing the FMEP (Friction Mean Effective Pressure) [bar] on the power stroke. The reduction of friction as a result of bearing loading and axial piston to cylinder loading is a direct result of a reduced  $P_{Cyl,max}$ . The cycle average FMEP will also be fractionally reduced on the intake, compression and exhaust stroke as the PEMP are reduced. Overall the friction of the rotating assembly is reduced over an entire engine cycle as the in-cylinder pressures are lower across the entire cycle, improving efficiency, see Figure 9.11.

$$FMEP = FMEP_{Const} + A \cdot P_{Cyl,max} + B \cdot c_{p,m} + C \cdot c_{p,m}^2$$

with

FMEP	Friction Mean Effective Pressure [bar]
$FMEP_{const}$	Constant Part of FMEP [bar]
A	Peak Cylinder Pressure Factor [-]
B	Mean Piston Speed Factor [ $bars/m$ ]
C	Mean Piston Speed Squared Factor [ $bars^2/m^2$ ]
$c_{p,m}$	Mean Piston Speed [ $m/s$ ]
$P_{Cyl,max}$	Maximum Cylinder Pressure [bar]

$$MMEP = FMEP - PMEP$$

with

MMEP	Mechanical Mean Effective Pressure [bar]
------	--

$$BMEP = IMEP - FMEP$$

with

BMEP	Break Mean Effective Pressure [bar]
IMEP	Indicated Mean Effective Pressure [bar]

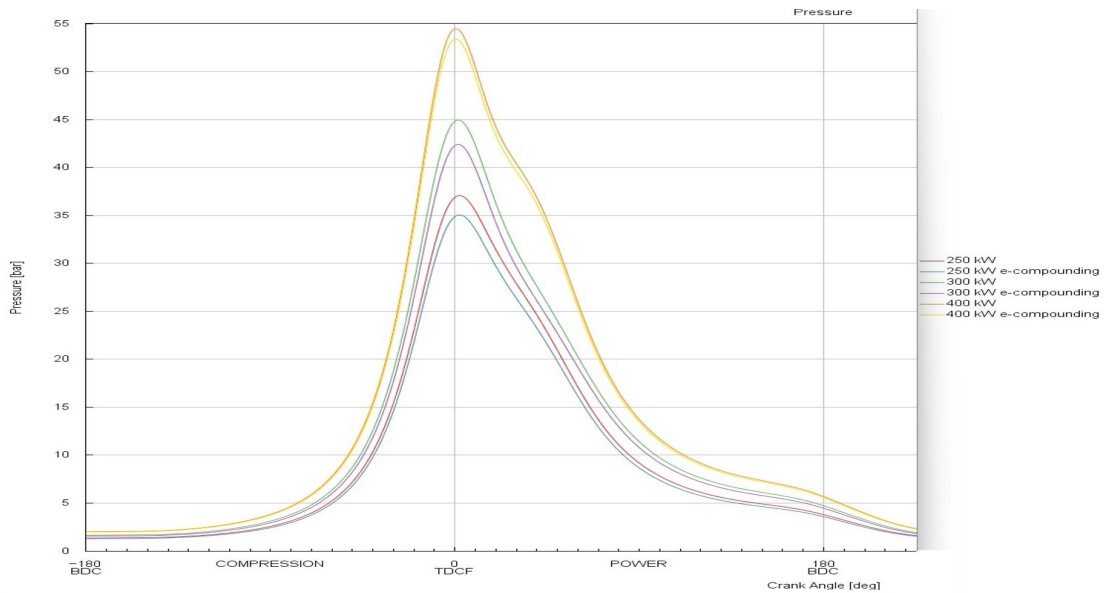


**Figure 9.11:** Indicated pressure for cylinder 1 for power settings 250 to 400 [kW] for non-compounding and e-compounding settings.

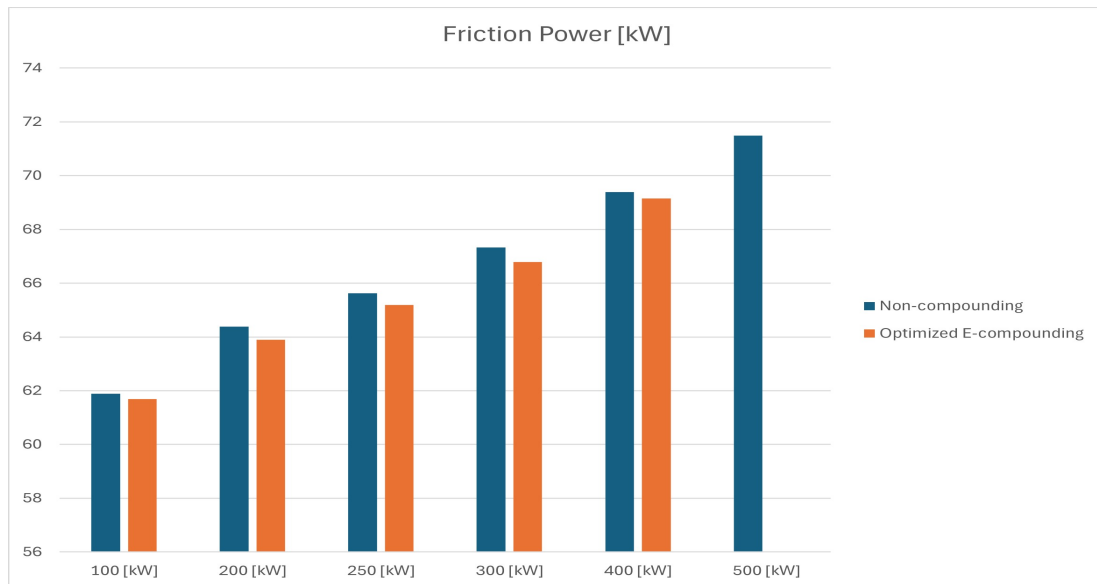


**Figure 9.12:** Friction power for all cases.

## 9.8. Efficiency exchange

The Cranktrain object in GT-ISE also monitors the BSFC of the engine. This object does not recognize the power development by the e-compounding turbochargers. It only takes the fuel mass flow and crank power into consideration. The BSFC for only crank power shows that the engine efficiency decreases when compounding is utilized. The MAP indicates that the e-compounding system shows a reduction in charge pressure. Indicating at a reduced filling efficiency of fresh air. This is supported by the residual mass fraction at the start of combustion in Figure 9.15. Here it can be seen that the residual mass fraction of each e-compounding case is slightly higher, indicating at a reduced filling efficiency and subsequent deteriorated combustion process.

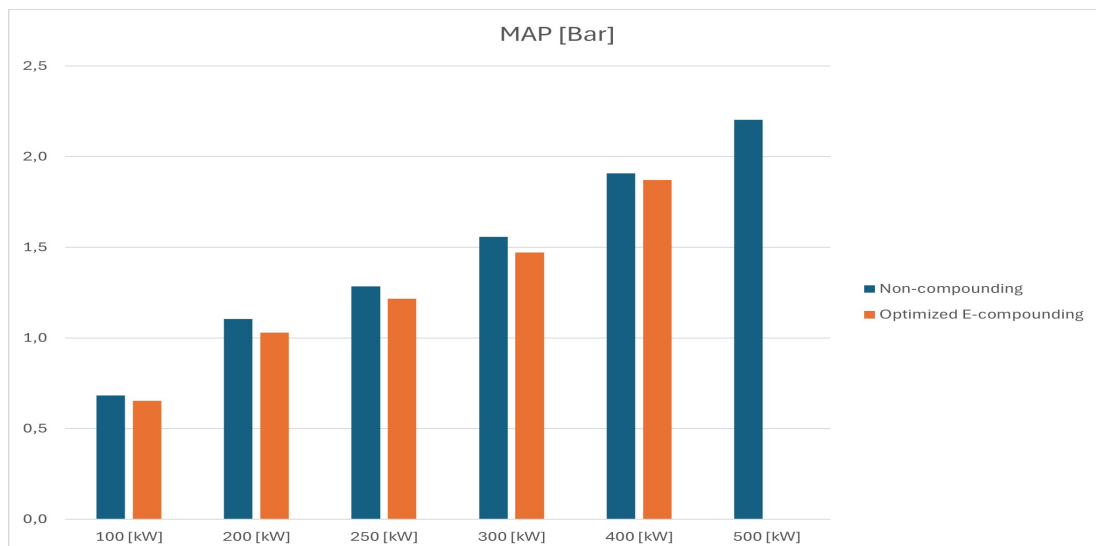


Figure 9.13: MAP (Manifold Absolute Pressure) for all cases.

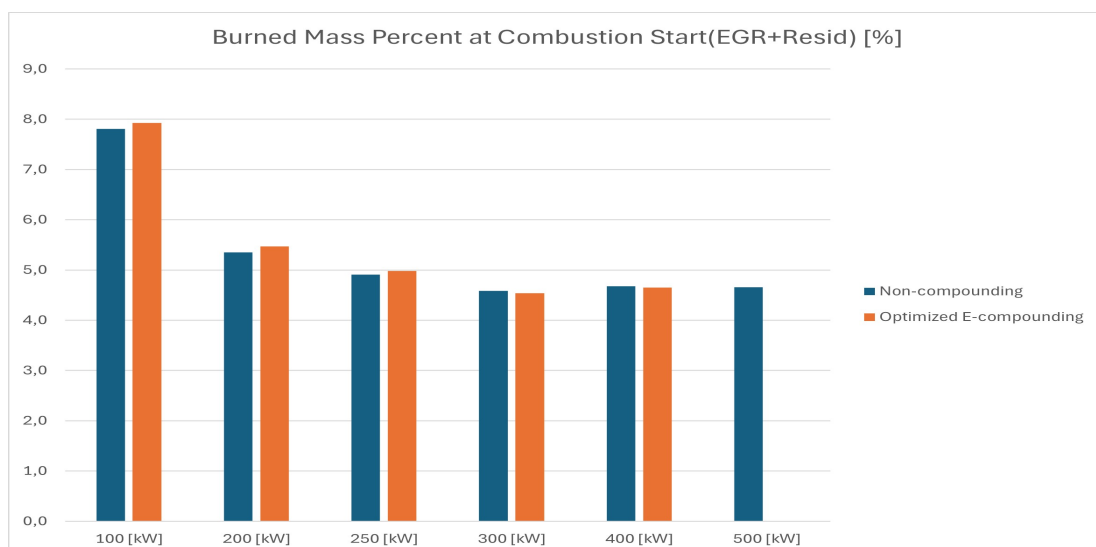


Figure 9.14: Average residual mass fraction in cylinders at start of combustion for all cases.

The impact of e-compounding has the tendency to having the ability to decrease the injected fuel mass flow at a more significant rate than deterioration of the combustion process. This indicates that the engine efficiency decrease is less significant than the gains of the energy recuperation of the e-compounding, resulting in an increase in system efficiency.

A potential benefit of this effect is the potential for the reduction of NO<sub>x</sub> emissions. An increase in residual mass in the cylinder is similar to the working of an EGR system. Residual gasses have a higher specific heat and consequently reduce peak combustion temperatures, reducing the NO<sub>x</sub> content at Exhaust Valve Opening (EVO). GT-ISE reports a NO<sub>x</sub> emission reduction of approximately 4 [%] for the lowest power settings, and fractional reduction for the higher power settings. However, it must be noted that the developed GT-ISE model of the CAT G3508a with its eturbo modification and its combustion model has not been focussed on the in-cylinder process. Additionally, the emission aspect of the model has not been validated, so these findings are to be further examined. Still, a reduction of NO<sub>x</sub> emissions would be a very attractive benefit of an e-compounding system. Figari et al. (2022) [31] reported an increase of 15 [%] in NO<sub>x</sub> emissions for a duel fuel engine running in diesel mode. These contradictory findings are interesting and are presumably rooted in the difference between a CI engine without a throttle and the SI throttle controlled G3508a that can run at WOT.

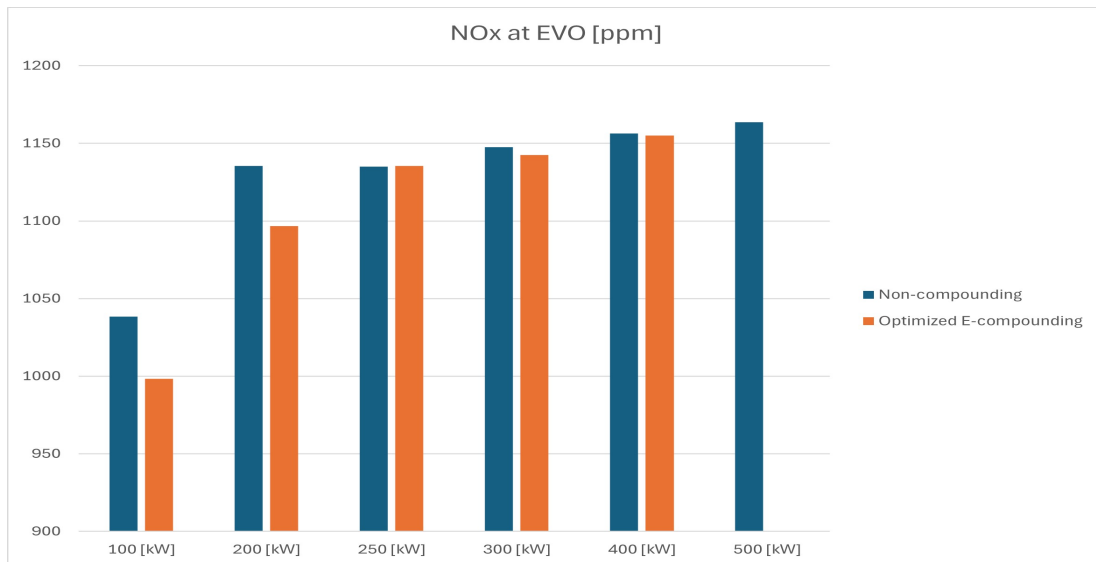


Figure 9.15: Average NOx emissions of all 8 cylinders at EVO for all cases.

## 9.9. Turbine exit temperature

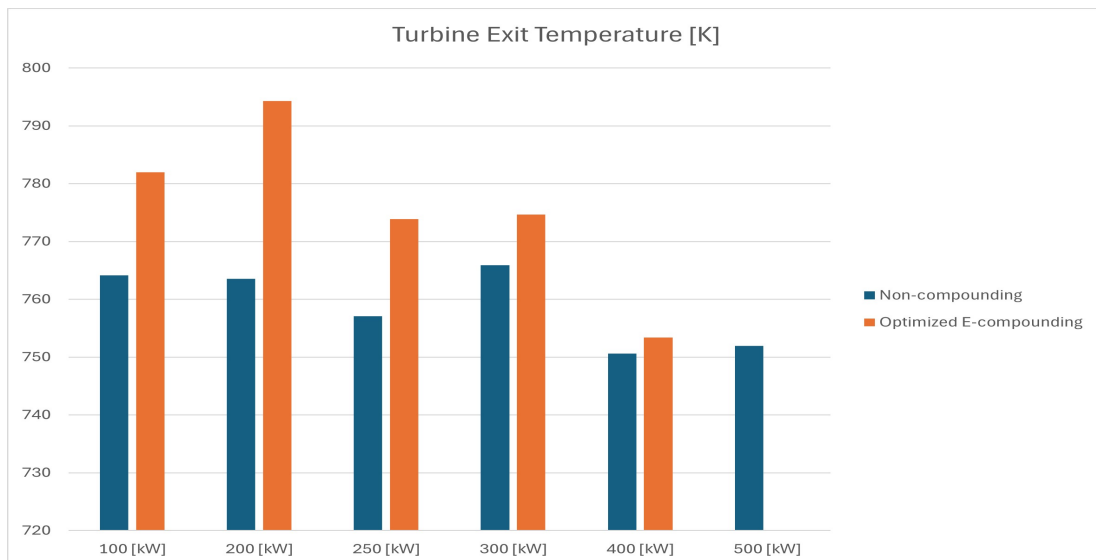
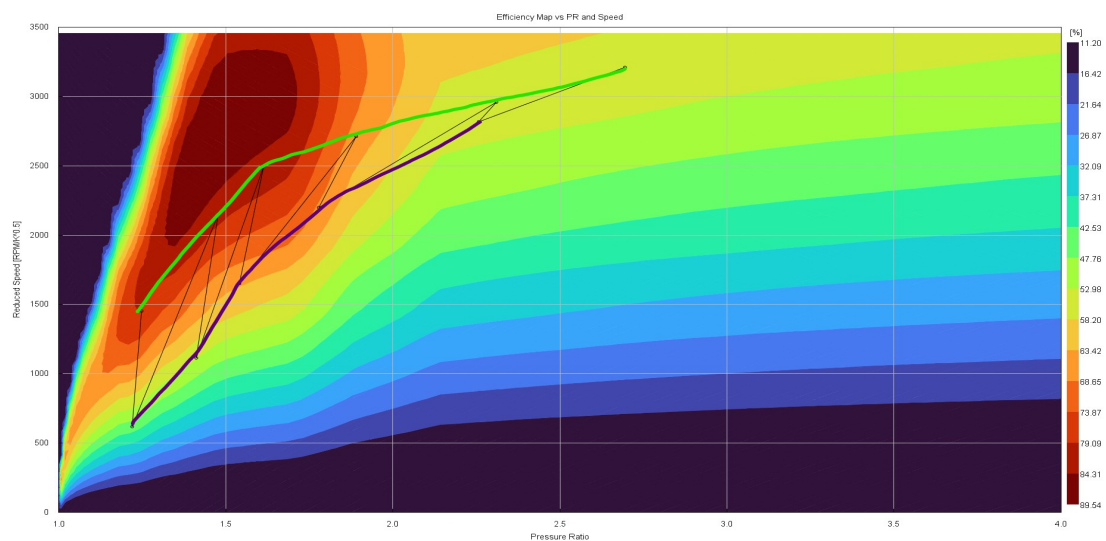


Figure 9.16: Turbine exit temperature on bank 1 for all cases.

Some other notable change is the consistent raise in turbine exit temperature across the e-compounding cases. Depicted in Figure 9.16 is the turbine exit temperature of bank 1, where it can be seen that all e-compounding cases show an increase in exit temperature over their non-compounding cases. This seems counter intuitive at first as the system has gained in efficiency, so less exergy should be wasted to the environment. This is a drawback for naval purposes as the thermal signature of vessels is to be reduced to minimum. Although, it must be noted that the mass flow is also reduced, so there is a lower mass of heated gas being expelled into the atmosphere. A higher turbine exit temperature could be an indication of a system that is less efficient that in this case that is only partly true. The turbine entry temperature is relatively consistent across all cases. Some e-compounding cases reporting higher entry temperature and some lower, all varying not more than  $\pm 10$  [K]. The exit temperature is consistently raised for the e-compounding cases, some cases by more than 30 [K]. The reduced system BSFC is a clear indication that the system overall is more efficient, the raised turbine exit temperature mainly is caused on component level by the efficiency of the turbine. The efficiency map of the turbine of the turbocharger on bank 1 gives a clear indication on what caused this.

The trace of operational points on the Reduced Speed  $[RPM/K^{0.5}]$  over Pressure Ratio mapping shows this. The upper operational points on the green line are the odd cases without compounding active, going from 100 [kW] on the left to 500 [kW] on the right. The lower operational points on the purple line are the even cases with e-compounding active, again 100 [kW] on the left and 400 [kW] on the right. It is clear that the general trend of the e-compounding operational line is shifted further out the area of peak efficiency. This means that the turbine is less capable in recuperating the available exergy to mechanical energy, instead it gets wasted to the exhaust temperature. This is a natural effect of recuperating energy with an e-compounding system on the Garrett TW6146 turbochargers (A/R of 1.37) of the CAT G3508a, or at least with the corresponding estimated Stapersma mappings

When a turbocharger supplier would develop a turbocharger capable of e-compounding they would logically develop a new turbocharger assembly. A new turbocharger assembly would then have its operational area better suited to its region of peak efficiency. When this is done more of the available exergy would be recuperated to mechanical energy, allowing for an increase in turbo torque and power. This should increase system efficiency even further and consequently reduce the exhaust gas temperature and its thermal signature.



**Figure 9.17:** The change in operational line of the turbine shows a shift in nominal efficiency. The lower operational points on the purple line are the even cases with e-compounding active, the operational points on the green line are the odd cases with compounding inactive.

When the same is done for the compressor a similar phenomena is observed but opposing direction. Here the operational line (purple) of the e-compounding cases is shifted towards a more efficient region. However, the absolute efficiency gain isn't as profound as the efficiency loss of the turbine, +/- gain 10 [%] against +/- 20 [%] loss. It also can be seen that the operational line moves away from the stall line. For the 100 [kW] e-compounding case even so much that it is placed on the edge of the map, on the pressure ratio is 1 [-] limit.

Hybrid electric turbocharging is a more versatile practice than what is explored in this study. Here, the focus is on the efficiency potential in e-compounding mode, through energy recuperation. However, the opposite approach is also possible, where the electric machine assists the turbine in generating power for the compressor. By examining how energy recuperation shifts the operational line on the compressor map, one can visualize the potential inverse outcome of turbine assistance. An overpowered compressor could possibly surpass the surge limit as there is little headroom in low power settings, making this an important factor to consider, especially for assist during load steps. This is however not a definitive conclusion about assisting hybrid electric turbocharging, but rather an observation of assisting the specific Garrett TW6146 turbochargers on the CAT G3508a. There are naturally plethora of turbochargers available on the market that reshape the compressor map to suit assisted hybrid electric turbocharging.

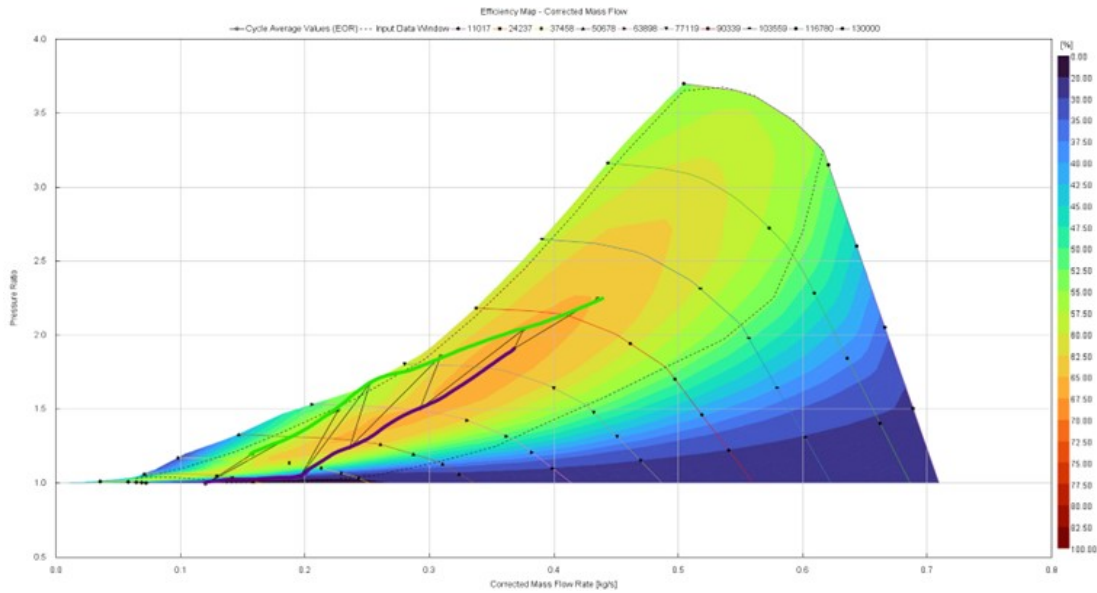


**Figure 9.18:** The change in operational line of the compressor shows a shift in nominal efficiency. The lower operational points on the purple line are the even cases with e-compounding active, the operational points on the green line are the odd cases with compounding inactive.

### 9.10. Summary table

Affected parameter as a result of E-compounding	General effect
System power	= Equal
BSFC	- Reduced
Turbocharger speed	- Reduced
Charge pressure	- Reduced
MAP	- Reduced
Pumping losses	- Reduced
Friction losses	- Reduced
Residual burned mass	+ Increased
NOx emissions	- Reduced
Exhaust exit temperature	+ Increased

**Figure 9.19:** Summary of the effects of eturbo compounding

# 10

## Conclusion

This research sets out to investigate the feasibility and benefits of hybrid electric turbocharging (HET) for improving the efficiency and performance of a spark-ignited internal combustion engine. Using the CAT G3508a as a case study, a detailed GT-ISE (Part of the GT-POWER suite, widely acknowledged engine simulation software) model was developed, validated, and analysed to assess the effects of integrating an electrically assisted turbocharger. The results indicate that hybrid electric turbocharging can enhance system efficiency through energy recuperation while also having potential for improving transient response.

### 10.1. Model Development, Placement and Validation

The foundation of this study was the construction of a high-fidelity engine model capable of accurately simulating the thermodynamic, mechanical, and aerodynamic behaviour of the CAT G3508a. The development of this model required a systematic approach, incorporating multiple subsystems in stages to ensure accuracy and stability. The first step in constructing the model was gathering comprehensive data about the engine and its components. This included geometric specifications like; cylinder bore, stroke, compression ratio, piston shape, and valve timing data. This data was sourced from manufacturer documentation and physical measurements. The layout of the intake manifold, exhaust runners, aftercooler, turbochargers and throttle were carefully modelled to replicate the real world airflow dynamics. Extra attention was given to replicate the staggered valve arrangement, which influences the flow behaviour. The model incorporates CNG fuel injection and combustion characteristics. A load setting dependant Wiebe function was used to model the combustion process, ensuring realistic pressure and temperature profiles. Since turbocharger performance is highly dependent on turbine and compressor characteristics, extensive efforts were made to integrate Stapersma method generated compressor and turbine maps for the best available turbomachinery flow data.

The model was developed incrementally to ensure accuracy, inspired by the Performance Tutorial that is included with the GT-POWER suite. The initial model featured only the core engine cylinders, crank train, valves, fuelling, throttle and aftercooler operating in a naturally aspirated configuration, using boost figures as boundary condition. This allowed calibration of fundamental combustion parameters without interference of the turbochargers. The turbochargers were added in two separate validation steps: first, the compressor system was implemented and tested in isolation, followed by the turbines. Both were driven by simulated control inputs to replicate their behaviour before full coupling. Coupling is done via a turboshaft object that has a specialized function to stabilize the model during startup and ensures that the model converges quickly. Once all components were setup, the full turbocharged model was assembled and subjected to extensive validation. A range of steady-state operating points were tested to ensure the model accurately represented real-world performance. The real world performance being measured on the experimental CAT G3508a that is operated in the facilities of the NLDA in Den Helder.

The model underwent the validation cycles twice using experimental and reference data. The key parameters used for validation included: Power output and mass and fuel flow, ensuring the engine produced the expected power output for a given fuel input was crucial. Manifold Air Temperature (MAT) and Intake Pressure were particularly important for evaluating turbocharger performance and ensuring the charge air cooling system was correctly modelled. The speed of the turbochargers and the corresponding intake and exhaust pressure ratios were compared with measured data, allowing adjustments to turbine and compressor efficiencies. Exhaust gas temperatures were monitored to assess thermal efficiency and modelling accuracy. Despite achieving good correlation in most areas, some discrepancies were observed at extreme load conditions, particularly in high-power scenarios. This highlighted limitations in the turbine related data and these will be suggested areas for further refinement.

The GT-ISE model of the CAT G3508a is a comprehensive model that represents the air path of the engine by dividing it into 283 separate flow volumes, which is an order of magnitude higher when compared to common models. This increase in flow volumes increases the resolution of the physical aspect of the engine over other engine model types, such as MAP-based and Mean-Value models.

MAP-based models rely on pre-measured data stored in look-up tables and sensors data, providing a fast, computationally efficient, and is widely used in engine control units (ECUs). However, they lack physical insight and don't adapt well to changes of engine parameters as they are mostly based on empirical methods.

Mean-Value models, on the other hand, rely on a more physics-based approach and capture average behavior of engine subsystems, typically over an entire cycle. They provide a good balance between computational speed and accuracy, useful for system optimization but may not capture transient effects at high resolution.

CFD models, on the other hand, feature a great increase in resolution, based on up to three-dimensional high-fidelity numerical simulations that solve the fundamental equations of fluid motion. These models are known for high accuracy and deep insights into local flow fields, combustion, and heat transfer but are computationally expensive and not suitable for real-time applications.

The GT-ISE model is a physics-based approach that captures air and fuel flow, pressure dynamics, and thermal effects at crank angle time resolution. With the one-dimensional air path modelling and zero-dimensional in-cylinder modelling, it is positioned between Mean-Value and CFD type models, offering improved resolution without being overly computationally intensive. The 283 separate flow volumes makes it attractive for transient behaviour modeling. The crank angle level resolution adds to its appeal when compared to time cycle averaged methods. The steady state simulation of a given power level takes approximately 10 minutes or less when running on a regular computer, which is considerably less intensive than a CFD model.

The GT-ISE model is well-positioned between Mean-Value and CFD models, improving physical and time resolution without excessive computational investments. Therefore, after the validation it has been concluded that the GT-ISE model represents the CAT G3508a to a satisfactory qualitative scientific level and is suitable for research purposes.

## 10.2. Key findings:

### 10.2.1. Efficiency Gains Through Energy Recuperation and its optimization.

The hybrid turbocharger's ability to recuperate exhaust energy in e-compounding mode and convert it into usable power resulted in significant reductions in fuel consumption at mid-range power levels. Up to 5.5 [%] fuel flow reduction for equivalent system power levels when compared to non-compounding settings. This is ultimately one of the key benefits of hybrid electric turbocharging as it reduces OPEX and OPEC dependence.

The system power is comprised of crank power and the added mechanical power of the electrified turbocharger. The resistive torque of the electrified turbos (e-turbos) was determined by GT-ISE's inbuilt optimizer, targeting for a minimum BSFC at a target system mechanical power. The electrification of the turbocharger changed the conventional power balance between the turbine and compressor. While energy recuperation improves system efficiency, it also reduced available power for the compressor, reducing boost pressure in compounding scenarios. The models throttle controller compensates for this decrease in air density by opening the throttle further, up to maximum in optimized cases. This decreases the pumping losses for the intake stroke, reducing PMEP results in a gain in efficiency. The effect is therefore greatest for mid-range power levels, as that is where the throttle is moderating air flow the most. Additionally, the engine load is reduced due to the additional power by the turbochargers, the sum of them producing an equal system power. The lower loading of the engine reduces the frictional losses of the rotating assembly.

### 10.2.2. Engine output control by hybrid electric turbocharging.

From this it can be concluded that the throttle functionality can also be accomplished by regulation of the resistive e-turbo torque. All optimized e-compounding cases run at WOT, with the exception of the 100 [kW] e-compounding case, so the total system power output is no longer regulated by the throttle. The energy extraction of the turbocharger compounding and the turbochargers behavioural response to that action is sufficient in regulating the system power output. This is similar in how BMW utilizes the aforementioned Valvetronic system [41], that can open the throttle further and regulate the engines power output by controlling the variable valve lift and consequent the mass air flow. It should be possible for a digital electronic control system to vary the applied resistive torque and regulate the engines power output by that method, complementary to an electrically controlled throttle body. Targeting the control system to regulate the engine as much as possible with the e-compounding system and run at WOT as much as possible.

### 10.2.3. NO<sub>x</sub> reduction in e-compounding

A possible benefit of e-compounding is the potential for the reduction of NO<sub>x</sub> emissions. The reduced available power for the compressor makes for a decrease in charge pressure and MAP. Subsequently, the residual mass in the cylinder is increased at Intake Valve Closing (IVC). This is similar to the working of an EGR system. The higher specific heat of residual gasses reduce peak combustion temperatures, reducing the NO<sub>x</sub> content at Exhaust Valve Opening (EVO). GT-ISE reports a NO<sub>x</sub> emission reduction of approximately 4 [%] for the lowest power settings, and fractional reduction for the higher power settings. It must be noted that the developed GT-ISE model of the CAT G3508a with its eturbo modification and its combustion model has not been focussed on the in-cylinder process. Additionally, the emission aspect of the model has not been validated, so these findings are to be further examined. Still, a reduction of NO<sub>x</sub> emissions would be a very attractive benefit of an e-compounding system.

### 10.2.4. Thermal signature and more efficiency potential.

The changed power balance of the turbocharger in e-compounding has resulted in a shift of the operational line of the compressor and turbine on their generated respective mappings. The shift of operational line has put the turbine outside the area of peak efficiency. This has multiple consequences; firstly, the turbine is less effective in expanding the exhaust gasses for energy recuperation, so available exergy is wasted to the environment. This results in a higher turbine exit temperature. This is a negative aspect when this setup would be used for naval purposes, for naval purposes a low exhaust temperature is desired to keep the thermal signature to a minimum. Secondly, the turbine is not as

effective as could be possible, so energy is wasted. When the e-compounding operational line would be positioned in the area of maximum efficiency the power potential for the e-turbos increases, this increases system efficiency even further. For these reasons it is advised for suppliers of electrified turbos to design a turbine for maximum turbine efficiency in e-compounding settings to utilize the maximum available system efficiency and to decrease the exhaust gas temperatures.

### 10.2.5. Hybrid electric turbocharging versatility

Hybrid electric turbocharging is a more versatile practice than what is being assessed in this study, this study focussed on the efficiency potential in e-compounding mode due to energy recuperation. The reverse is also a possibility, where the electric machine assists the turbine in producing power for the compressor. However, when the trend is seen of the shift of the operational line on the compressor map due to the recuperation, one can imagine what the result is of assisting the turbine. It is likely that an overpowered compressor can easily breach the surge limit, this should be taken into consideration when this is practiced. The operational line of conventional non-compounding running leaves little room to the surge line.

### 10.2.6. Study scope and model limitations.

This study focuses on assessing the efficiency potential of hybrid electric turbocharging in a large SI internal combustion engine, specifically the CAT G3508a, using a GT-ISE simulation model. The scope is limited to steady-state analysis, with transient behavior, eturbo control strategies, and dynamic load changes falling outside the research focus, despite GT-ISE's capability to simulate such effects. Additionally, the study does not address system integration challenges in a real-world maritime environment, long-term operational factors such as mechanical wear or thermal management complexities. The model development was constrained by available empirical data, with certain assumptions made regarding turbocharger characteristics, engine combustion behaviour, and control parameters. Furthermore, while alternative fuels like methanol are of growing interest, their direct implementation within the model was not explored in detail.

Additionally, E-compounding has turned out to be ineffective at maximum power of 500 [kW]. This is a model limitation as the model is unable to reach this target in non-compounding cases as the throttle is maxed out at approximately 446 [kW]. Introducing power recuperation of the turboshaft in these conditions only reduces the achieved system power. The models air path has a flow restrictive nature at high power levels, making the model unable to achieve target max. power, even at wide open throttle. The quality of the turbine mapping is suspected to be the cause as the constant speed lines at high speed show a trend that is deemed too vertical. Whether the dis-correlation of the throttle behaviour is due to the turbine mapping or throttle extrapolation to 90 degrees domain can be examined when higher quality turbine mapping becomes available. In the low power regions the correlation seems to be reasonably accurate.

Future research should extend the findings by investigating transient dynamics, adaptive hybrid electric turbo control strategies, alternative fuel compatibility, and real-world validation of hybrid electric turbocharging in operational maritime conditions.

## 10.3. Final takeaway

This research has demonstrated that hybrid electric turbocharging can play a transformative role in improving fuel efficiency. By integrating an electric machine into the turbocharger system, system efficiency can be enhanced, making this a viable technology for future internal combustion engines. Especially in modern times where a dependence on potential untrustworthy OPEC is to be reduced. With further development and refinement, hybrid electric turbocharging could provide a crucial bridge toward more sustainable engine solutions, particularly as industries transition toward alternative fuels. The results and model development for this study could serve as a foundation for future research, guiding the continued evolution of high-efficiency internal combustion engine technology.

## Recomendations for further research

- The boost assist aspect of hybrid electric turbocharging the CAT G3508a is still to be studied. This requires the addition of a transient loading controller, which is still to be developed. Additionally, a controller for transient turbo torque needs to be added. This controller needs to take various aspects into consideration like; max boost, max boost power, only boosting on target undershoot and prevention of breaching the surge limit by means of a separate bypass valve for example, etc. The boost assist has considerable performance potential for transient operations. The boost assist gives the opportunity for proactive anticipation of load steps, completely eliminating the perceived boost threshold and turbo lag. Through this method a specific AFR can be controlled to a much more advanced degree, allowing for larger load steps and shorter transient operations. Precedent for this has been set in automotive and motorsport. Implementation of this practice for large SI internal combustion engines could be very beneficial for high performance marine engines running on alternative fuels.
- The model of the CAT G3508a has been developed from scratch during this study. During the validation it has been found to represent the CAT to satisfactory levels, most parameters falling well in the set tolerance of max. +/- [10%]. However, it has also become clear that the developed model is only scratching the surface of the capabilities of the GT-POWER suite. When one browses through the examples catalog it becomes clear that GT-ISE alone is capable of simulating entire vehicles in precise detail, down to effects of the auto-HVAC on fuel consumption for a WLTP cycle to name an example. It is also used for FEM mechanical analysis of vibrations, lubrication models, high fidelity models of turbocharger dynamics and many more. If one wants to get an impression, take a look at example 'FRM\_Vehicle\_eTurbo.gtm' (under File, Examples to Engine\_1D\_Gas\_Exchange\_Combustion\Boosting\e-Turbo\FRM\_Vehicle\_eTurbo.gtm).

The point being that even though the developed model is found fit for purpose for this study, it can be developed much further.

Specifically for the CAT G3508a; the turbocharger mapping are to be further examined. The optimizer could be helpful for this objective as it is capable of solving and optimizing entire maps supposedly. Just beware of long computational times for this task. Additionally, the assumptions that are made regarding the flow characteristics of the valves and throttle can be reevaluated. The 'Discharge Coefficients' which are implemented are borrowed from the model that is build in GT-ISE's Performance Tutorial, they are found sufficient but it is unknown how accurate they represent the flow behaviour of the valvetrain of the CAT G3508a. Moreover, the fuel map which is used is questionable in its calibration. The data is taken directly from the MCAT control system in Den Helder. Still, the injected fuel mass flow doesn't match as accurately as imagined, the mass air flow is almost as close as could be possible, yet fuel mass flow is off.

In a broader sense; after development of the engine model and taking inspiration from various examples. It has become clear that simulation of the power and propulsion systems of an entire vessel are possible. The TU-Delft Diesel-B model is currently very frequently used for this aspect. GT-ISE seems similarly very capable in modelling and simulation of larger marine systems, like vessels. This way the loading profiles of a vessel in waves can be used to assess the dynamic behaviour of engines to a higher level. It is expected that the increase of resolution due to numerous flow volumes, as with the CAT 3508a's GT-ISE model, is consistent also when other engines are used. This can be beneficial when for example studying dynamic prime mover behaviour in marine conditions.

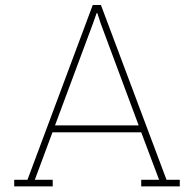
- The optimized Wiebe parameters have not been fully validated during this study. The parameter set for the 500 and 300 [kW] mark have been verified to be close to real values. But concrete validation of these parameters has not been accomplished. The validation of these parameters could present short comings of the model if the values turn out to be unrealistic.
- Controller for variable speed could be introduced to the model. A recent development at the facility of NLDA in Den Helder is the introduction of variable speed control to the CAT G3508a. This has not been implemented into the model at this stage. Additionally, the principle of control could be re-considered. The CAT G3508a is set up by specifying a desired loading for the load bank, the engine control system then controls the torque output which is corresponding to the set loading by targeting a desired speed of 1500 rpm. The developed model uses an inverse principle, it is targeting a desired torque at a set speed of 1500 rpm. In other words; the CAT G3508a sets a power goal and targets a speed, the model sets a speed and targets a power goal. This difference has not been constraining during this study. But in a later stage it could be beneficial to correct this principle.
- A validation of the NO<sub>x</sub> emissions of the developed model could give valuable insights into new aspects that are not widely considered in this study. The model is capable of predicting in-cylinder NO<sub>x</sub> levels at the opening of the exhaust valves. This again highlights the versatility and capabilities of the GT-ISE tool.

# References

- [1] International Maritime Organization. *Index of MEPC Resolutions and Guidelines related to MARPOL Annex VI*. URL: <https://www.imo.org/en/OurWork/Environment/Pages/Index-of-MEPC-Resolutions-and-Guidelines-related-to-MARPOL-Annex-VI.aspx> (visited on 06/10/2024).
- [2] Consilium. *FuelEU Maritime initiative: Provisional agreement to decarbonise the maritime sector*. 2023. URL: <https://www.consilium.europa.eu/en/press/press-releases/2023/03/23/fueleu-maritime-initiative-provisional-agreement-to-decarbonise-the-maritime-sector/> (visited on 06/27/2024).
- [3] AA Banawan, M Morsy El Gohary, and IS Sadek. “Environmental and economical benefits of changing from marine diesel oil to natural-gas fuel for short-voyage high-power passenger ships”. In: *Proceedings of the Institution of Mechanical Engineers, Part M: Journal of Engineering for the Maritime Environment* 224.2 (2010), pp. 103–113.
- [4] Defence Energy. *Defence Energy Transition Plan of Action*.
- [5] NL. Times. *Defense wants to strengthen Dutch industry with new frigates, costing up to €8 billion*. 2024. URL: <https://nltimes.nl/2024/03/03/defense-wants-strengthen-dutch-industry-new-frigates-costing-eu8-billion> (visited on 06/27/2024).
- [6] OPERATIONELE ENERGIESTRATEGIE. 2015. URL: <https://zoek.officielebekendmakingen.nl/blg-683462.pdf>.
- [7] Charles J McKinlay, Stephen R Turnock, and Dominic A Hudson. “Route to zero emission shipping: Hydrogen, ammonia or methanol?”. In: *International Journal of Hydrogen Energy* 46.55 (2021), pp. 28282–28297.
- [8] Faculteit Militaire Wetenschappen. *Nieuwe uitbreiding motorenlab*. URL: <https://faculteitmilitairewetenschappen.nl/news/view/5becc098-68ab-4b81-b07b-b4a9d8235bb6/nieuwe-uitbreiding-motorenlab> (visited on 06/20/2024).
- [9] Faculteit Militaire Wetenschappen. *Duurzame aanwinst dieselmotor verrijkt motorenlab*. URL: <https://faculteitmilitairewetenschappen.nl/news/view/aea83e95-14a0-4bf3-811c-8a97cb9f8627/duurzame-aanwinst-dieselmotor-verrijkt-motorenlab> (visited on 06/21/2024).
- [10] Jan Westhoeve. “Hybrid Electric Turbocharging: Improving the loading capability and efficiency of a dual fuel engine”. MA thesis. Delft University of Technology (DUT), 2018.
- [11] Joris Rusman. “Charge air configurations for propulsion diesel engines aboard fast naval combatants: a simulation study on efficiency and performance”. MA thesis. Delft University of Technology (DUT), 2018.
- [12] Seiichi Ibaraki et al. “Development of the hybrid turbo, an electrically assisted turbocharger”. In: *Mitsubishi Heavy Industries Technical Review* 43.3 (2006), pp. 1–5.
- [13] KEIICHI Shiraishi et al. “Energy savings through electric-assist turbocharger for marine diesel engines”. In: *Mitsubishi Heavy Ind. Tech. Rev* 52.1 (2015), pp. 36–41.
- [14] D. Stapersma. *Diesel Engines Volume 1 Performance Analysis*. Technical report, Delft University of Technology. Jan. 2010.
- [15] D. Stapersma. *Diesel Engines Volume 2 Turbocharging*. Technical report, Delft University of Technology. Jan. 2010.
- [16] Ioana Georgescu et al. “Characterisation of large gas and dual-fuel engines”. In: *MTZ industrial* 6.3 (2016), pp. 64–71.
- [17] Wikipedia contributors. *Deflagration*. Apr. 2024. URL: <https://en.wikipedia.org/wiki/Deflagration>.
- [18] La Xiang, Enzhe Song, and Yu Ding. “A two-zone combustion model for knocking prediction of marine natural gas SI engines”. In: *Energies* 11.3 (2018), p. 561.

- [19] Neil Watson and Marian Stefan Janota. *Turbocharging the internal combustion engine*. Macmillan Education UK, 1982.
- [20] D. Stapersma. *DIESEL ENGINES: A fundamental approach to performance analysis, turbocharging, combustion, emissions and heat transfer including thermodynamical principles*. Jan. 2010.
- [21] John B Heywood. *Internal combustion engine fundamentals*. McGraw-hill, 1988.
- [22] Avinash Kumar Agarwal et al. *Engine Modeling and Simulation*. Springer, 2022.
- [23] C. Westfall. *Understanding Compressor maps – Sizing a turbocharger*. 2018. URL: <https://www.enginelabs.com/engine-tech/power-adders/understanding-compressor-maps-sizing-a-turbocharger/> (visited on 2024).
- [24] Habib Aghaali and Hans-Erik Ångström. “A review of turbocompounding as a waste heat recovery system for internal combustion engines”. In: *Renewable and sustainable energy reviews* 49 (2015), pp. 813–824.
- [25] C. Csere. *Things You Must Know about Porsche’s 911 GTS T-Hybrid Powertrain*. 2024. URL: <https://www.caranddriver.com/news/a60914997/2025-porsche-911-gts-t-hybrid-engine-details/> (visited on 06/27/2024).
- [26] Federation Internationale de l’Automobile (FIA). *Formula One Power Unit Regulations 2014*. 2014. URL: <https://www.fia.com/sites/default/files/publication/file/FIA%20F1%20Power%20Unit%20leaflet.pdf>.
- [27] Yoshihisa Ono, KEIICHI Shiraishi, and Yukio Yamashita. “Application of a large hybrid turbocharger for marine electric-power generation”. In: *Mitsubishi Heavy Industries Technical Review* 49.1 (2012), p. 29.
- [28] RD Geertsma et al. “Pitch control for ships with diesel mechanical and hybrid propulsion: Modelling, validation and performance quantification”. In: *Applied energy* 206 (2017), pp. 1609–1631.
- [29] Mike Loonstijn. “Diesel AM (A-Modular) Model Proposed: Expanding the Diesel A model for advanced turbocharging capabilities”. In: (2017).
- [30] van Putten Colonna and H Van Putten. “Dynamic modeling of steam power cycles.: Part I—Modeling paradigm and validation”. In: *Applied Thermal Engineering* 27.2-3 (2007), pp. 467–480.
- [31] Massimo Figari et al. “Parametric investigation and optimal selection of the hybrid turbocharger system for a large marine four-stroke dual-fuel engine”. In: *Applied Thermal Engineering* 208 (2022), p. 117991.
- [32] Yukio Yamashita et al. “Development of electric supercharger to facilitate the downsizing of automobile engines”. In: *Mitsubishi Heavy Industries Technical Review* 47.4 (2010), pp. 7–12.
- [33] Keiichi Shiraishi, Yoshihisa Ono, and Kiyoko Sugishita. “Development of large marine hybrid turbocharger for generating electric power with exhaust gas from the main engine”. In: *Mitsubishi Heavy Industries Technical Review* 47.3 (2010), pp. 53–58.
- [34] Hao Dong et al. “Experiment and simulation investigation on energy management of a gasoline vehicle and hybrid turbocharger optimization based on equivalent consumption minimization strategy”. In: *Energy Conversion and Management* 226 (2020), p. 113518.
- [35] Robert G Sargent. “Verification and validation of simulation models”. In: *Proceedings of the 2010 winter simulation conference*. IEEE. 2010, pp. 166–183.
- [36] Gamma Technologies. *GT-Suite engine performance tutorials (Version 2022)*. 2022.
- [37] K. J. Saurwalt. “Nog steeds zorgen in de scheepsbouwwereld”. In: *Schip en Werf* 49.18 (Sept. 1982). URL: <https://swzmaritime.nl/wp-content/uploads/2021/07/1982-18.pdf>.
- [38] G. Woschni. “A Universally Applicable Equation for the Instantaneous Heat Transfer Coefficient in the Internal Combustion Engine”. In: *SAE Technical Paper* 76.670931 (1967). DOI: 10.4271/670931.
- [39] Günter P Merker et al. *Simulating Combustion: Simulation of combustion and pollutant formation for engine-development*. Springer Science & Business Media, 2005.

- 
- [40] D. Stapersma. "A general model for off-design performance of a single-stage turbomachine". In: *Marine Engineering & Platform Systems, TU Delft KIM-PFS-97-111*, issue D (July 2013).
- [41] Harald Unger et al. "The valvetronic". In: *MTZ worldwide* 69.7 (2008), pp. 30–37.



# Remaining Re-validation graphs

## A.1. Re-validation graphs

The remaining re-validation graphs are given below for sake of completion. The graphs show little difference between the initial and recalibrated model, this again remarks the fact that the model is robust and can run stable when significant parameters are varied. The orange line displays the latest iteration with the 'name3' reference. The power settings are identical as the initial validation, starting with the red dot at 100 [kW], increasing to 200, 250, 300, 400 [kW] and finalizing at max power (=500 [kW]).

## A.2. Pressure compressor in

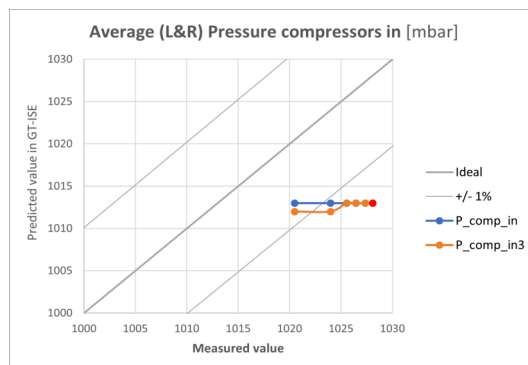


Figure A.1: Pressure compressor in of previous (blue) and latest iteration (orange), Predicted vs. Measured values.

## A.3. Pressure compressor out

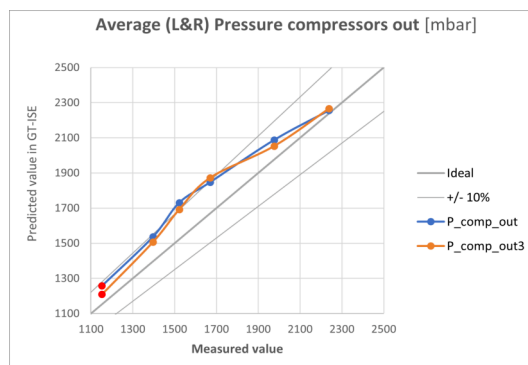


Figure A.2: Pressure compressor out of previous (blue) and latest iteration (orange), Predicted vs. Measured values.

## A.4. Pressure ratio compressors

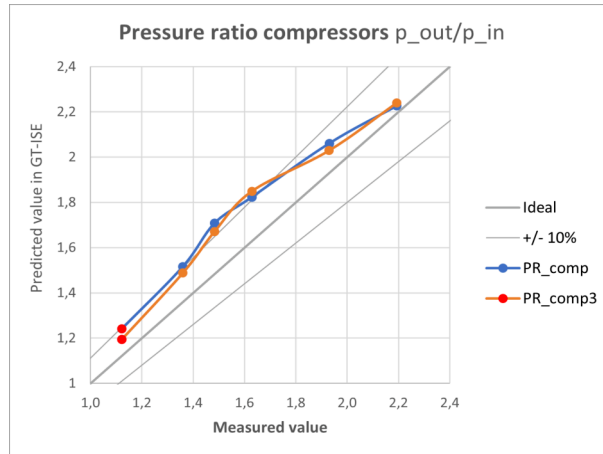


Figure A.3: Pressure ratio compressor of previous (blue) and latest iteration (orange), Predicted vs. Measured values.

## A.5. Temperature compressor in

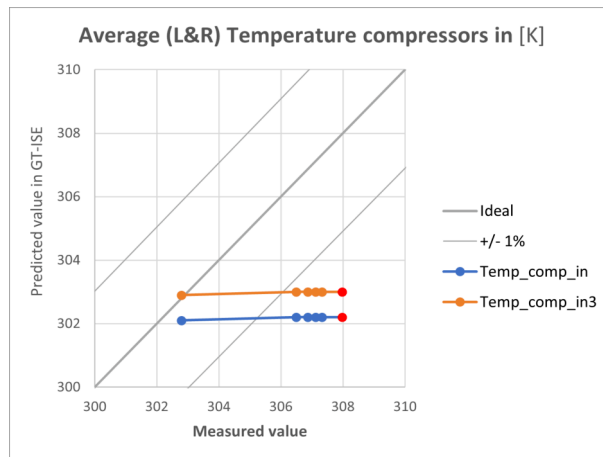


Figure A.4: Temperature compressor in of previous (blue) and latest iteration (orange), Predicted vs. Measured values.

## A.6. Temperature compressor out

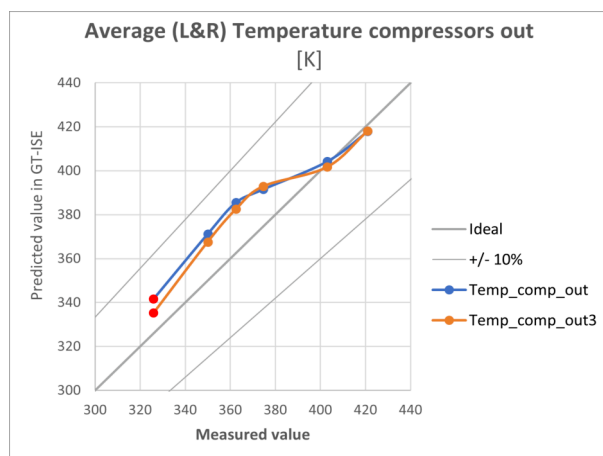


Figure A.5: Temperature compressor out of previous (blue) and latest iteration (orange), Predicted vs. Measured values.

## A.7. Pressure ratio aftercooler

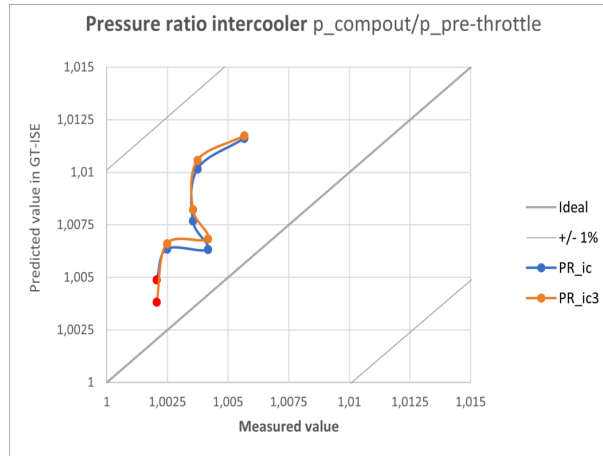


Figure A.6: Pressure ratio aftercooler of previous (blue) and latest iteration (orange), Predicted vs. Measured values.

## A.8. Pressure pre-throttle

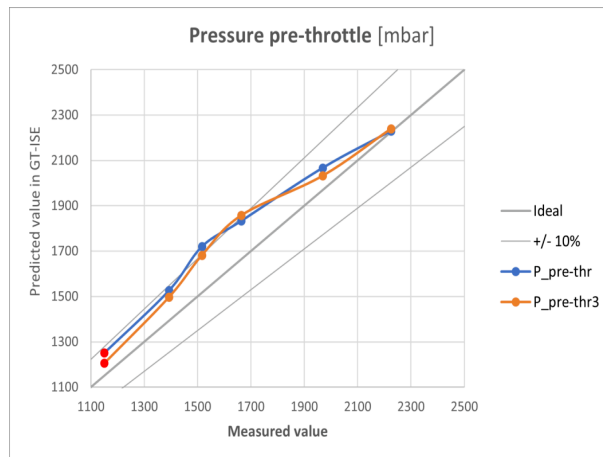


Figure A.7: Pressure pre-throttle of previous (blue) and latest iteration (orange), Predicted vs. Measured values.

## A.9. Pressure ratio throttle

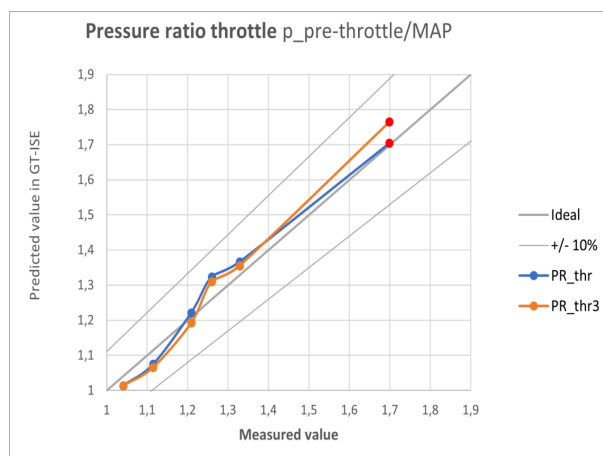


Figure A.8: Pressure ratio throttle of previous (blue) and latest iteration (orange), Predicted vs. Measured values.

## A.10. Manifold Absolute Pressure (MAP)

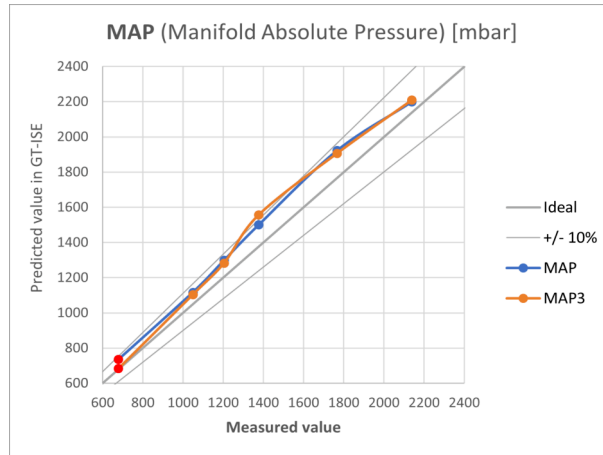


Figure A.9: Manifold absolute pressure of previous (blue) and latest iteration (orange), Predicted vs. Measured values.

## A.11. Pressure turbines in

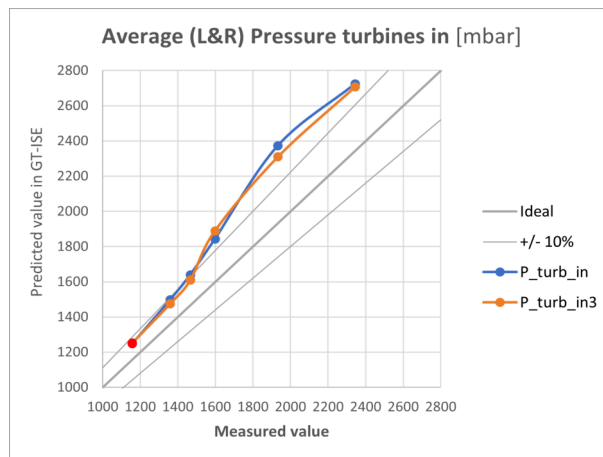


Figure A.10: Pressure turbine in of previous (blue) and latest iteration (orange), Predicted vs. Measured values.

## A.12. Pressure turbines out

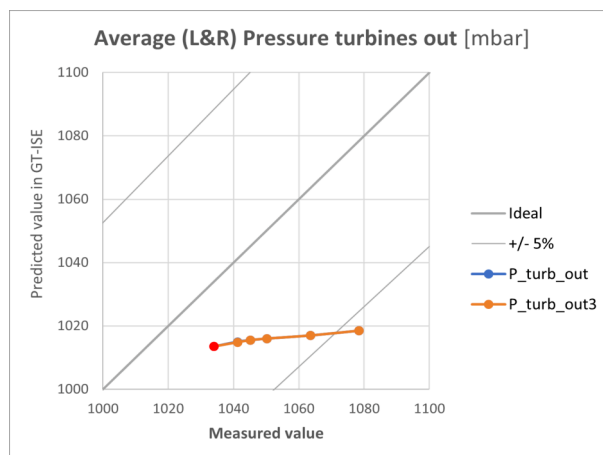


Figure A.11: Pressure turbine out of previous (blue) and latest iteration (orange), Predicted vs. Measured values.